UNIVERSITY OF CALIFORNIA

Los Angeles

Non-linear Evolution

of an Obliquely Propagating

Langmuir Wave

A dissertation submitted in partial fulfillment of the

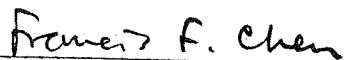requirements for the degree Doctor of Philosophy

in Physics

by

Curtis Robert Menyuk

1981
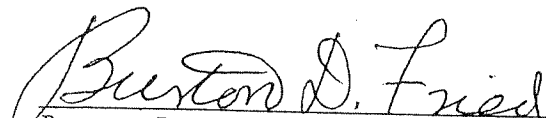
The dissertation of Curtis Robert Menyuk is approved.

_____
Francis F. Chen

_____
John M. Dawson

_____
Neville C. Luhmann

_____
George J. Morales

_____
Burton D. Fried, Committee Chairman

University of California, Los Angeles

1981

ii

TABLE OF CONTENTS

Latin Alphabet

$E(x,t)$	electrostatic field variation
$E_k(t)$	coefficient of the kth component of the electrostatic field
$E_0(t)$	amplitude of the electrostatic field
f	electron distribution function
f_ℓ	linear response function
f_r	linear response function contribution to ϵ_r
f_i	linear response function contribution to ϵ_i
f_k	coefficient of the kth component of the distribution function response
$f_{k\ell}$	linear contribution to f_k
$f_{kn\ell}$	non-linear contribution to f_k
f_{kr}	contribution of $f_{k\ell}$ to ϵ_r
f_{ki}	contribution of $f_{k\ell}$ to ϵ_i
f_0	spatially averaged f
$\mathcal{f}_0$	normalized f_0
k	wave-number magnitude
$k_{\shortparallel}$	parallel wave-number
$k_\perp$	perpendicular wave-number
k_D	Debye wave-number
ℓ	normalized lower bound of simulation region (laboratory frame)

ℓ_i	normalized lower bound of the ith resonant region (laboratory frame)
n_0	plasma density
$P(t)$	normalized wave power, $\Phi^2(t)/\Phi^2(0)$
$P_z(z)$	normalized wave power in the boundary-value problem
r	tangent of the wave's angle of propagation, $k_\perp/k_{\shortparallel}$
R	asymptotic ($t = \infty$) total damping
$R(t)$	total damping as a function of time
R_z	asymptotic ($z = \infty$) total damping
$R_z(z)$	total damping as a function of z.
s	normalized upper bound of simulation region (laboratory frame)
s_i	normalized upper bound of the ith resonant region (laboratory frame)
T	plasma temperature
u	normalized frequency, $\omega/k_{\shortparallel}v_t$; normalized phase velocity, v_p/v_t
u_i	normalized damping rate, $\gamma/k_{\shortparallel}v_t$
u_c	normalized complex frequency
v_g	parallel group velocity
v_p	phase velocity
v_s	velocity separation between resonances, $\Omega/k_{\shortparallel}$
v_t	electron root-mean-square velocity
w	resonance width

Greek Alphabet

α normalized plasma frequency, $\omega_p/kv_t = (k\lambda_D)^{-1}$

γ damping rate

γ_z spatial damping rate

ε dielectric function

ε_r real part of the dielectric function evaluated at real frequencies

ε_i imaginary part of the dielectric function evaluated at real frequencies

ζ normalized perpendicular velocity, $v_\perp/v_t$

η non-linear phase shift

θ gyro-angle, $\tan^{-1}(-v_x/v_y)$

κ normalized wave-number, kv_t/Ω

$\kappa_{\shortparallel}$ normalized parallel wave-number; inverse of the normalized gyrofrequency, $\Omega/k_{\shortparallel}v_t$; inverse of the normalized separation between resonances, v_s/v_t

$\kappa_\perp$ normalized perpendicular wave-number

ν normalized parallel velocity (wave frame), $(v_z-v_p)/v_t$

ρ_k coefficient of the kth component of the charge density

$\rho_{k\ell}$ linear contribution to ρ_k

ρ_{kr} contribution of $\rho_{k\ell}$ to ε_r

ρ_{ki} contribution of $\rho_{k\ell}$ to ε_i

τ_b bounce period, $2\pi/\omega_b$

ϕ	normalized potential amplitude, $e\Phi/T$
Φ	wave potential amplitude
$\tilde{\Phi}(x,t)$	wave potential variation
χ	susceptibility function
χ_r	real part of the susceptibility function at real frequencies
χ_i	imaginary part of the susceptibility function at real frequencies
$\omega,\ \omega_0$	wave frequency
ω_c	complex wave frequency
$\delta\omega$	non-linear frequency shift
$\delta\omega_c$	complex, non-linear frequency shift
ω_b	bounce frequency
ω_{bn}	bounce frequency in the nth resonance at a given $v_\perp$
ω_p	plasma frequency
Ω	cyclotron frequency

LIST OF FIGURES

LIST OF TABLES

VITA

March 26, 1954 -- Born, Newton, Massachusetts

          1975 -- Certificat C1, Maitrise de Physique,

               Université de Paris VI, Paris, France

          1976 -- B.S., M.S., Massachusetts Institute of Tech-

               nology, Cambridge, Massachusetts

   1977 - 1979 -- Research Assistant, Department of Physics,

               University of California, Los Angeles

   1979 - 1981 -- Staff Research Associate, Department of Physics,

               University of California, Los Angeles

PUBLICATIONS

Menyuk, C. R., Shapiro, I. I., Wittels, J. J., Hinteregger, H. F.,
    Knight, C. A., Rogers, A. E., Whitney, A. R., Clark, T. A.,
    and Hutton, L. K., "VLBI Observations of 3C 345 and NRAO 512
    in Right and Left Circular Polarization," Ap. J. 220, L27
    (1978).

Zweben, S. J., Menyuk, C. R., and Taylor, R. J., "Small-Scale
    Magnetic Fluctuations Inside the Macrotor Tokamak," Phys.
    Rev. Lett. 42, 1270 (1979).

Zweben, S. J., Menyuk, C. R., and Taylor, R. J., "Vacuum Photo-
    diode Array for U.V. Detection in a Tokamak Plasma," Rev.

Sci. Instr. <u>50</u>, 972 (1979).

Menyuk, C. R., and Lee, Y. C., "Finite Bandwidth Induced Stochas-
ticity in a Magnetic Mirror," Phys. Fluids <u>23</u>, 2225 (1980).

ABSTRACT OF THE DISSERTATION

Non-linear Evolution of an

Obliquely Propagating Langmuir Wave

by

Curtis Robert Menyuk

Doctor of Philosophy in Physics

University of California, Los Angeles, 1981

Professor Burton D. Fried, Chairman

The transition between regular and stochastic motion which occurs when resonances overlap plays an important role in present-day plasma physics research, and has recently been the subject of intensive study. However, investigations to date have been primarily concerned with single-particle motion in given wave fields, and there has been little attempt to determine how particle motion feeds back on the wave to affect its evolution. We explore this problem here in the simple context of an obliquely propagating Langmuir wave. Electrons are resonant with the wave whenever $v_{\shortparallel} = (\omega - n\Omega)/k_{\shortparallel}$, where n is any integer.

This wave has three distinct evolution regimes whose locations in parameter space are given roughly by the following relations: If ω_b (the electron bounce frequency) $< \gamma$ (the linear damping rate), then linear theory is valid, and the wave damps away. If $\gamma < \omega_b < \Omega$ (the

xv

cyclotron frequency), then electrons can be trapped in individual reso-
nances. In this trapping regime, the wave evolution can be treated
in a fashion analogous to O'Neil's treatment of a parallel-propagating
wave. We find that the amplitude oscillations disappear at propagation
angles greater than 14° due to a "super-phase-mixing" of the many
bounce frequencies. Finally, if $\gamma < \Omega < \omega_b$, then resonances overlap
and electron motion is stochastic. In this regime, particle motion is
nearly diffusive in the region of velocity space where resonances over-
lap, and the wave evolution can be treated using quasilinear theory
with resonance broadening. However, because most of the stochastic
electrons are initially on the edge of the stochastic region in velo-
city space, where large regular regions exist, their motion is not
entirely diffusive, and this theory's results, while qualitatively use-
ful, are not quantitatively accurate, as comparison with numerical si-
mulation shows.

In the transition regime between regular and stochastic motion,
the electron orbits are complicated and an analytic solution does not
appear possible. It is possible, however, to determine the asymptotic
total damping of the wave using two different approaches. In the
first, we assume that the distribution function is asymptotically flat-
tened over the resonant regions. In the second, we use "mini-simula-
tions," following the orbits of the resonant electrons numerically and
treating the rest of the electrons as a background linear dielectric
medium. Using this approach, the wave evolution is determined self-
consistently by updating the field at each time step. The two methods
lead to asymptotic amplitudes which agree to within a factor of two,

and the wave's total damping is found to increase significantly when a transition is made between the regular and stochastic regimes, i.e. when resonances overlap.

In order to make contact with possible experiments, an idealized boundary-value problem in which ω and $k_\perp$ are fixed and $k_{||}$ is then determined by the plasma is considered. The principal qualitative results which should be observable in experiments and full-particle simulations are found also in the boundary-value problem.

We restate the principal qualitative results: 1) the amplitude oscillations in the trapping regime disappear due to super-phase-mixing of the many bounce frequencies when the angle of propagation is increased past 14°; 2) the wave exhibits increased total damping when a transition is made between the regular and stochastic regimes.

1. INTRODUCTION

1.1 Intrinsic Stochasticity and the Resonance Overlap Criterion

The study of intrinsic stochasticity, the apparently random be-
havior of deterministic systems, has found application in the fields
of hydrodynamic turbulence,[1] semiconductor physics,[2] many-wave coup-
ling in plasmas,[9-12] particle confinement in mirror machines,[13-16]
particle transport in Tokamaks,[17-18] and others.[19]

These theoretical applications can be divided into two classes,
those concerned with dissipative (non-Hamiltonian) systems,[1-5] and
those concerned with conservative (Hamiltonian) systems.[6-18] In the
conservative systems, which include most of the plasma physics appli-
cations to date, one generally considers the dynamics of particles
moving in fixed-amplitude waves and is interested in determining the
character of particle motion as a function of the wave amplitudes.
If the motion is regular,* then particles can diffuse, leading to heat-
ing or loss of confinement, depending on the application.

The point at which the transition between regular and stochastic
behavior occurs may be determined analytically using the resonance
overlap criterion developed by Chirikov.[20] Consider the simple exam-
ple of a one-dimensional potential which is a superposition of plane
waves. The Hamiltonian of a particle with unit mass and charge is
given by

*then particles are trapped in a small region of phase space.
If the motion is stochastic,

1

$$H(z, p_z) = \frac{p_z^2}{2} + \varepsilon \sum_{n=1}^{\infty} a_n \cos\left[k_n(z - v_n t)\right],$$

(1.1)

where z is the particle coordinate, p_z is the particle momentum, and εa_n gives the amplitude of the nth wave. When $\dot{z} = p_z = v_n$, the particle will be resonant with the nth wave, and, if ε is small, the effect of the other waves on the particle will be small. The Hamiltonian may then be approximated by

$$H(z, p_z) \simeq \frac{p_z^2}{2} + \varepsilon a_n \cos\left[k_n(z - v_n t)\right].$$

(1.2)

Eliminating time by moving to the wave frame will yield the usual pendulum Hamiltonian which has regular solutions with a resonance (trapping) width $\Delta p_z = 4(\varepsilon a_n)^{1/2}$ (see Ref. 20, Sec. 1). As ε is increased, the approximation of neglecting all but one wave breaks down when the resonance widths associated with neighboring resonances (n and n±1) overlap; in effect, the particle is now trapped in many waves, responds to all of them at once, and hence moves stochastically. It has been shown in many numerical studies that this overlap condition tends to overestimate the value of ε at which some particles are free to move from one resonance to another and to underestimate the value at which essentially all particles are free to move. Nonetheless, it is relatively easy to calculate and therefore quite useful.

Theories to date which examine the transition between regular and stochastic motion have generally focused on the particle motion

in a fixed amplitude wave. There has been little attempt to determine how the particle motion feeds back on the waves to affect their evolution, or to demonstrate that this evolution differs significantly in the regular and stochastic regimes. Because it is waves, not particles, which are the primary observables in most experiments and full particle simulations, a determination of the wave evolution and a discussion of the differences between the regular and stochastic regimes is important. It is one of the major purposes of this thesis to address this issue.

In this thesis, the particular example of a Langmuir wave propagating obliquely to a magnetic field is considered. This wave has the virtue of being a promising candidate for experimantal study. Single particles are resonant with it whenever

$$v_z = \frac{\omega - n\Omega}{k_{\shortparallel}} \, , \tag{1.3}$$

where v_z is the particle velocity parallel to the magnetic field, ω is the wave frequency, Ω is the cyclotron frequency, $k_{\shortparallel}$ is the parallel wavenumber, and n is any integer. Hence, this single wave has many resonances which can overlap, leading to stochastic particle behavior[9] and, as we will show, increased asymptotic change in the wave amplitude (increased total damping).

It should be borne in mind that plasmas are influenced by a myriad of non-linear phenomena,[21] several of which can be seen mixed together at one time in many experiments and full-particle simulations.[22] Because we consider a single wave, wave-wave coupling is

3

not important in our problem. To reduce shock formation and other wave generation as much as possible, we consider a wave satisfying $\phi \equiv (e\Phi/T) \lesssim 0.1$, which is the range where experiments on parallel-propagating waves have been done.[23] To avoid confusion with enhanced Landau damping,[24] we not only consider small wave amplitudes, but also set $v_p \gtrsim 4v_t$, where v_p is the phase velocity and v_t is the thermal velocity. Finally, to demonstrate that resonance overlap leads to effects different from trapping, so that the two phenomena may be distinguished, we show that when resonance overlap occurs, particles can gain considerably more energy than when they are trapped, because they are free to move from resonance to resonance. As a result, they take more energy from the wave, leading to an increase in the total asymptotic damping.

1.2 Obliquely Propagating Waves

Obliquely propagating waves are worth studying for reasons that go well beyond verification of the resonance overlap condition. Nonlinear wave-particle interactions lie at the root of many important plasma physics phenomena,[21] of which resonance overlap is just one. Great progress has been made theoretically,[25-31] experimentally,[23,32] and in simulations[24,33-35] in understanding these phenomena in parallel-propagating waves, but there has been far less progress in understanding these phenomena in obliquely propagating waves, where the presence of many resonances leads to behavior quite different from that of parallel-propagating waves.

4

In this thesis, the evolution of a Langmuir wave propagating obliquely to a magnetic field in an infinite, homogeneous, Maxwellian plasma is studied. We consider only a single wave, ignoring the possible existence of other waves due to harmonic generation, sideband instabilities, or other non-linear processes. Particle motion in electrostatic waves has been discussed by Smith and Kaufman,[9] and earlier, for non-stochastic particles, by Palmadesso.[36] Electron waves are studied here, rather than ion waves, because the non-linear evolution of electron waves is only affected by the electron dynamics, considerably complicating the theoretical analysis.

We can distinguish three different regimes for the evolution of an obliquely propagating Langmuir wave, depending on the wave amplitude. If the linear damping rate γ is greater than the electron bounce frequency ω_b, then linear damping dominates the evolution; if $\gamma < \omega_b < \Omega$, then electrons are trapped in well-separated resonances and trapped particle oscillations dominate the wave evolution; finally, if $\gamma < \Omega < \omega_b$, then electrons move stochastically, and their diffusion dominates the wave evolution.

Study of the non-linear evolution of any wave must be based on a good understanding of the linear regime where $\omega_b < \gamma$. It is straightforward to claculate the linear dispersion relation of obliquely propagating Langmuir waves;[37] however, the usual treatment does not clarify the physical origin of the multiple resonances and of the damping. In Chapter 2 of this thesis, the dispersion relation is derived. Next, the dimensionless variables which will be used to describe the wave and the plasma are introduced, and the parameter regime where our

work was done is described. The physical origin of the many resonances and the associated damping is then discussed, and it is shown that the damping is caused by essentially the same machanism as the usual Landau damping in parallel-propagating Langmuir waves. The linear dispersion relation is then solved exactly using root-finding techniques and the result compared to the usual asymptotic approximations. The contributions of the separate resonances to the damping are also evaluated and discussed.

Consideration of non-linear effects begins with Chapter 3, where the equations governing the evolution of waves in the trapping regime, $\gamma < \omega_b < \Omega$, are derived, and the result is shown to reduce to that of O'Neil[26] in the case of parallel propagation. In the course of this derivation, it is demonstrated that the bounce frequency of electrons trapped in the nth resonance is given by

$$\omega_{b_n} = k_{\shortparallel} \left[\frac{e \Phi}{m} J_n \left(\frac{k_\perp v_\perp}{\Omega} \right) \right]^{1/2} , \qquad (1.4)$$

where e is the electron charge, m is the electron mass, Φ is the wave potential amplitude, $k_\perp$ is the perpendicular wavenumber, $v_\perp$ is is the electron perpendicular velocity, and $J_n(x)$ is the Bessel function of order n. The equation governing the wave amplitude is then solved numerically, and it is shown that when the angle of propagation with respect to the magnetic field is increased from 0° to 14°, the amplitude oscillations discovered by O'Neil disappear due to "super-phase-mixing" of electrons with different bounce frequencies.

In discussing the transition between the trapping and stochas-

tic regimes, an analytic description of the particle motion does not appear possible since phase space is composed of regular and stochastic regions pathologically interwoven. Nonetheless, progress can be made in discussing the asymptotic (t=∞) change in the wave amplitude using momentum conservation arguments similar to arguments previously used by Dawson and Shanny.[24] One calculates the fraction R of the wave energy required to flatten the electron distribution function over the width of a resonance, or, if several resonances overlap, over their combined width. If R<1, then the wave energy will decrease by a fractional amount approximately equal to R before saturating; if R>>1, then the wave will damp away. This model is used in Chapter 4 to demonstrate that the "total damping", the fractional decrease in wave energy, increases when resonance overlap occurs, and to derive scaling laws which could be verified in experiments and simulations. The time evolution of the wave energy in the stochastic regime $\gamma < \omega_b < \Omega$ is then investigated; the assumption that particle motion is diffusive is examined, and, given this assumption, the appropriate diffusion coefficient is derived and used to estimate $R(t)$.

In order to check our theoretical results and accurately determine the time-development in the stochastic regime, we have used a "mini-simulation" technique[33,38-39] in which a small region of velocity space is simulated, while most of the plasma is treated as a background linear dielectric. The results, which are presented in Chapter 5, essentially confirm the theoretical predictions of Chapters 3 and 4. Moreover, they show that the evolution in the stochastic regime is quite slow compared to evolution in the trapping

regime. In the stochastic regime, the wave is only halfway towards saturation after ten bounce periods and takes hundreds of bounce periods more to get all the way there; while, in the trapping regime, the wave has essentially saturated after five bounce periods.

In theories and simulations, one generally solves initial-value problems, and the results are not directly appropriate for comparisons with experiments, where waves are typically launched from a grid. To facilitate comparison with experiments, we consider an idealized boundary-value problem in Chapter 6. A planar phased array which fixes both ω and $k_{\perp}$ is assumed to be embedded in the plasma, with its normal parallel to the magnetic field. The dispersion relation determines the real and imaginary parts of $k_{\shortparallel}$. The familiar relation $\gamma_z = \gamma v_g$, where γ_z is the spatial linear damping rate and v_g is the group velocity is reviewed. It is shown that in the trapping regime the bounce wavenumber k_{bz} in the nth resonance is equal to ω_b / v_n, where $v_n = (\omega - n\Omega)/k_{\shortparallel}$. As a result, the relationshipt between the temporal and spatial evolution is usually complicated; however, in the special case of parallel propagation, the spatial evolution is self-similar to the temporal. In this case, the total spatial damping R_z is shown to equal $(v_p/v_g)R$. If the resonances are closely packed, as is the case in the stochastic regime, then this result is shown to be approximately valid for obliquely propagating waves as well.

Chapter 7 contains the conclusions. Our principal results are that super-phase-mixing leads to disappearance of the amplitude oscillations in the trapping regime, and that the onset of stochas-

ticity leads to increased total damping of the wave.

2. LINEAR REGIME

2.1 Derivation of the Dispersion Relation

Landau[40] was the first to calculate the complete dispersion relation for unmagnetized electron waves, including the imaginary part; before then, only the real part had been derived. Landau's prediction that the wave damps was confirmed experimentally[41] and in simulations[42] in the early '60's. The work of extending Landau's theory to a magnetized plasma was done by a number of authors and essentially completed by 1962.[37]

The standard derivation of the dispersion relation begins with the Vlasov equation

$$\frac{\partial f}{\partial t} + \underset{\sim}{v} \cdot \frac{\partial f}{\partial \underset{\sim}{x}} - \frac{e}{m}\left(\underset{\sim}{E} + \frac{\underset{\sim}{v} \times \underset{\sim}{B_o}}{c}\right) = 0 , \qquad (2.1)$$

where $f \equiv f(\underset{\sim}{x}, \underset{\sim}{v}, t)$ is the electron distribution function, $\underset{\sim}{x}$ is the electron coordinate, $\underset{\sim}{v}$ is the electron velocity, $\underset{\sim}{B}_0 \equiv B_0 \underset{\sim}{e}_z$ is the magnetic field, chosen to be in the z-direction, and

$$\underset{\sim}{E} \equiv -i \, \Phi \left(k_{\shortparallel} \underset{\sim}{e}_z + k_{\perp} \underset{\sim}{e}_y\right) \exp\left[i\left(k_{\shortparallel} z + k_{\perp} y - \omega t\right)\right] \qquad (2.2)$$

is the electrostatic field, with the perpendicular component chosen to be in the y-direction. In linear theory, the electrostatic field is considered small, and the Vlasov equation is linearized to yield

$$\frac{\partial f_1}{\partial t} + \underset{\sim}{v} \cdot \frac{\partial f_1}{\partial \underset{\sim}{x}} - \frac{e}{m}\left(\frac{\underset{\sim}{v} \times \underset{\sim}{B_0}}{c}\right) \cdot \frac{\partial f_1}{\partial \underset{\sim}{v}} = \frac{e}{m}\underset{\sim}{E} \cdot \frac{\partial f_0}{\partial \underset{\sim}{v}} , \qquad (2.3)$$

where $f_0(\underset{\sim}{v})$ is the unperturbed part of the distribution function and

$$f_1(\underset{\sim}{x}, \underset{\sim}{v}, t) \equiv f_1(\underset{\sim}{v}) \exp\left[i\left(k_{\shortparallel} z + k_\perp y - \omega t\right)\right] \qquad (2.4)$$

is the perturbed part of the distribution function. Solving for f_1 from Eq. (2.3) and substituting into Poisson's equation

$$\nabla \cdot \underset{\sim}{E} = -4\pi e n_0 \int d^3v\, f_1 , \qquad (2.5)$$

where n_0 is the plasma density, yields

$$k^2 \Phi = \omega_p^2 \Phi \sum_{n=-\infty}^{\infty} \int d^3v \left(\frac{n\Omega}{v_\perp}\frac{\partial f_0}{\partial v_\perp} + k_{\shortparallel}\frac{\partial f_0}{\partial v_{\shortparallel}}\right) \frac{J_n^2\left(\frac{k_\perp v_\perp}{\Omega}\right)}{n\Omega + k_{\shortparallel} v_z - \omega} , \qquad (2.6)$$

where $\omega_p \equiv (4\pi n_0 e^2/m)^{1/2}$ is the plasma frequency. In the v_z integration in Eq. (2.6) and subsequent equations, we assume $\mathrm{Im}(\omega) > 0$. If $\mathrm{Im}(\omega) < 0$, the integration is determined by the analytic continuation from the upper half plane. The dielectric function may now be written

$$\varepsilon\left(k_{\shortparallel}, k_\perp, \omega\right) = 1 - \frac{\omega_p^2}{k^2} \sum_{n=-\infty}^{\infty} \int d^3v \left(\frac{n\Omega}{v_\perp}\frac{\partial f_0}{\partial v_\perp} + k_{\shortparallel}\frac{\partial f_0}{\partial v_z}\right)$$

$$\frac{J_n^2\left(\frac{k_\perp v_\perp}{\Omega}\right)}{n\Omega + k_{\shortparallel} v_z - \omega} . \qquad (2.7)$$

To find the dispersion relation $\omega(k_{\shortparallel}, k_\perp)$, one sets the dielectric function equal to zero and solves for ω given $k_{\shortparallel}$ and $k_\perp$. If ω is almost real, then it is legitimate to break the dielectric into two

pieces $\varepsilon = \varepsilon_r + \varepsilon_i$, where

$$\varepsilon_r \equiv 1 - \frac{\omega_p^2}{k^2} \sum_{n=-\infty}^{\infty} P \int d^3v \left(\frac{n\Omega}{v_\perp} \frac{\partial f_o}{\partial v_\perp} + k_\parallel \frac{\partial f_o}{\partial v_z} \right) \frac{J_n^2\left(\frac{k_\perp v_\perp}{\Omega}\right)}{n\Omega + k_\parallel v_z - \omega} ,$$

(2.8)

$$\varepsilon_i = \pi \frac{\omega_p^2}{k^2} \sum_{n=-\infty}^{\infty} \int d^2v_\perp \left(\frac{n\Omega}{k_\parallel v_\perp} \frac{\partial f_o}{\partial v_\perp} + \frac{\partial f_o}{\partial v_z} \right) J_n^2\left(\frac{k_\perp v_\perp}{\Omega}\right) .$$

One can then solve for ω_r, the real part of ω, by setting ε_r equal to zero, and then solve for ω_i, the imaginary part of ω, using the relation

$$\left. \frac{\partial \varepsilon_r}{\partial \omega} \right|_{\omega_r} (i\omega_i) = i\varepsilon_i .$$

(2.9)

Noting that $\gamma = -\omega_i$, one obtains the standard result

$$\gamma = -\pi \left(\frac{\partial \varepsilon_r}{\partial \omega} \right)^{-1} \frac{\omega_p^2}{k^2} \sum_{n=-\infty}^{\infty} \int d^2v_\perp \left(\frac{n\Omega}{k_\parallel v_\perp} \frac{\partial f_o}{\partial v_\perp} + \frac{\partial f_o}{\partial v_z} \right) J_n^2\left(\frac{k_\perp v_\perp}{\Omega}\right) .$$

(2.10)

In the case of a Maxwellian plasma, the distribution function is

$$f_o = \left(\frac{m}{2\pi T} \right)^{1/2} \exp\left[-\left(\frac{m}{T} \right)\left(\frac{v_z^2}{2} + \frac{v_\perp^2}{2} \right) \right] ,$$

(2.11)

where T is the temperature, and Eq. (2.7) becomes

$$\varepsilon = 1 + \frac{k_D^2}{k^2} \left\{ 1 + \sum_{n=-\infty}^{\infty} \Lambda_n \left(\frac{k_\perp^2}{\Omega^2} \frac{T}{m} \right) \right.$$

$$\left. \frac{\omega}{k_\parallel} \left(\frac{m}{2T} \right)^{1/2} Z\left[\frac{\omega - n\Omega}{k_\parallel} \left(\frac{m}{2T} \right)^{1/2} \right] \right. ,$$

(2.12)

where $\Lambda_n(x) \equiv I_n(x)\exp(-x)$, $I_n(x)$ being the modified Bessel function of order n, $k_D \equiv (4\pi n_0 e^2/T)^{1/2}$ is the inverse Debye length, and

$$Z(x) \equiv \frac{1}{\pi^{1/2}} \int_{-\infty}^{\infty} du \frac{\exp(-u^2)}{u - \chi}$$

is the plasma dispersion function of Fried and Conte.[43]

2.2 Normalized Variables and the Parameter Regime Considered

An obliquely propagating electrostatic wave in a Maxwellian plasma with a homogeneous magnetic field is completely characterized by seven variables which may be chosen to be the wave potential Φ, the plasma density n_0, the plasma temperature T, the cyclotron frequency Ω, the wave frequency ω, the parallel wave-number $k_{||}$, and the perpendicular wave-number $k_\perp$. One can replace this set of variables with another as long as the two sets are equivalent, and, in our work, we often replace n_0 and T with the plasma frequency ω_p and the inverse Debye length k_D. Of the seven variables needed, two only serve to set the length and time scales, and can be removed by suitably normalizing the original variables. In this thesis, we use the normalized variables

$$\varphi \equiv \frac{e\Phi}{T} \, , \qquad \alpha \equiv \frac{k_D}{k} \, , \qquad u \equiv \frac{\omega}{k_{||} v_t} \, ,$$

$$K_{||} \equiv \frac{k_{||} v_t}{\Omega} \, , \qquad K_\perp \equiv \frac{k_\perp v_t}{\Omega} \, ,$$

(2.13)

where $v_t \equiv (T/m)^{1/2}$ is the root-mean-square electron velocity. This

choice of variables implicitly assumed $k_{\shortparallel} \neq 0$; in fact, in our numerical work, the angle of propagation is never greater than $45°$. Other variables, dependent on those already defined, which will be useful in the course of our work are

$$r \equiv k_{\perp}/k_{\shortparallel} , \qquad K \equiv k v_t /\Omega .$$

(2.14)

The dimensionless quantities we have defined in Eqs. (2.13-14) have definite physical meaning and are the natural ones to use. The quantity $\alpha \equiv k_D/k = (k\lambda_D)^{-1} = \omega_p/kv_t$ is the inverse of the parameter generally used in full particle simulations to characterize wavelengths. The quantity $u \equiv \omega/k_{\shortparallel}v_t = v_p/v_t$ is the normalized phase velocity, the velocity of the $n = 0$ resonance, and the quantity $\kappa_{\shortparallel}^{-1} \equiv (\Omega/k_{\shortparallel}v_t) = (v_s/v_t)$ is the normalized velocity separation between adjacent resonances. This situation is shown schematically in Fig. (2.1). The effect of increasing u, which is to move all the resonances farther out on the tail of the distribution function, and the effect of increasing $\kappa_{\shortparallel}$, which is to bunch all the resonances closer to the $n = 0$ resonance, are also shown. Finally, the quantity $r \equiv k_{\perp}/k_{\shortparallel}$ is the tangent of the angle of propagation with respect to the magnetic field.

Letting $u_c \equiv u + u_i$ be the normalized complex frequency, the linear dispersion relation, Eq. (2.12) becomes

$$\varepsilon = 1 - \alpha^2 \left[1 + \sum_{h=-\infty}^{\infty} \Lambda_h (K_{\perp}^2) \frac{u_c}{\sqrt{2}} Z \left(\frac{u_c}{\sqrt{2}} - \frac{n}{\sqrt{2} K_{\shortparallel}} \right) \right] = 0 ,$$

(2.15)

when expressed in terms of normalized variables. In the linear re-
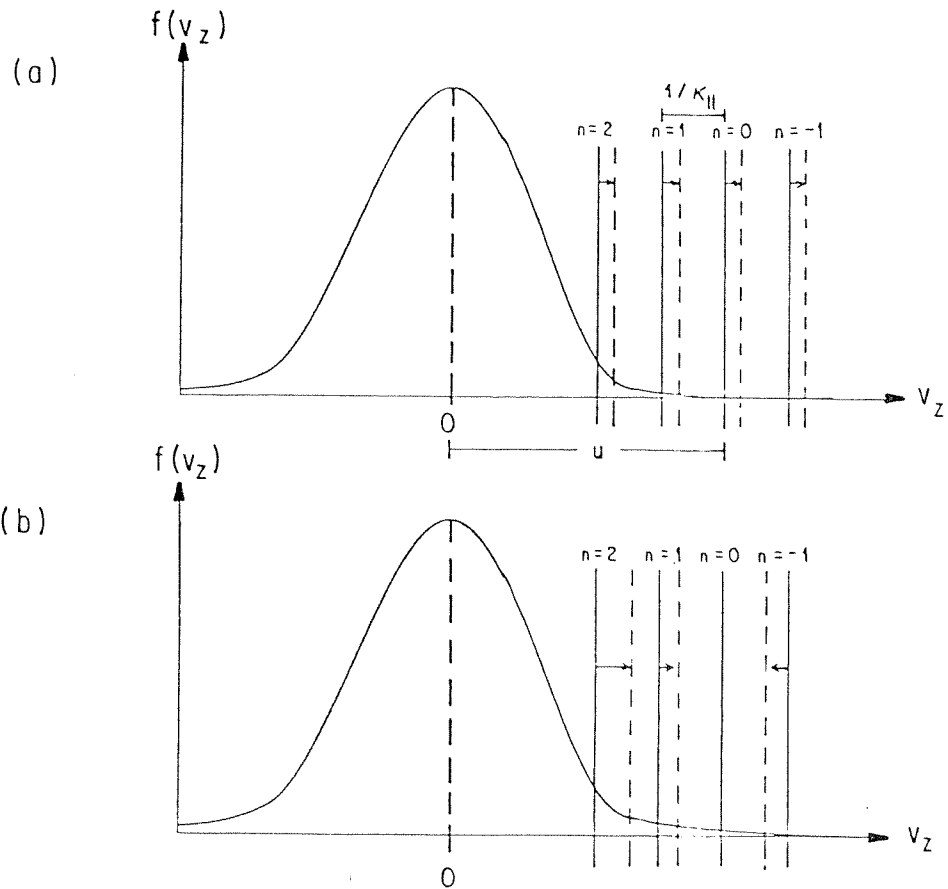
Fig. 2.1   Schematic illustration of the resonance structure.   (a) The effect of increasing u is shown by the arrows leading from the solid to dashed lines.   (b) The effect of increasing $\kappa_{\parallel}$ is similarly shown.

15

gime, this relation determines u in terms of α, $\kappa_{||}$, and $\kappa_{\perp}$, eliminating it as an independent parameter. In the non-linear regime as well, the linear dispersion relation determines u to good approximation, because the frequency is only slightly shifted from the linear value in the parameter regimes we will be considering. Whether the wave is linear or non-linear, the number of independent variables is reduced from five to four, and, in the linear regime, it is further reduced to three because ϕ is irrelevant to the wave evolution.

In order to reduce the possibility of non-linear wave generation as much as we can, we always consider the parameter regimes $\phi \lesssim 0.1$, which is the range where experiments on parallel-propagating waves have been done.[23] In order to be in a regime where resonances can overlap, we consider $\kappa_{||} \gtrsim 1.0$, which is the warm plasma limit. Finally, in order to be in a regime where non-linear effects are not overwhelmed by linear damping, we consider $\alpha \gtrsim 3.5$, which, in combination with our condition on $\kappa_{||}$ implies that $(\omega_p/\Omega) \gtrsim 3.5$, so that the wave is in the weakly magnetized limit.

In these limits, the asymptotic solution of the unmagnetized dispersion relation

$$\mathcal{E} = 1 - \frac{\alpha^2}{2} Z' \left(\frac{\kappa_{||}}{\kappa} \frac{u_c}{\sqrt{2}} \right) = 0 , \tag{2.16}$$

gives a good approximation to the real part of the frequency, although it does not represent the imaginary part very well. Using the asymptotic expansion of $Z'(x)$[43] in Eq. (2.16) yields in the weak damping case, $\gamma \ll u$, for the real part of Eq. (2.16)

$$\varepsilon_r = 1 - \alpha^2 \frac{K^2}{K_\parallel^2} \frac{1}{u^2} - 3\alpha^2 \frac{K^4}{K_\parallel^4} \frac{1}{u^4} = 0 \; . \tag{2.17}$$

To second order in α^{-1}, Eq. (2.17) is just the usual Bohm-Gross dispersion relation. Solving Eq. (2.17) to second order in α^{-1}, we find

$$u = \left(\alpha + \frac{3}{2\alpha} \right) \frac{K}{K_\parallel} \; . \tag{2.18}$$

Evaluating the quantity $\omega(\partial \varepsilon_r / \partial \omega) = u(\partial \varepsilon_r / \partial u)$, which is needed in Eq. (2.9) to solve for u_i, we find

$$u \frac{\partial \varepsilon_r}{\partial u} = 2 + \frac{6}{\alpha^2} \; . \tag{2.19}$$

In order to obtain a reasonably accurate solution for $u_i = -\gamma/k_\parallel v_t$, it is necessary to use Eq. (2.10) which contains the effects for all the resonances:

$$|u_i| = \sqrt{\frac{\pi}{2}} \, \alpha^2 u^2 \left(u \frac{\partial \varepsilon_r}{\partial u} \right)^{-1} \sum_{h=-\infty}^{\infty} \Lambda_h(K_\perp^2) \exp\left[-\tfrac{1}{2}\left(u - \tfrac{h}{K_\parallel} \right)^2 \right] , \tag{2.20}$$

where we have used Eq. (2.9) and the relation

$$\varepsilon_i = \sqrt{\frac{\pi}{2}} \, \alpha^2 u \sum_{h=-\infty}^{\infty} \Lambda_h(K_\perp^2) \exp\left[-\tfrac{1}{2}\left(u - \tfrac{h}{K_\parallel} \right)^2 \right] , \tag{2.21}$$

which may be obtained from Eq. (2.8).

2.3 Physical Origin of the Multiple Resonances

The multiple resonance structure which was discussed in the Introduction and is apparent in Eq. (2.6) and the subsequent equations can be understood physically using ideas very similar to those familiar from the case of single electrostatic wave in an unmagnetized plasma.[44]

The wave which we are considering is a normal mode of the infin-
ite, homogeneous plasma, and its time variation in the laboratory frame
is sinusoidal. An electron moving rectilinearly with respect to the
laboratory frame, as in an unmagnetized plasma, "sees" a potential whose
variation is also sinusoidal. However, an electron moving on a spiral
path, as is the case in a magnetized plasma experiences a potential of
the form

$$\Phi(\underset{\sim}{x},t) = \Phi \cos\left(k_{\parallel} z + k_{\perp} y + k_{\perp}\rho \sin\theta - \omega t\right), \tag{2.22}$$

where Y is the y-coordinate of the gyrocenter, $\rho \equiv v_{\perp}/\Omega$ is the gyro-
radius, and θ is the gyroangle. Along the spiral path of the electron's
unperturbed motion, $\theta = \theta_0 + \Omega t$ and $z = z_0 + v_z t$. Hence Eq. (22) be-
comes

$$\Phi(t) = \Phi \cos\left[k_{\parallel} z_0 + k_{\parallel} v_z t + k_{\perp}\rho \sin(\theta_0 + \Omega t) - \omega t\right]. \tag{2.23}$$

This potential and the associated electric field have a nonsinu-
soidal dependence on time, and a Fourier decomposition yields

$$\Phi(t) = \sum_{n=-\infty}^{\infty} \Phi J_n(k_{\perp}\rho) \sin\left(k_{\parallel} v_z t + n\Omega t - \omega t + \xi_n\right), \tag{2.24}$$

where $\xi_n \equiv k_{\parallel} z_0 + k_{\perp} Y + n\theta_0$ is a constant phase. Thus, an electron sees
a field composed of many "partial waves" whose amplitudes depend on the
electron's velocity. As a result, the electron will be resonant with
the nth particle wave when $v_z = (\omega - n\Omega)/k_{\parallel}$, and can gain or lose energy
depending on its phase. The partial waves are not real waves and cannot

separately gain or lose energy; only the wave as a whole can do so. Nonetheless, electrons can be trapped in the individual partial waves, and, when the partial waves overlap, electrons move stochastically.

The physical picture of oblique wave damping is that electrons interact strongly with any of the partial waves with which they are resonant, taking energy from, or giving energy to, the wave as a whole. If there are more electrons that take energy than give energy, the wave damps, just as in the usual physical picture of Landau damping.[45]

2.4 Solution of the Dispersion Relation

In the nonlinear regimes, the quantities u and $u(\partial\epsilon_r/\partial u)$ play an important role, similar to the role they play in determining u_i in Eq. (2.20). Hence, it is important to accurately relate these quantities to α, $\kappa_{||}$, and r. Obvious candidates for doing so are the asymptotic relations, Eq. (2.18) and (2.19). To compare Eq. (2.18) to the solution of the complete dispersion relation, Eq. (2.15), we used a root-finding technique described by McCune,[45] which yields the complex root u_c as a function of α, $\kappa_{||}$, and r. The quantity $u_c(\partial\epsilon/\partial u_c)$ was then evaluated at the root.

Fig. 2.2 shows that in the ranges of interest for the non-linear theory, $\alpha > 3.5$ when $r = 0.0$, $\alpha > 4.0$ when $r = 0.25$, and $\alpha > 4.5$ when $r = 0.5$, the asymptotic approximation for u is quite good, deviating by less than 2%. By contrast Fig. 2.3 shows that the asymptotic relation, Eq. (2.19) is not very good, deviating by more than 10% in some cases of interest. In our numerical work, we therefore used the exact
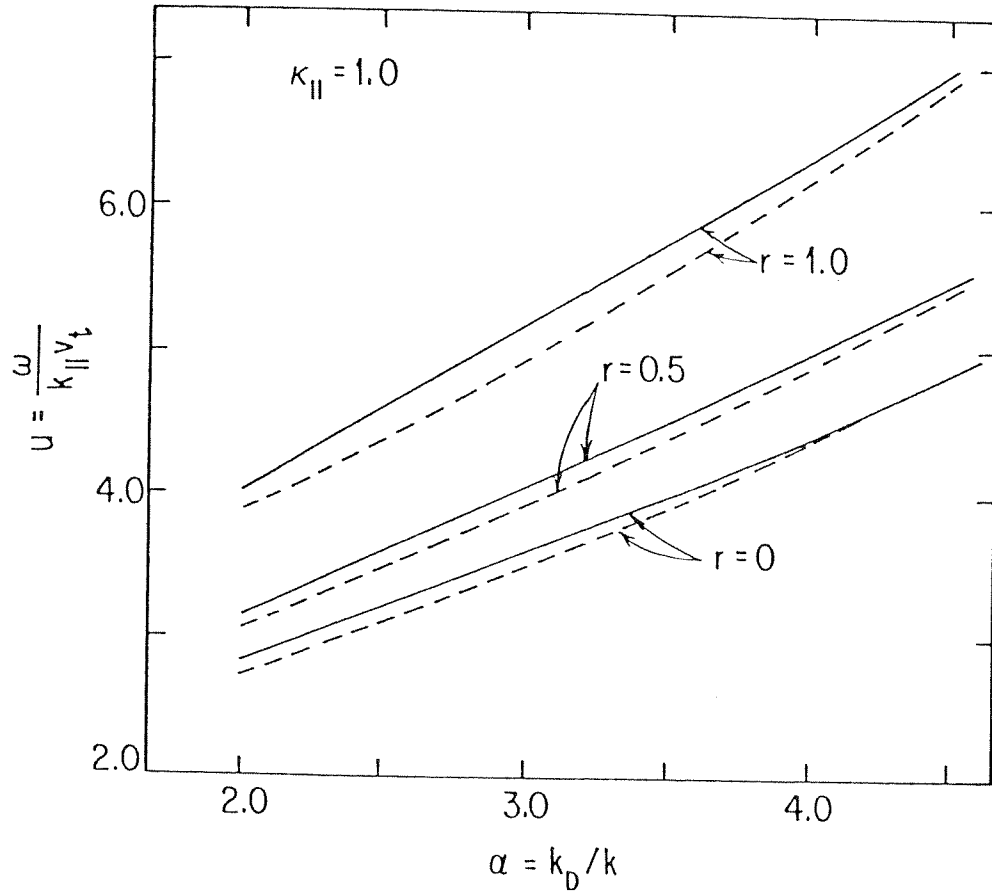
Fig. 2.2 Variation of the phase velocity $u = \omega/k_\parallel v_t$ with $\alpha = k_D/k$. Solid lines indicate solutions of the complete dispersion relation Eq. (2.15). Dashed lines indicate solutions of the asymptotic relation Eq. (2.18).
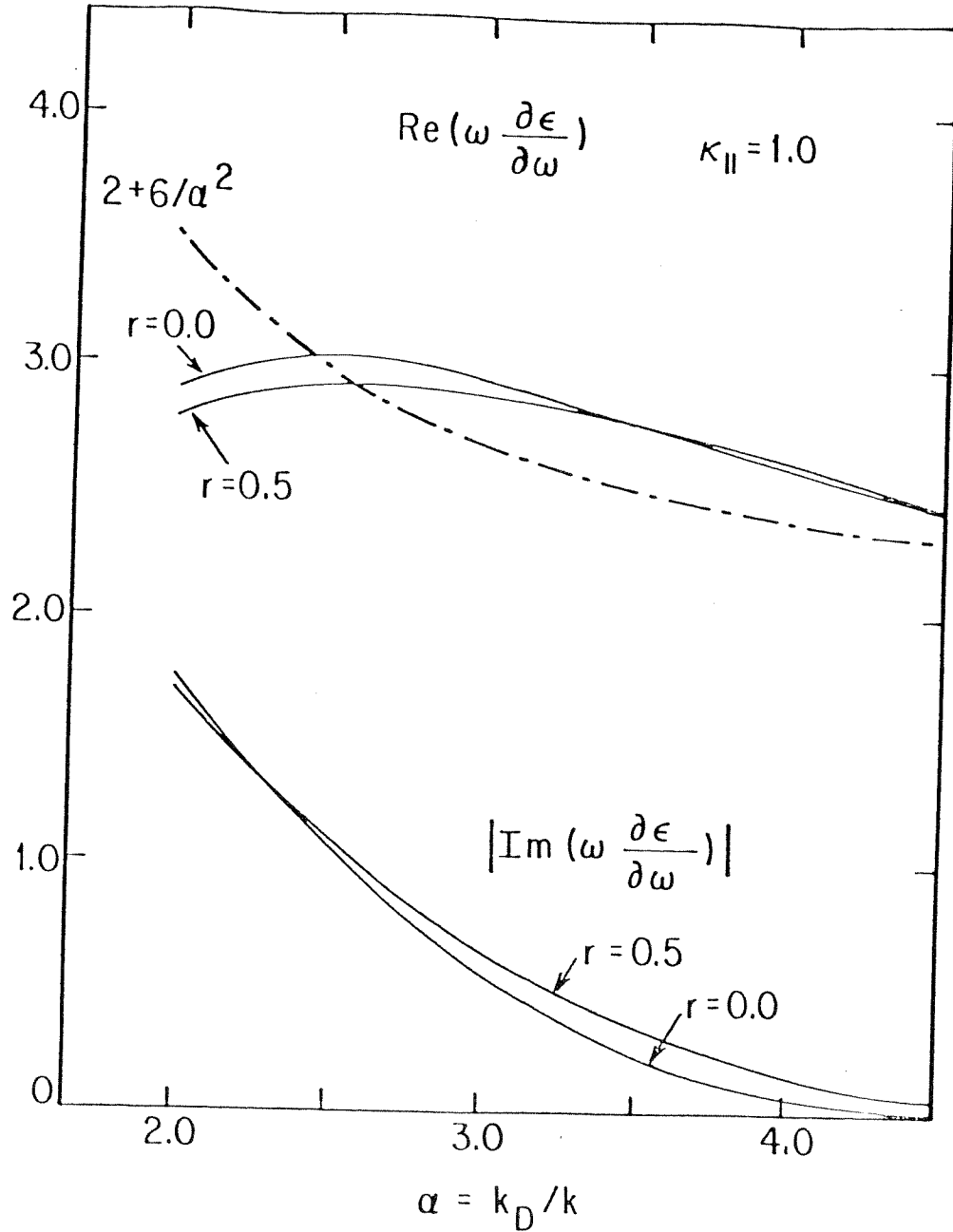
Fig. 2.3 Variation of $u_c(\partial\epsilon/\partial u_c)$ with α. Solid lines indicate solutions determined from Eq. (2.15). The dash-dot line indicates the asymptotic relation, Eq. (2.19).

values of $u(\partial \varepsilon_r / \partial u)$ obtained from Eq. (2.15).

Eq. (2.18) and Eq. (2.19) may be substituted into Eq. (2.20) to determine u_i and the results compared to those obtained from Eq. (2.15). This comparison is shown in Fig. 2.4 which displays $|u_i|$ in a semi-log plot as a function of α. The large deviations, up to 30% in the range of interest, are almost entirely due to small deviations in u, which are magnified by the appearance of u in the exponentials of Eq. (2.20), and the deviations of $u(\partial \varepsilon_r / \partial u)$. If $|u_i|$ is plotted as a function of u rather than α, and the exact values of $u(\partial \varepsilon_r / \partial u)$ are used, the deviations are reduced to less than 4%.

It is of interest to examine the fractional contribution of the nth resonance to the damping, i.e. the quantity

$$\frac{\gamma_n}{\gamma} = \frac{\Lambda_n(\kappa_\perp^2) \, \exp\left[-\frac{1}{2}\left(u - \frac{n}{\kappa_{||}}\right)^2\right]}{\sum_{\ell=-\infty}^{\infty} \Lambda_\ell(\kappa_\perp^2) \, \exp\left[-\frac{1}{2}\left(u - \frac{\ell}{\kappa_{||}}\right)^2\right]} \tag{2.25}$$

shown in Fig. 2.5, where Eq. (2.18) is used to calculate u as a function α. As α increases, and with it the phase velocity u, resonances at higher values of n become increasingly important.

The damping per cycle, γ/ω, is shown in Fig. 2.6 as a function of α. As α increases, the phase velocity u increases without affecting the separation between the resonances which is fixed by $\kappa_{||}$. Thus, all of the resonant velocities increase, sharply reducing the number of resonant electrons and, with them, the damping. The fall-off with increasing α becomes less rapid when r is increased because the fractional contributions of the high-n resonances, which are proportional to $\Lambda_n(\kappa_\perp^2)$, increase.
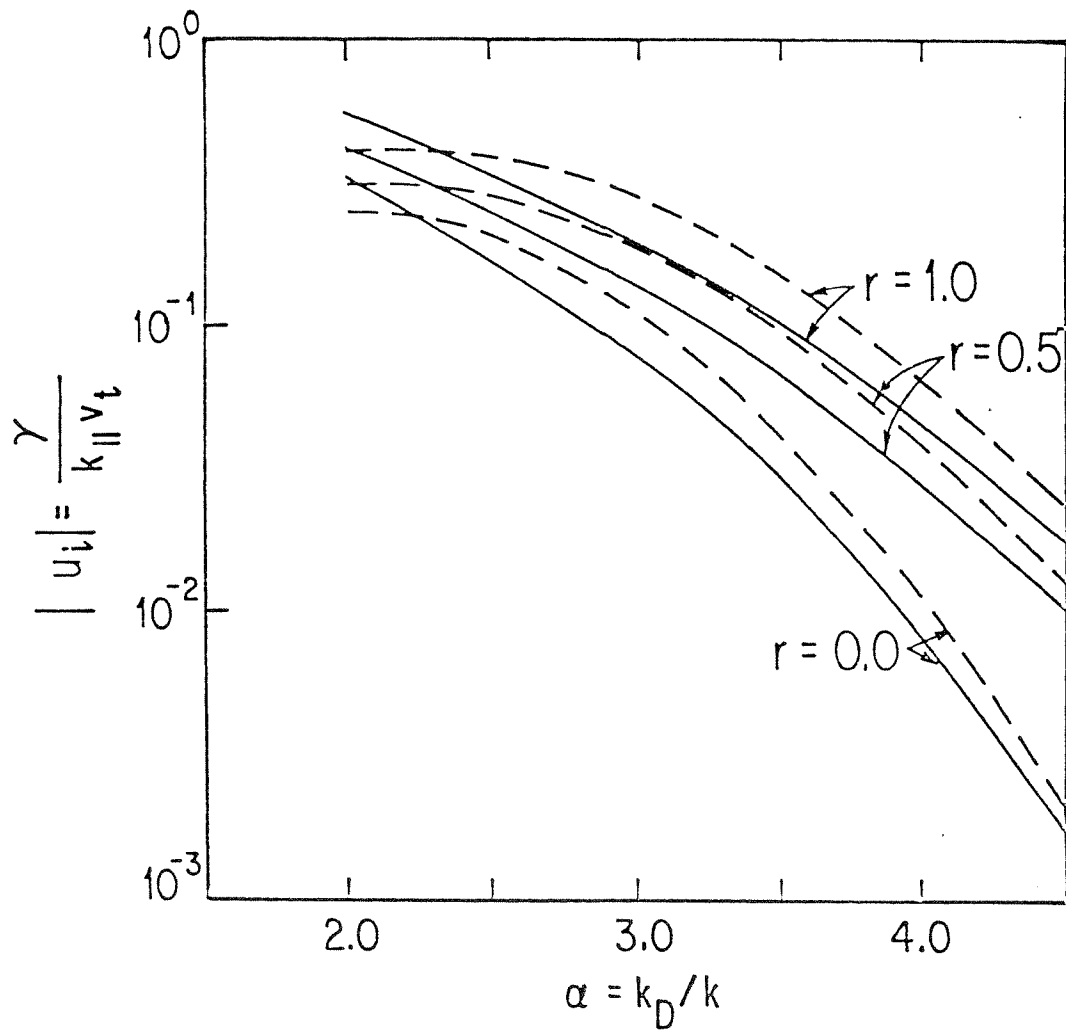
Fig. 2.4 Variation of u_i with α. Solid lines indicate solutions of the complete dispersion relation. Dashed lines indicate solutions of the asymptotic relation.
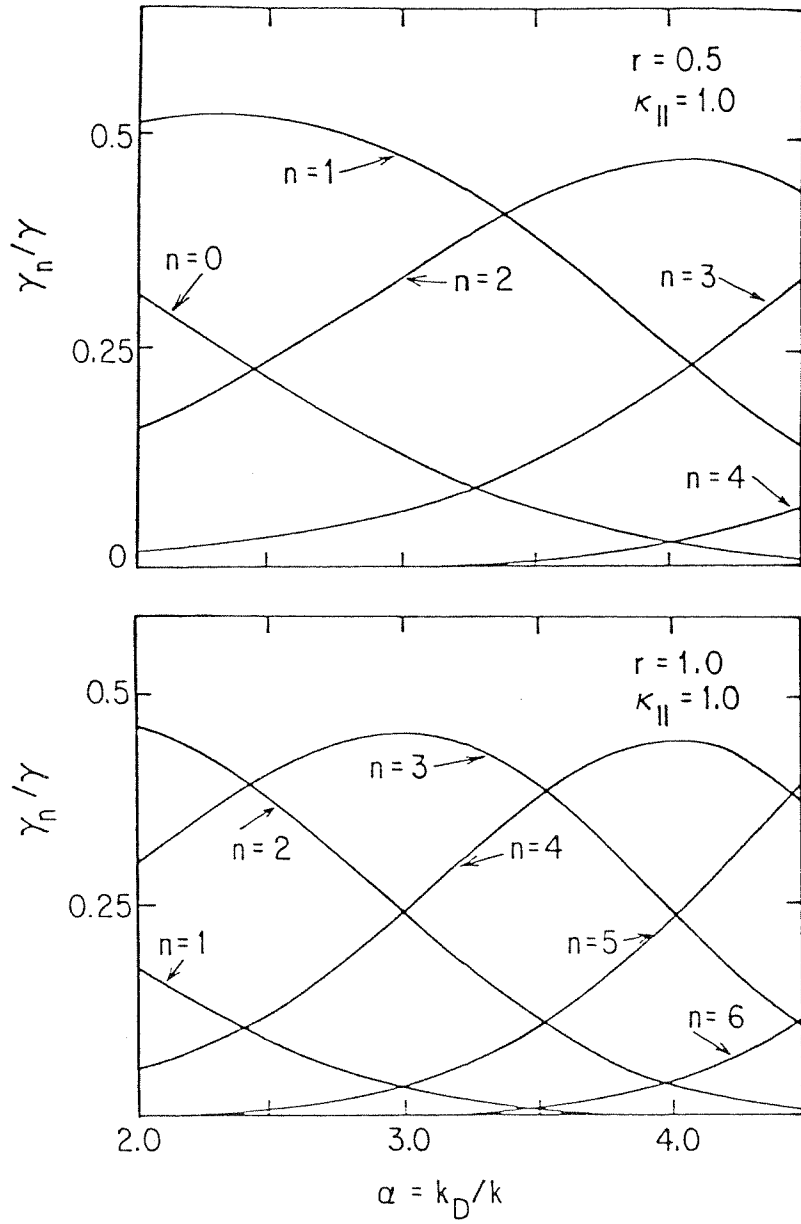
Fig. 2.5   Fractional contribution of individual resonances to γ as a function of α.
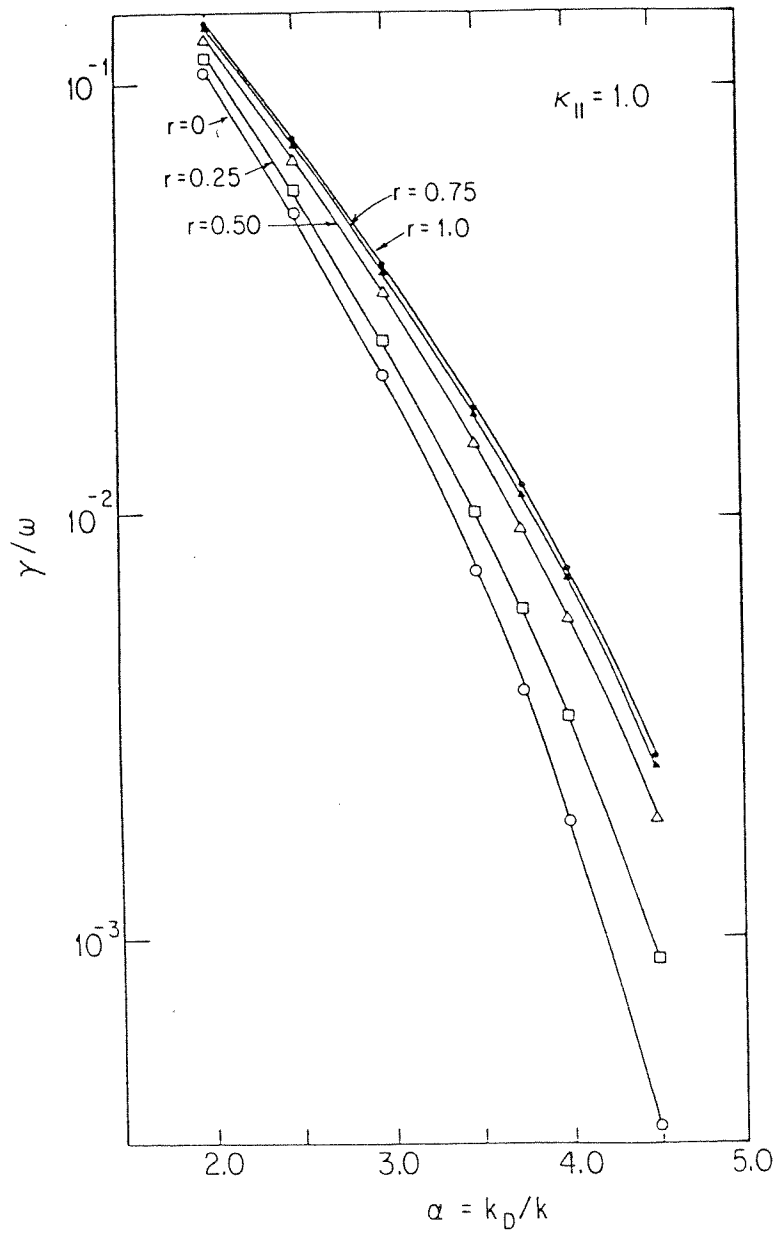
Fig. 2.6 Variation of γ/ω with α for various values of $r \equiv k_\perp/k_{||}$.

The solution to the complete dispersion relation, Eq. (2.15), is shown in Fig. 2.7 as a function of $\kappa_{\parallel}$. Since increasing $\kappa_{\parallel}$ while keeping α and r fixed is equivalent to reducing the magnetic field, the dispersion relation eventually approaches the unmagnetized limit where u and u_i are independent of $\kappa_{\parallel}$ for given r and α. The real part of the frequency u deviates only slightly from the $\Omega = 0$ ($\kappa_{\parallel} = \infty$) limiting value in the entire range $\kappa_{\parallel} \geq 1.0$, justifying the use of the unmagnetized limit approximation. The imaginary part of the frequency u_i deviates significantly from the $\Omega = 0$ ($\kappa_{\parallel} = \infty$) limiting value until $\kappa_{\parallel} \geq 2.0$. Two competing effects are at work here. Since $\kappa_{\perp}$ increases with $\kappa_{\parallel}$ for fixed r, the higher-n resonances, whose contributions are proportional to $\Lambda_n(\kappa_{\perp}^2)$, make a more important contribution to the overall damping rate as shown in Fig. 2.8. At the same time, recalling that $v_n = (\omega - n\Omega)/k_{\parallel}$, the resonances with n > 0 increase in velocity, so that they "bite" less deeply into the distribution and affect fewer electrons. For $\kappa_{\parallel} \gtrsim 2.0$, the latter effect dominates over the former, and the damping increases with $\kappa_{\parallel}$. However, at larger values of $\kappa_{\parallel}$, these two effects exactly cancel each other, and the damping is independent of $\kappa_{\parallel}$, consistent with Eq. (2.16).
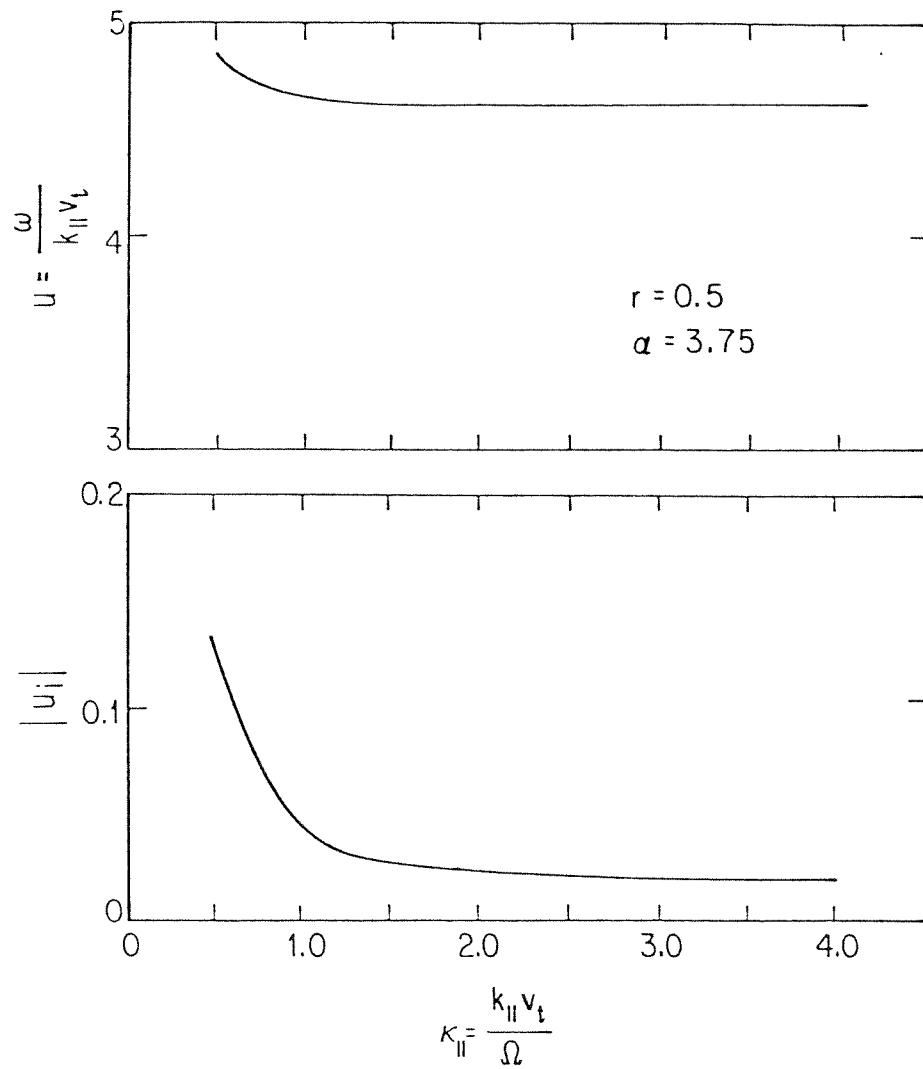
Fig. 2.7 Variation of u and u_i with $\kappa_{\parallel} = k_{\parallel}v_t/\Omega$. As $\kappa_{\parallel}$ increases, the functions approach their unmagnetized limits.
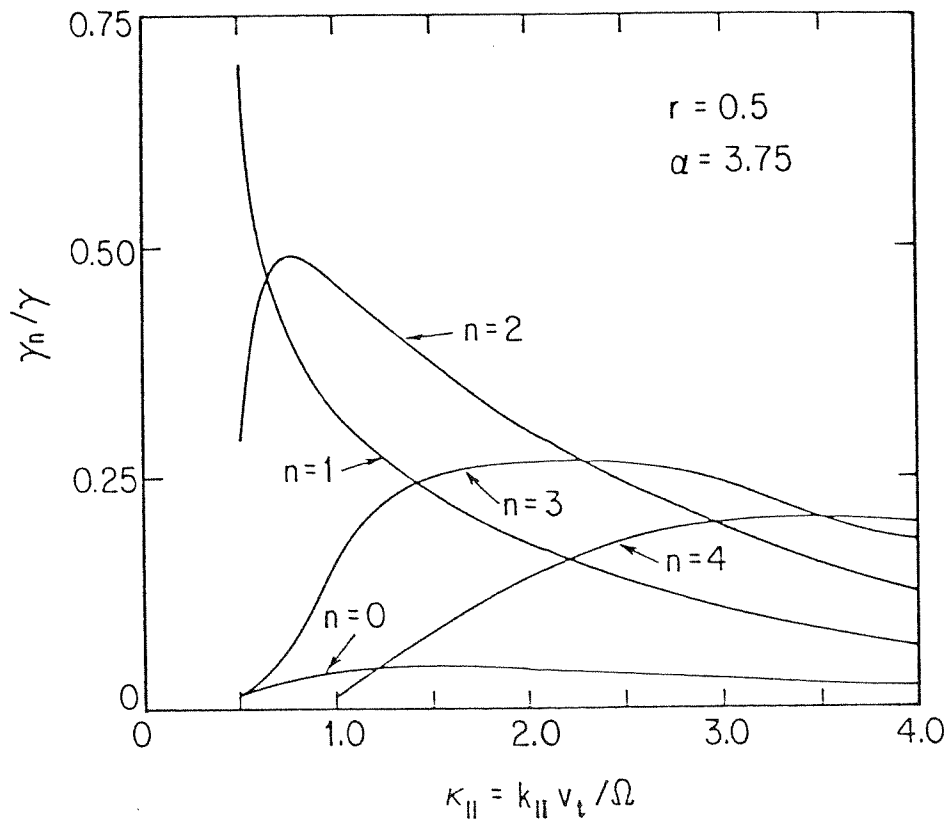
Fig. 2.8   Fractional contribution of the individual resonances to γ as a function of $\kappa_{\parallel}$.

3. TRAPPING REGIME

3.1 Historical Overview and Discussion

The non-linear evolution of a Langmuir wave in an unmagnetized plasma was first treated by O'Neil[26] and independently by Mazitov.[25] The amplitude oscillations predicted by O'Neil were observed experimentally by Malmberg and Wharton[23] and in particle simulations by Matsuda and Crawford,[35] who used a quiet start technique and periodic smoothing to avoid the need for many particles. Tsai[33] used a mini-simulation for the spatial problem, following the resonant electrons numerically and using linear theory for the background.

Since O'Neil's work, the theory has been extended in two ways. First, since O'Neil solved for the electron orbits holding the electric field constant, his theory is strictly valid only in the limit $\gamma \ll \omega_b$. Various authors[30] have shown that even when the electron orbits are treated exactly, O'Neil's results are essentially correct in almost the whole range $\gamma < \omega_b$, but the time between the amplitude oscillation maxima increases somewhat relative to O'Neil's prediction as γ/ω_b, increases. Second, O'Neil approximates the distribution function as a linear function of v near $v = v_p$. Morales and O'Neil,[28] by keeping the quadratic terms in $(v - v_p)$, obtained the non-linear frequency shift in the frequency as well as the damping rate. This shift has been seen both experimentally[32] and in simulations.[33, 35]

In this chapter, we extend the theories of O'Neil[26] and Morales and O'Neil[28] to magnetized plasmas in the regime where $\gamma < \omega_b < \Omega$. We

find that because the different resonances have different bounce fre-
quencies, the amplitude oscillations of the wave undergo a "super-phase-
mixing", disappearing at angles greater than about 14°.

3.2 Review of the Single Particle Motion

We consider a Langmuir wave with the potential given by

$$\Phi(\underset{\sim}{x}, t) = \Phi \cos(k_{\shortparallel} z + k_{\perp} y - \omega_o t),$$

(3.1)

where Φ is the potential amplitude. The equations of motion in this
wave are

$$\dot{\underset{\sim}{x}} = \underset{\sim}{v},$$

(3.2)

$$\dot{\underset{\sim}{v}} = -e \frac{\underset{\sim}{v} \times \underset{\sim}{B_o}}{c} - \frac{e\Phi}{m}(k_{\shortparallel} \underset{\sim}{e}_z + k_{\perp} \underset{\sim}{e}_y) \sin(k_{\shortparallel} z + k_{\perp} y - \omega_o t).$$

It is useful to transform from Cartesian coordinates to the six variables
z and p_z, θ and μ, the gyro-angle and lowest order adiabatic moment, and
X and Y, the guiding center coordinates. In terms of x, y, v_x, and v_y,
the precise definitions of θ, μ, X, and Y are

$$\theta \equiv \tan^{-1}(-v_x/v_y),$$

$$\mu \equiv \frac{m}{2\Omega}(v_x^2 + v_y^2) = \frac{m v_{\perp}^2}{2\Omega},$$

(3.3)

$$X \equiv x - \rho \cos\theta,$$

$$Y \equiv y - \rho \sin\theta ,$$

where $\rho \equiv (2\mu/m\Omega)^{1/2} = v_\perp/\Omega$. In these variables, the equations of motion become

$$\dot{z} = p_z/m ,$$

$$\dot{p}_z = -ek_\parallel \Phi \sin\left[k_\parallel z + k_\perp (Y + \rho \sin\theta) - \omega_0 t\right] ,$$

$$\dot{\theta} = \Omega + \frac{ek_\perp \rho}{2\mu} \Phi \sin\theta \, \sin\left[k_\parallel z + k_\perp (Y + \rho \sin\theta) - \omega_0 t\right] ,$$

(3.4)

$$\dot{\mu} = -ek_\perp \rho \Phi \cos\theta \, \sin\left[k_\parallel z + k_\perp (Y + \rho \sin\theta) - \omega_0 t\right] ,$$

$$\dot{X} = k_\perp \dot{p}_z / k_\parallel m \Omega ,$$

$$\dot{Y} = 0 .$$

The change in X, which is due to the $\underset{\sim}{E} \times \underset{\sim}{B}$ drift, is determined exactly from p_z, so X is a redundant variable. Eliminating Y and $\omega_0 t$ by re-defining z and p_z, $z \to z - (k_\perp/k_\parallel)Y + (1/k_\parallel)\omega_0 t$, $p_z \to p_z + (m/k_\parallel)\omega_0$, the equations of motion become

$$\dot{z} = p_z/m ,$$

$$\dot{p}_z = -ek_\parallel \Phi \sin\left(k_\parallel z + k_\perp \rho \sin\theta\right) ,$$

(3.5)

$$\dot{\theta} = \Omega + \frac{e k_\perp \rho}{2 \mu} \Phi \sin\theta \, \sin(k_{\shortparallel} z + k_\perp \rho \sin\theta),$$

$$\dot{\mu} = -e k_\perp \rho \, \Phi \cos\theta \, \sin(k_{\shortparallel} z + k_\perp \rho \sin\theta).$$

Eq. (3.5) can be derived directly from the Hamiltonian of Smith and Kaufman[9]

$$H = \frac{p_z^2}{2m} + \mu \Omega - e \Phi \cos(k_{\shortparallel} z + k_\perp \rho \sin\theta), \tag{3.6}$$

in which p_z and μ are conjugate to z and θ, respectively.

Solving Eq. (3.5) yields the particle motion on a four-dimensional torus. A two-dimension, graphical representation of the solution can be obtained by plotting the phase point (z, p_z) whenever θ becomes equal to some constant θ_0, on a constant energy surface, $H(z, p_z, \theta, \mu) =$ constant. Alternatively, we can use the discrete Hamiltonian method to replace Eq. (3.5) with two discrete equations which describe the mapping on the surface-of-section $\theta = \theta_0$, $H =$ constant.[46] Using either method, one finds resonances in which there are trapped electrons, as shown in Fig. 3.1. Recalling that we have moved into the wave frame, these resonances occur when $p_z/m = -n\Omega/k_{\shortparallel}$.

In treating the wave evolution in this chapter, we hold the wave amplitude fixed when we calculate particle orbits; this approximation was also used by O'Neil[26] when he studied the evolution of a parallel-propagating wave. We further assume that the resonances are well-separated. These approximations are strictly valid only when $\gamma \ll \omega_b \ll \Omega$,
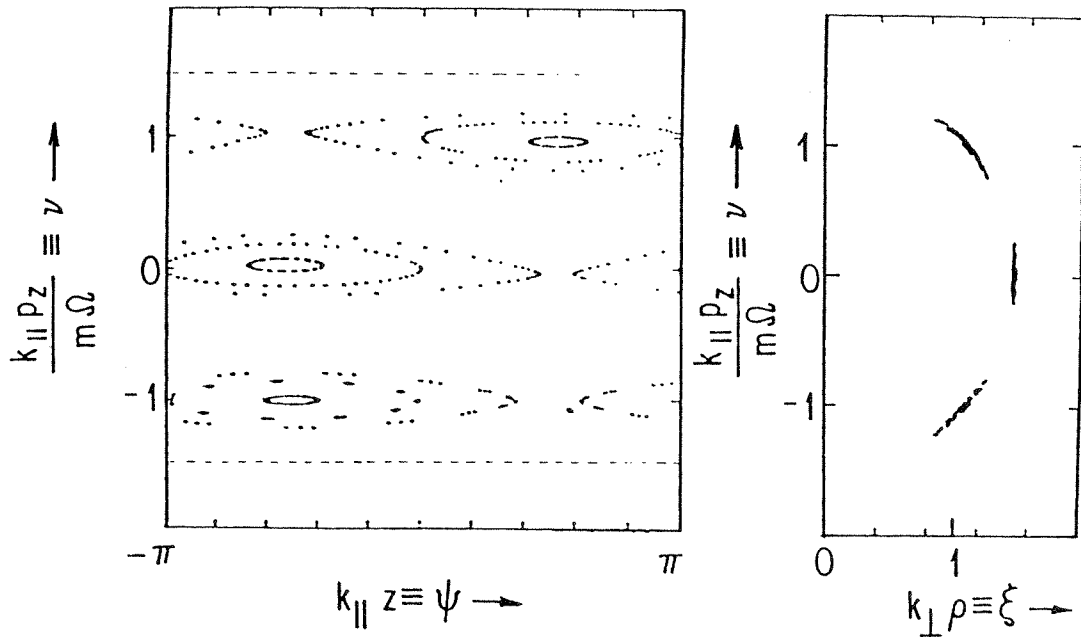
Fig. 3.1 Surface-of section plots of electron trajectories on the energy surface $\zeta_m \equiv (2H/T)^{1/2} = 1.44$. The plots shown here were made using the discrete Hamiltonian method.

but, from our experience with parallel-propagating waves[26] and single-particle orbits in obliquely propagating waves,[9] we conclude that they should be qualitatively valid over the whole range $\gamma < \omega_b < \Omega$. Referring to Eq. (3.5), and noting that $\mu \equiv m v_{\perp}^2 / 2\Omega \sim T/\Omega$, we see that $\dot{\theta} = \Omega[1 + 0(\phi)]$. Recalling that $\phi << 1$, we conclude that it is legitimate to neglect all but the lowest order variation in θ, so that we may approximate $\dot{\theta} = \Omega$. By contrast, we will retain the full, non-linear variation of z.

3.3 Theoretical Formulation

Writing the potential variation, Eq. (3.1) in the form

$$\Phi(\underset{\sim}{r}, t) \equiv \frac{\Phi}{2} \left\{ \exp\left[i(k_{\shortparallel} z + k_{\perp} y - \omega_0 t)\right] \right.$$
$$\left. + \exp\left[-i(k_{\shortparallel} z + k_{\perp} y - \omega_0 t)\right] \right\} , \tag{3.7}$$

we see that both the amplitude variation of $\Phi(r, t)$ and the nonlinear frequency shift can be accounted for by replacing $\omega_0 t$ with

$$\int_0^t \omega_c(t') \, dt' \quad ,$$

where $\omega_c(t')$ can be considering to be the complex frequency of the wave. The problem of determining the non-linear evolution of the wave is just the problem of determining $\omega_c(t')$. We shall make this determination subject to the assumption that the time scale for the non-linear evolution of the wave is slow compared to the wave period in the laboratory frame $2\pi/\omega_0$, where ω_0 is the solution of $\epsilon_r(\underset{\sim}{k}, \omega_0) = 0$, i.e., that $\delta\omega_c \equiv \omega_c - \omega_0$ is small compared to ω_0.

In this section, we will take advantage of the smallness of $\delta\omega_c$ to establish our basic equation using the subtraction procedure of Morales and O'Neil.[28] Letting $E_{\sim 0}$ be the wave amplitude and defining a phase difference

$$\eta(t) \equiv \int_0^t \delta\omega(t')\,dt, \qquad (3.8)$$

the electric field may be written quite generally in the form

$$\underset{\sim}{E}(\underset{\sim}{x},t) = \underset{\sim}{E}_{\underset{\sim}{k}}(t)\,\exp\left[i\left(\underset{\sim}{k}\cdot\underset{\sim}{x}-\omega_0 t\right)\right] \qquad (3.9)$$
$$+ \underset{\sim}{E}_{\underset{\sim}{k}}^{*}(t)\,\exp\left[-i\left(\underset{\sim}{k}\cdot\underset{\sim}{x}-\omega_0 t\right)\right],$$

where

$$\underset{\sim}{E}_{\underset{\sim}{k}}(t) = \frac{E_{\sim 0}}{2i}\,\exp\left[-i\eta(t)\right]. \qquad (3.10)$$

Poisson's equation may be written in the form

$$ik\,E_{\underset{\sim}{k}}(t) = 4\pi\rho_{\underset{\sim}{k}} = 4\pi\left(\rho_{\underset{\sim}{k}\ell} + \rho_{\underset{\sim}{k}n\ell}\right), \qquad (3.11)$$

where $\rho_{\underset{\sim}{k}\ell}$ is the linear charge response and $\rho_{\underset{\sim}{k}n\ell}$ is the non-linear charge response. These charge densities can be written as

$$\rho_{\underset{\sim}{k}} = -e\,n_0\int d^3v\,f_{\underset{\sim}{k}}\,,$$

$$\rho_{\underset{\sim}{k}\ell} = -e\,n_0\int d^3v\,f_{\underset{\sim}{k}\ell}\,, \qquad (3.12)$$

where

$$f_{\underset{\sim}{k}} = \int_0^{\lambda_\shortparallel} \frac{dz}{\lambda_\shortparallel} \int_0^{\lambda_\perp} \frac{dy}{\lambda_\perp} \; \exp\left[-i\left(k_\shortparallel z + k_\perp y - \omega_0 t\right)\right] f ,$$

$$\tag{3.13}$$

$$f_{\underset{\sim}{k}\ell} = \int_0^{\lambda_\shortparallel} \frac{dz}{\lambda_\shortparallel} \int_0^{\lambda_\perp} \frac{dy}{\lambda_\perp} \; \exp\left[-i\left(k_\shortparallel z + k_\perp y - \omega_0 t\right)\right] f_\ell ,$$

$\lambda_\shortparallel = 2\pi/k_\shortparallel$, $\lambda_\perp = 2\pi/k_\perp$, $f(\underset{\sim}{x}, \underset{\sim}{v}, t)$ is the full distribution function and $f_\ell(\underset{\sim}{x}, \underset{\sim}{v}, t,)$ is the linear response.

By definition, we have

$$\varepsilon\left(\underset{\sim}{k}, \omega\right) = 1 - \frac{4\pi e n_0}{ik E_{\underset{\sim}{k}}} \int d^3 v \; f_{\underset{\sim}{k}\ell} ,$$

$$\tag{3.14}$$

where $f_{k\ell}$ is the linear response to a wave of a given frequency. For real frequencies, $f_{k\ell}$ can be divided into two parts; f_{kr} which is 90° out of phase with E_k and is responsible for supporting the wave, and f_{ki}, which is in phase with E_k, and is responsible for the usual linear damping. We then have

$$\varepsilon_r\left(\underset{\sim}{k}, \omega\right) = 1 - \frac{4\pi e n_0}{ik E_{\underset{\sim}{k}}} \int d^3 v \; f_{\underset{\sim}{k}r} .$$

$$\tag{3.15}$$

The explicit long-time ($t = \infty$) form of f_{kr} and ε_r for an obliquely propagating wave is given by Eq. (2.8), and these quantities can be extended to complex frequencies by analytical continuation. Noting that near $\omega = \omega_0$, $\varepsilon_r(k, \omega) \simeq (\partial \varepsilon_r/\partial \omega)\delta\omega_c$, and combining Eq. (3.15) with Eq. (3.12), we conclude

$$ik\left(\frac{\partial \varepsilon_r}{\partial \omega}\right)\delta\omega_c \, E_{\underset{\sim}{k}} = -4\pi e n_0 \int d^3 v \left(f_{\underset{\sim}{k}} - f_{\underset{\sim}{k}r}\right).$$

$$\tag{3.16}$$

36

Eq. (3.16) forms the basis for the remaining analysis in this chapter. A more rigorous derivation of this equation using a method described by Landau and Lifshitz[47] is included in Appendix A.

Like Morales and O'Neil, we assume that the electrostatic field is constant when determining f_k and f_{kr}. In this case, $f_\ell(x, v, t)$ has the form

$$f_\ell(\underset{\sim}{x}, \underset{\sim}{v}, t) = f_r(\underset{\sim}{x}, \underset{\sim}{v}, t) + f_i(\underset{\sim}{x}, \underset{\sim}{v}, t), \tag{3.17}$$

where

$$f_r(\underset{\sim}{x}, \underset{\sim}{v}, t) = A(\underset{\sim}{v}, t) \cos(\underset{\sim}{k} \cdot \underset{\sim}{x} - \omega_0 t),$$

$$f_i(\underset{\sim}{x}, \underset{\sim}{v}, t) = B(\underset{\sim}{v}, t) \sin(\underset{\sim}{k} \cdot \underset{\sim}{x} - \omega_0 t). \tag{3.18}$$

The functions A and B are explicitly calculated later in this chapter. Given Eq. (3.18), it follows that

$$f_{\underset{\sim}{k} r} = \int_0^{\lambda_{\shortparallel}} \frac{dz}{\lambda_{\shortparallel}} \int_0^{\lambda_\perp} \frac{dy}{\lambda_\perp} \exp\left[-i\left(k_{\shortparallel} z + k_\perp y - \omega_0 t\right)\right] f_r(\underset{\sim}{x}, \underset{\sim}{v}, t). \tag{3.19}$$

3.4 Determination of the Complex Frequency Shift

In order to calculate the complex frequency shift from Eq. (3.16), we must first determine f_k and f_{kr} from the equations of motion, Eq. (3.5). To do so, we first recall that $f = f_0[v_0(x,v,t)]$, where f_0 is the initial distribution function and $v_0(x,v,t)$ is the initial velocity of an electron with coordinates (x, v) at time t. Assuming that the

excursions $\Delta \underset{\sim}{v} = \underset{\sim}{v}_0 - \underset{\sim}{v}$ are small, we may then expand $f - f_r$ in a Taylor series. In order to obtain the real part of the frequency shift, we must retain terms through second order, and we find

$$f - f_r = \frac{\partial f_0}{\partial \underset{\sim}{v}} \cdot (\Delta \underset{\sim}{v} - \Delta \underset{\sim}{v}_r) + \frac{1}{2} \frac{\partial^2 f_0}{\partial \underset{\sim}{v} \partial \underset{\sim}{v}} : \Delta \underset{\sim}{v} \Delta \underset{\sim}{v} \ . \tag{3.20}$$

No second order term in $\Delta \underset{\sim}{v}_r$ appears because it would be non-linear. We may calculate $\Delta \underset{\sim}{v}_r$ from the linear response $\Delta \underset{\sim}{v}_\ell$, by recalling that $\Delta \underset{\sim}{v}_\ell$ may be quite generally resolved into two places, $\Delta \underset{\sim}{v}_\ell = \Delta \underset{\sim}{v}_r + \Delta \underset{\sim}{v}_i$, where $\Delta \underset{\sim}{v}_r$ has the form $a(v,t) \cos[i(\underset{\sim}{k} \cdot \underset{\sim}{x} - \omega_0 t)]$ and $\Delta \underset{\sim}{v}_i$ has the form $b(v,t) \sin[i(\underset{\sim}{k} \cdot \underset{\sim}{x} - \omega_0 t)]$. Substituting Eq. (3.20) into Eq. (3.16), and using Eqs. (3.13) and (3.19), we find

$$i k \left(\frac{\partial \mathcal{E}_r}{\partial \omega}\right) \delta \omega_c \underset{\sim}{E}_k = -4\pi e n_0 \int_0^{\lambda_{\shortparallel}} \frac{dz}{\lambda_{\shortparallel}} \int_0^{\lambda_\perp} \frac{dy}{\lambda_\perp} \int d^3 v \ \exp\left[-i\left(k_{\shortparallel} z\right.\right.$$

$$\left.\left. + k_\perp y - \omega_0 t\right)\right] \left\{ \frac{\partial f_0}{\partial \underset{\sim}{v}} \cdot (\Delta \underset{\sim}{v} - \Delta \underset{\sim}{v}_r) + \frac{\partial^2 f_0}{\partial \underset{\sim}{v} \partial \underset{\sim}{v}} : \Delta \underset{\sim}{v} \Delta \underset{\sim}{v} \right\} \ . \tag{3.21}$$

Noting that $E_k = k\phi/2i$, where the factor $\exp[-i\eta(t)]$ is ignored, consistent to lowest order in $\delta \omega_c$, and changing to the coordinate system used to describe single-particle motion in Eq. (3.5), we can write Eq. (3.21) as

$$k^2 \left(\frac{\partial \mathcal{E}_r}{\partial \omega}\right) \frac{\delta \omega_c}{2} \phi = -4\pi e n_0 \int_0^{\lambda_{\shortparallel}} \frac{dz}{\lambda_{\shortparallel}} \int_0^{\lambda_\perp} \frac{d\Box}{\Box} \int d^3 v \ \exp\left[-i\left(k_{\shortparallel} z\right.\right.$$

$$\left.\left. + k_\perp \rho \sin\theta\right)\right] \left\{ \frac{\partial f_0}{\partial \underset{\sim}{v}} \cdot (\Delta \underset{\sim}{v} - \Delta \underset{\sim}{v}_r) + \frac{1}{2} \frac{\partial^2 f_0}{\partial \underset{\sim}{v} \partial \underset{\sim}{v}} : \Delta \underset{\sim}{v} \Delta \underset{\sim}{v} \right\} \ . \tag{3.22}$$

From studies of the single-particle behavior, we know that the motion is non-linear only in a region on the order of $\omega_b/k_{\shortparallel}$, surround-

ing the resonant velocities $v_z = -n\Omega/k_{\shortparallel}$. By hypothesis, $(\omega_b/k_{\shortparallel}) < < v_s \equiv \Omega/k_{\shortparallel}$, the separation between resonances, and it will be useful to take advantage of this fact to write Eq. (3.22) in the form

$$k^2 \left(\frac{\partial \varepsilon_r}{\partial \omega}\right) \frac{\delta \omega_c}{2} \Phi = -4\pi e n_0 \sum_{n=-\infty}^{\infty} \int_0^{\lambda_{\shortparallel}} \frac{dz}{\lambda_{\shortparallel}} \int_0^{2\pi} \frac{d\theta}{2\pi} \int 2\pi v_\perp \, dv_\perp \, dv_z$$

$$\sum_{\ell=-\infty}^{\infty} J_\ell (k_\perp \rho) \, \exp\left[-i(k_{\shortparallel} z + \ell\theta)\right] \left\{ \frac{\partial f_0}{\partial \underset{\sim}{v}} \cdot (\Delta \underset{\sim}{v}_n - \Delta \underset{\sim}{v}_{rn}) \right. \tag{3.23}$$

$$\left. + \frac{1}{2} \frac{\partial^2 f_0}{\partial \underset{\sim}{v} \partial \underset{\sim}{v}} : \Delta \underset{\sim}{v}_n \, \Delta \underset{\sim}{v}_n \right\} \quad ,$$

where $\Delta \underset{\sim}{v}_n$ is the deviation in the neighborhood of the nth resonance. In writing Eq. (3.23), we have also made use of the relation

$$\exp\left[-i(k_{\shortparallel} z + k_\perp \rho \sin\theta)\right] = \sum_{\ell=-\infty}^{\infty} J_\ell (k_\perp \rho) \, \exp\left[-i(k_{\shortparallel} z + \ell\theta)\right] \quad . \tag{3.24}$$

Expanding $\partial f_0/\partial \underset{\sim}{v}$ to second order about $v_z = v_n \equiv n\Omega/k_{\shortparallel}$,

$$\frac{\partial f_0}{\partial \underset{\sim}{v}} = \left(\frac{\partial f_0}{\partial \underset{\sim}{v}}\right)_{v_n} + \left(\frac{\partial^2 f_0}{\partial \underset{\sim}{v} \partial \underset{\sim}{v}}\right)_{v_n} \cdot (\underset{\sim}{v} - \underset{\sim}{v}_n) \quad , \tag{3.25}$$

we find

$$k^2 \left(\frac{\partial \varepsilon_r}{\partial \omega}\right) \frac{\delta \omega_c}{2} \Phi = -4\pi e n_0 \sum_{n=-\infty}^{\infty} \int_0^{\lambda_{\shortparallel}} \frac{dz}{\lambda_{\shortparallel}} \int_0^{2\pi} \frac{d\theta}{2\pi} \int 2\pi v_\perp \, dv_\perp \, dv_z$$

$$\sum_{\ell=-\infty}^{\infty} J_\ell (k_\perp \rho) \, \exp\left[-i(k_{\shortparallel} z + \ell\theta)\right] \left\{ \left(\frac{\partial f_0}{\partial \underset{\sim}{v}}\right)_{v_n} \cdot (\Delta \underset{\sim}{v}_n - \Delta \underset{\sim}{v}_{rn}) \right. \tag{3.26}$$

$$\left. + \frac{1}{2} \left(\frac{\partial^2 f_0}{\partial \underset{\sim}{v} \partial \underset{\sim}{v}}\right)_{v_n} : \left(2 \underset{\sim}{v} \, \Delta \underset{\sim}{v}_n + \Delta \underset{\sim}{v}_n \, \Delta \underset{\sim}{v}_n - 2 \underset{\sim}{v} \, \Delta \underset{\sim}{v}_{rn}\right) \right\} \quad .$$

We now determine $\Delta \underset{\sim}{v}_n$ from the electron's equations of motion, Eq. (3.5). Using the definitions $p_z \equiv mv_z$ and $\mu \equiv mv_\perp^2/2\Omega$, it is convenient to re-write the equations for $\dot{p}_z$ and $\dot{\mu}$ in the form

$$\dot{v}_z = -e \frac{k_\parallel \Phi}{m} \sin \left(k_\parallel z + k_\perp \rho \sin \theta \right),$$

$$\dot{v}_\perp = -e \frac{k_\parallel \Phi}{m} \cos \theta \, \sin \left(k_\parallel z + k_\perp \rho \sin \theta \right) . \tag{3.27}$$

The procedure we use in solving Eq. (3.27) is to first integrate along the unperturbed orbits for one cyclotron period, taking advantage of the relation $\omega_b \ll \Omega$ to ignore the change in v_z over one cyclotron period. Averaging these integrated equations over the cyclotron orbit, we obtain coarse-grained equations of motion which may be explicitly solved. Eq. (3.27), when integrated over the unperturbed orbits, has the form

$$\delta v_z = -\frac{e \, k_\parallel \Phi}{m} \int_0^{\frac{2\pi}{\Omega}} \sin \left[k_\parallel z_0 + k_\parallel v_z t + k_\perp \rho \sin \left(\theta_0 + \Omega t\right)\right] dt,$$

$$\delta v_\perp = -\frac{e \, k_\parallel \Phi}{m} \int_0^{\frac{2\pi}{\Omega}} \cos \left(\theta_0 + \Omega t\right) \sin \left[k_\parallel z_0 + k_\parallel v_z t + k_\perp \rho \sin \left(\theta_0 + \Omega t\right)\right] dt . \tag{3.28}$$

Dropping the "0" subscripts and substituting the relation

$$\sin \left[k_\parallel z + k_\parallel v_z t + k_\perp \rho \sin \left(\theta + \Omega t\right)\right]$$

$$= \sum_{h=-\infty}^{\infty} J_h \left(k_\perp \rho\right) \sin \left(k_\parallel z + k_\parallel v_z t + h\theta + h\Omega t\right) , \tag{3.29}$$

we find near the nth resonance ($k_\parallel v_z + n\Omega = 0$), that these integrals

become

$$\dot{v}_z = \frac{\delta v_z}{\delta t} = -\frac{e k_{\shortparallel} \Phi}{m} \, J_n(k_{\perp}\rho) \, \sin(k_{\shortparallel} z + n\theta),$$

(3.30)

$$\dot{v}_{\perp} = \frac{\delta v_{\perp}}{\delta t} = -\frac{e n \Omega \, \Phi}{m \, v_{\perp}} \, J_n(k_{\perp}\rho) \, \sin(k_{\shortparallel} z + n\theta),$$

where $\delta t = 2\pi/\Omega$. In order to solve these coarse-grained equations of motion, we must first eliminate the θ-dependence, which we do by letting $z \to z-(n/k_{\shortparallel})\theta$. Then, Eq. (3.30) becomes

$$\dot{v}_z = -\frac{e k_{\shortparallel} \Phi}{m} \, J_n(k_{\perp}\rho) \, \sin(k_{\shortparallel} z),$$

(3.31.a)

$$\dot{v}_{\perp} = \frac{n \Omega}{k_{\shortparallel} v_{\perp}} \, \dot{v}_z \quad .$$

(3.31.b)

To be consistent, we must substitute the same change of variables into Eq. (3.26). Doing so and integrating over θ, we find

$$k^2 \left(\frac{\partial \varepsilon_r}{\partial \omega}\right) \frac{\delta \omega_c}{2} \, \Phi = -4\pi e n_0 \sum_{n=-\infty}^{\infty} \int_0^{\lambda_{\shortparallel}} \frac{dz}{\lambda_{\shortparallel}} \int 2\pi v_{\perp} \, dv_{\perp} \, dv_z$$

$$\exp(-i k_{\shortparallel} z) \, J_n(k_{\perp}\rho) \left\{ \left(\frac{\partial f_0}{\partial \underset{\sim}{v}}\right)_{\underset{\sim}{v}_n} \cdot (\Delta \underset{\sim}{v}_n - \Delta \underset{\sim}{v}_{rn}) \right.$$

(3.32)

$$\left. + \frac{1}{2}\left(\frac{\partial^2 f_0}{\partial \underset{\sim}{v} \, \partial \underset{\sim}{v}}\right)_{\underset{\sim}{v}_n} : \left(2 \underset{\sim}{v} \, \Delta \underset{\sim}{v}_n + \Delta \underset{\sim}{v}_n \, \Delta \underset{\sim}{v}_n - 2 \underset{\sim}{v} \, \Delta \underset{\sim}{v}_{rn}\right) \right\} \quad .$$

If we ignore the variation of $J_n(k_{\perp}\rho)$ in Eq. (3.31), which is legitimate in the limit

41

$$\frac{d J_n(k_\perp \rho)}{d v_\perp} (\Delta v_\perp) << J_n(k_\perp \rho) , \tag{3.33}$$

where $\Delta v_\perp$ is the perpendicular resonance width, then Eq. (3.31.a) is just the standard pendulum equation, whose solution may be determined in the usual fashion. (See, e.g., the beginning of reference 20.)

To solve Eq. (3.31.a), we integrate once to obtain

$$\frac{1}{2} v_z^2 - \frac{e \Phi}{m} J_n(k_\perp \rho) \cos(k_\parallel z) = W . \tag{3.34}$$

Letting $\xi \equiv k_\parallel z/2$, this equation becomes

$$\dot{\xi} = \pm \frac{\omega_{bn}}{K} (1 - K \sin^2 \xi)^{1/2} , \tag{3.35}$$

where $\omega_{bn}^2 \equiv ek_\parallel^2 \Phi |J_n(k_\perp \rho)|/m$, and $K^2 \equiv \omega_{bn}^2/(k_\parallel^2 W/2m + \omega_{bn}^2/2.)$ When $K < 1$, the solution to Eq. (3.35) may be written[48]

$$u_0 = u \mp H_n(k_\perp \rho) \frac{\omega_{bn} t}{K} , \tag{3.36}$$

where $H_n(\kappa_\perp \rho) \equiv J_n(k_\perp \rho)/|J_n(k_\perp \rho)|$, $u \equiv F(K,\xi)$, and $u_0 \equiv F(K, \xi_0)$ is the initial value of u. As a result, we find $\sin(\xi) = sn(u)$, $\dot{\xi} = \pm(\omega_{bn}/K) dn(u)$, and letting $\hat{v}_z$ and $\hat{v}_\perp$ be unit vectors in the v_z and $v_\perp$ directions,

$$\Delta \underset{\sim}{v}_n = (\underset{\sim}{v}_0 - \underset{\sim}{v}) = \pm \frac{2}{k_\parallel} \frac{\omega_{bn}}{K} \left\{ dn \left[u \mp H_n(k_\perp \rho) \frac{\omega_{bn} t}{K} \right] \right.$$
$$\left. - dn(u) \right\} \hat{v} , \tag{3.37}$$

where $\hat{\underset{\sim}{v}} \equiv [\hat{\underset{\sim}{v}}_z + (n\Omega/k_\parallel v_\perp)\hat{\underset{\sim}{v}}_\perp]$. If $K \gtrsim 1$, it is useful to define a new quantity ξ' such that $K\sin(\xi) = \sin(\xi')$. The solution to Eq. (3.35) may then be written

$$w_0 = w \mp H_n(k_\perp\rho) \omega_{bn} t , \qquad (3.38)$$

where $w \equiv F(K^{-1},\xi')$ and $w_0 \equiv F(K^{-1},\xi_0')$. As a result, we find $\dot{\xi} = \pm(\omega_{bn}/K)cn(w)$, and

$$\Delta\underset{\sim}{v}_n = \pm\frac{2}{k_\parallel}\frac{\omega_{bn}}{K}\left\{cn\left[w \mp H_n(k_\perp\rho)\omega_{bn}t\right] - cn(w)\right\}\hat{\underset{\sim}{v}}. \qquad (3.39)$$

The quantity $\Delta\underset{\sim}{v}_{\ell n}$ is

$$\Delta\underset{\sim}{v}_{\ell n} = \frac{\omega_{bn}^2}{k_\parallel^2 v_z}\left\{\cos\left[k_\parallel z - H_n(k_\perp\rho)k_\parallel v_z t\right] - \cos(k_\parallel z)\right\}\hat{\underset{\sim}{v}}, \qquad (3.40)$$

so that $\Delta\underset{\sim}{v}_{rn}$ is

$$\Delta\underset{\sim}{v}_{rn} = -\frac{\omega_{bn}^2}{k_\parallel^2 v_z}\cos(k_\parallel z)\left[1 - \cos(k_\parallel v_z t)\right]\hat{\underset{\sim}{v}}. \qquad (3.41)$$

From Eqs. (3.37). (3.39), and (3.41), we see that $\Delta\underset{\sim}{v}_n$ and $\Delta\underset{\sim}{v}_{nr}$ are anti-symmetric with respect to the exchange $(\underset{\sim}{v},\underset{\sim}{z}) \to (-\underset{\sim}{v},-\underset{\sim}{z})$; whereas, the quadratic terms $2\underset{\sim}{v}\Delta\underset{\sim}{v}_n$, $\Delta\underset{\sim}{v}_n\Delta\underset{\sim}{v}_n$, and $2\underset{\sim}{v}\Delta\underset{\sim}{v}_{nr}$ are symmetric. Noting that $\delta\omega_c = \delta\omega - i\gamma$, where $\delta\omega$ is the real frequency shift and γ is the damping, we may take advantage of these symmetries to split Eq. (3.32) into its real and imaginary parts as follows

43

$$k^2 \left(\frac{\partial \varepsilon_r}{\partial \omega} \right) \frac{\delta \gamma}{2} \Phi = -4\pi e n_0 \sum_{h=-\infty}^{\infty} \int_0^{\lambda_{\shortparallel}} \frac{dz}{\lambda_{\shortparallel}} \int 2\pi v_\perp \, dv_\perp \, dv_z$$

$$\sin(k_{\shortparallel} z) \; J_n(k_\perp \rho) \; \left(\frac{\partial f_0}{\partial \underset{\sim}{v}} \right)_{\underset{\sim}{v}_h} \cdot \Delta \underset{\sim}{v}_h \; , \tag{3.42.a}$$

$$k^2 \left(\frac{\partial \varepsilon_r}{\partial \omega} \right) \delta\omega \, \Phi = -4\pi e n_0 \sum_{h=-\infty}^{\infty} \int_0^{\lambda_{\shortparallel}} \frac{dz}{\lambda_{\shortparallel}} \int 2\pi v_\perp \, dv_\perp \, dv_z \; \cos(k_{\shortparallel} z)$$

$$J_n(k_\perp \rho) \; \left(\frac{\partial^2 f_0}{\partial \underset{\sim}{v} \, \partial \underset{\sim}{v}} \right)_{\underset{\sim}{v}_h} : \left(2 \underset{\sim}{v} \, \Delta \underset{\sim}{v}_h + \Delta \underset{\sim}{v}_h \, \Delta \underset{\sim}{v}_h - 2 \underset{\sim}{v} \, \Delta \underset{\sim}{v}_h \right) . \tag{3.42.b}$$

Because $\Delta \underset{\sim}{v}_{rn}$ has no component proportional to $\sin(k_{\shortparallel} z)$, it disappears completely from Eq. (3.42.a).

We now determine γ from Eq. (3.42.a). Transforming variables from (z, v_z) to (ξ, K) for $K < 1$ and to (ξ', K) for $K > 1$, we find

$$\sin(k_{\shortparallel} z) \, dv_z \, \frac{dz}{\lambda_{\shortparallel}} = \begin{cases} \dfrac{4}{k_{\shortparallel}} \dfrac{\omega_{bn}}{K^2} \dfrac{\sin\xi \cos\xi}{(1 - K^2 \sin^2\xi)^{1/2}} \, dK \, \dfrac{d\xi}{\pi} \; ; \quad K < 1 \\[2em] \dfrac{4}{k_{\shortparallel}} \dfrac{\omega_{bn}}{K^4} \sin\xi' \, dK \, \dfrac{d\xi'}{\pi} \; ; \quad K > 1 \end{cases} \tag{3.43}$$

Using Eqs. (3.37) and (3.39), and taking advantage of the antisymmetry of $\Delta \underset{\sim}{v}_n$, we find

$$k^2 \left(\frac{\partial \varepsilon_r}{\partial \omega} \right) \gamma \, \Phi = -4\pi e n_0 \sum_{h=-\infty}^{\infty} \int 2\pi v_\perp \, dv_\perp \; J_n(k_\perp \rho)$$

$$\left\{ \int_0^1 \frac{dK}{K^3} \int_0^{\frac{\pi}{2}} d\xi \, \frac{64}{\pi} \, \frac{\omega_{bn}^2}{k_{\shortparallel}^2} \, \frac{\sin\xi \cos\xi}{(1 - K^2 \sin^2\xi)^{1/2}} \; \frac{H_n(k_\perp \rho)}{2} \left[dn\left(u - \frac{\omega_{bn} t}{K} \right) \right. \right.$$

$$\left. \left. - dn\left(u + \frac{\omega_{bn} t}{K} \right) \right] + \int_1^\infty \frac{dK}{K^5} \int_0^{\frac{\pi}{2}} d\xi' \, \frac{64}{\pi} \, \frac{\omega_{bn}^2}{k_{\shortparallel}^2} \sin\xi' \right. \tag{3.44}$$

44

$$\frac{H_h(k_\perp \rho)}{2} \left[cn(w - \omega_{bn}t) - cn(w + \omega_{bn}t) \right] \left(\frac{\partial f_0}{\partial \underset{\sim}{v}} \right)_{v_h} \cdot \hat{\underset{\sim}{v}} \ .$$

Rewriting this equation, we conclude

$$\gamma = -\pi \frac{\omega_p^2}{k^2} \left(\frac{\partial \varepsilon_r}{\partial \omega} \right)^{-1} \sum_{h=-\infty}^{\infty} \int 2\pi v_\perp \, dv_\perp \ J_h^2(k_\perp \rho) \left(\frac{\partial f_0}{\partial \underset{\sim}{v}} \right) \cdot \hat{\underset{\sim}{v}}$$

$$\left\{ \frac{64}{\pi} \int_0^1 \frac{dK}{K^3} \int_0^{F(K)} sn(u) \, cn(u) \, \frac{1}{2} \left[dn \left(u - \frac{\omega_{bn}t}{K} \right) - dn \left(u + \frac{\omega_{bn}t}{K} \right) \right] du \right. \tag{3.45}$$

$$\left. + \frac{64}{\pi} \int_0^1 K^3 dK \int_0^{F(K)} sn(w) \, dn(w) \, \frac{1}{2} \left[cn(w - \omega_{bn}t) - cn(w + \omega_{bn}t) \right] dw \right\},$$

where F(K) is a complete integral of the first kind.

The function in curly brackets has been tabulated,[28] and will be referred to here as the function, $\sigma_0(\omega_{bn}t)$. O'Neil's derivation was somewhat less straightforward than the one presented here, and his final result was expressed as an integral over a sum rather than a double integral. We can obtain this result by first noting that the Fourier transforms of cn(u) and dn(u) may be written[49]

$$dn(u) = \frac{\pi}{2F} + \frac{2\pi}{F} \sum_{h=1}^{\infty} \frac{q^h}{1 + q^{2h}} \cos\left(\frac{h\pi u}{F} \right),$$

$$cn(u) = \frac{2\pi}{KF} \sum_{h=1}^{\infty} \frac{q^{h-1/2}}{1 + q^{2h-1}} \cos\left[\frac{(2h-1)\pi u}{2F} \right], \tag{3.46}$$

where $q \equiv \exp\{-\pi F[(1-K^2)^{1/2}]/F(K)\}$. It follows that

$$sn(u) \, cn(u) = -\frac{1}{K^2} \frac{d}{du} dn(u) = \frac{2\pi^2}{K^2 F^2} \sum_{h=1}^{\infty} \frac{h \, q^h}{1 + q^{2h}} \sin\left(\frac{h\pi u}{F} \right),$$

$$\frac{1}{2} \left[dn \left(u - \frac{\omega_{bn} t}{K} \right) - dn \left(u + \frac{\omega_{bn} t}{K} \right) \right]$$

$$= \frac{2\pi}{F} \sum_{h=1}^{\infty} \frac{q^h}{1 + q^{2h}} \sin \left(\frac{h\pi u}{F} \right) \sin \left(\frac{h\pi \omega_{bn} t}{KF} \right),$$

$$sn(u) \, dn(u) = -\frac{d}{du} cn \, u = \frac{2\pi^2}{KF^2} \sum_{h=1}^{\infty} \frac{(h-\frac{1}{2}) q^{h-\frac{1}{2}}}{1 + q^{2h-1}} \sin \left[\frac{(2h-1)\pi u}{2F} \right], \tag{3.47}$$

$$\frac{1}{2} \left[cn (u - \omega_{bn} t) - cn (u + \omega_{bn} t) \right]$$

$$= \frac{2\pi}{KF} \sum_{h=1}^{\infty} \frac{q^{h-1/2}}{1 + q^{2h-1}} \sin \left[\frac{(2h-1)\pi u}{2F} \right] \sin \left(\frac{h\pi \omega_{bn} t}{F} \right).$$

Substituting these expressions into the definition of $\sigma_0(\omega_{bn} t)$ and integrating over u, we find

$$\sigma_0 (\omega_{bn} t) = \sum_{h=0}^{\infty} \frac{64}{\pi} \int_0^1 dK \left\{ \frac{2h \pi^2 \sin \left(\frac{h\pi \omega_{bn} t}{KF} \right)}{K^5 F^2 (1 + q^{2h})(1 + q^{-2h})} \right.$$

$$\left. + \frac{(2h+1) \pi^2 K \sin \left[\frac{(2h+1)\pi \omega_{bn} t}{F} \right]}{F^2 (1 + q^{2h+1})(1 + q^{-2h-1})} \right\}, \tag{3.48}$$

which is just O'Neil's result. Our final result is

$$\gamma(t) = -\pi \frac{\omega_p^2}{k^2} \left(\frac{\partial \varepsilon_r}{\partial \omega} \right)^{-1} \sum_{h=-\infty}^{\infty} \int_0^{\infty} 2\pi v_\perp \, dv_\perp \left(\frac{\partial f_0}{\partial v_z} + \frac{h\Omega}{k_\| v_\perp} \frac{\partial f_0}{\partial v_\perp} \right)$$

$$J_h^2 (k_\perp \rho) \, \sigma_0 (\omega_{bn} t). \tag{3.49}$$

Comparing this result to Eq. (2.10) and noting that $\sigma_0(0) = 1$, we see that Eq. (3.49) yields the usual linear damping rate at t = 0, just as it ought to. Because $\omega_{bn} = [ek_\|^2 \phi | J_n(k_\perp \rho)|/m]^{1/2}$ depends

46

on $v_\perp$, the time-dependent damping rate must be determined by numerical integration even for a Maxwellian distribution.

The time-dependent frequency shift can be determined from Eq. (3.42.b). Recalling that $\underset{\sim}{v} + \underset{\sim}{\Delta v} = \underset{\sim}{v}_0$, it follows that $2\underset{\sim}{v}\underset{\sim}{\Delta v} - \underset{\sim}{\Delta v}\underset{\sim}{\Delta v} = \underset{\sim}{v}_0\underset{\sim}{v}_0 - \underset{\sim}{v}\underset{\sim}{v}$. From Eq. (3.37), we see that when $K < 1$,

$$\underset{\sim}{v}_0\underset{\sim}{v}_0 - \underset{\sim}{v}\underset{\sim}{v} = \frac{4}{k_\parallel^2}\frac{\omega_{bn}^2}{K^2}\left\{dn^2\left[u \mp H_n(k_\perp\rho)\frac{\omega_{bn}t}{K}\right] - dn^2(u)\right\}\underset{\sim}{\hat{v}}\,\underset{\sim}{\hat{v}}\,, \qquad (3.50)$$

and, from Eq. (3.39), that when $K > 1$,

$$\underset{\sim}{v}_0\underset{\sim}{v}_0 - \underset{\sim}{v}\underset{\sim}{v} = \frac{4}{k_\parallel^2}\frac{\omega_{bn}^2}{K^2}\left\{cn^2\left[w \mp H_n(k_\perp\rho)\omega_{bn}t\right] - cn^2(u)\right\}\underset{\sim}{\hat{v}}\,\underset{\sim}{\hat{v}}\,. \qquad (3.51)$$

From Eq. (3.41), we have

$$2\underset{\sim}{v}\underset{\sim}{\Delta v}_{rn} = -\frac{2\omega_{bn}^2}{k_\parallel^2}\cos(k_\parallel z)\left[1 - \cos(k_\parallel v_z t)\right]\underset{\sim}{\hat{v}}\,\underset{\sim}{\hat{v}}\,. \qquad (3.52)$$

Making use of the relationship

$$\cos(k_\parallel z) = H_n(k_\perp\rho)\left[1 - \frac{2}{K^2} + \frac{2}{K^2}dn^2(u)\right] = H_n(k_\perp\rho)\left[1 - \frac{2}{K^2} + \frac{2}{K^2}cn^2(w)\right]\,, \qquad (3.53)$$

and transforming variables

$$\cos(k_\parallel z)\,v_z\,\frac{dz}{\lambda_\parallel} = \begin{cases} \dfrac{2}{k_\parallel}\dfrac{\omega_{bn}^2}{K^2}H_n(k_\perp\rho)\left[1 - 2sn^2(u)\right]\dfrac{du}{\pi}dK; & K < 1 \\[3em] \dfrac{2}{k_\parallel}\dfrac{\omega_{bn}^2}{K^2}H_n(k_\perp\rho)\left[1 - 2sn^2(w)\right]\dfrac{du}{\pi}dK; & K > 1 \end{cases} \qquad (3.54)$$

47

we obtain from Eq. (3.42.b)

$$k^2 \left(\frac{\partial \varepsilon_r}{\partial \omega}\right) \delta\omega \ \Phi \ = \ - 4\pi e \, n_0 \sum_{n=-\infty}^{\infty} \int_0^{\infty} 2\pi v_\perp \, dv_\perp \ |J_n(k_\perp \rho)|$$

$$\frac{\omega_{bn}^3}{k_\parallel^3} \left(\frac{\partial^2 f_0}{\partial v \, \partial v}\right)_{v_\parallel} : \hat{v} \ \hat{v} \ \left(\frac{16}{\pi} \int_0^{F(K)} \frac{dK}{K^4} \int_0^{F(K)} [1 - sn^2(u)] \left\{ dn^2\left(u - \frac{\omega_{bn} t}{K}\right) \right. \right.$$

$$\left. + \ dn^2\left(u + \frac{\omega_{bn} t}{K}\right) - [K^2 - 2 + 2 \, dn^2(u)] \cos\left[\frac{2\omega_{bn} t}{K} dn(u)\right] + K^2 - 2 \right\} du$$

$$+ \frac{16}{\pi} \int_1^{\infty} \frac{dK}{K^4} \int_0^{F(1/K)} [1 - sn^2(w)] \left\{ cn^2(w - \omega_{bn} t) + cn^2(w + \omega_{bn} t) \right. \tag{3.55}$$

$$\left. \left. - [K^2 - 2 + 2 \, cn^2(w)] \cos\left[\frac{2\omega_{bn} t}{K} cn(w)\right] + K^2 - 2 \right\} dw \right) \ .$$

The quantity in curly brackets is a tabulated function[28] which will be referred to here as $\sigma_M(\omega_{bn} t)$. Because of the terms containing $\cos[(\omega_{bn} t/K) dn(u)]$ and $\cos[(\omega_{bn} t/K) cn(w)]$, there is no simple way to reduce the double integral to a single integral over a sum. Rewriting Eq. (3.55), we conclude at last

$$\delta\omega \ = \ - \frac{\omega_p^2}{k^2} \left(\frac{\partial \varepsilon_r}{\partial \omega}\right)^{-1} \left(\frac{e\Phi}{m}\right)^{1/2} \sum_{n=-\infty}^{\infty} \int_0^{\infty} 2\pi v_\perp \, dv_\perp \ \left(\frac{\partial^2 f_0}{\partial v_z^2}\right.$$

$$\left. + \frac{2n\Omega}{k_\parallel v_\perp} \frac{\partial^2 f_0}{\partial v_\perp \partial v_z} + \frac{n\Omega}{k_\parallel v_\perp} \frac{\partial}{\partial v_\perp} \frac{n\Omega}{k_\parallel v_\perp} \frac{\partial f_0}{\partial v_\perp}\right) |J_n(k_\perp \rho)|^{5/2} \tag{3.56}$$

$$\sigma_M(\omega_{bn} t) \ .$$

Eqs. (3.49) and (3.56) together determine the complex frequency shift.

3.5 Numerical Results

The solution of Eq. (3.49) when f_0 is Maxwellian will now be explored in order to determine the effect of the multiple resonances on the time-evolution of the amplitude. In dimensionless variables, Eq. (3.49) becomes

$$|u_i(\tau)| = \sqrt{\frac{\pi}{2}}\, \alpha^2 u^2 \left(u\, \frac{\partial \varepsilon_r}{\partial u}\right)^{-1} \sum_{n=-\infty}^{\infty} \int_0^{\infty} \zeta \, d\zeta \; \exp\left\{-\frac{1}{2}\left[\zeta^2 + \left(u - \frac{n}{\kappa_{\shortparallel}}\right)^2\right]\right\} \cdot$$

$$J_n^{\,2}(\kappa_\perp \zeta)\; \sigma_0\left[\varphi^{1/2} |J_n(\kappa_\perp \zeta)|^{1/2} \tau\right] \;, \tag{3.57}$$

where $\zeta \equiv v_\perp/v_t$, $\phi \equiv e\Phi/T$, and $\tau \equiv (k_{\shortparallel} v_t)t$. As discussed in Section 2.2, we must specify the four parameters α, $\kappa_{\shortparallel}$, r, and ϕ in order to determine the system. Noting that $[d\Phi(\tau)/d\tau] = -|u_i(\tau)|\Phi$, the power ratio evolution is described by

$$P(t) \equiv \frac{\Phi^2(t)}{\Phi^2(o)} = \exp\left(-2\int_0^t \gamma(t')\,dt'\right)$$

$$= \exp\left(-2\int_0^\tau |u_i(\tau')|\,d\tau'\right) \;. \tag{3.58}$$

Beyond the range $x = 5\pi$, $\sigma_0(x)$ has not been tabulated. Since we expect it to be small beyond this point, we set it equal to zero.

Calculated results for $\gamma(t)/\gamma(0) = |u_i(\tau)|/|u_i(0)|$ and $P(t)$ are shown in Fig. 3.2 with $\kappa_{\shortparallel} = 1.0$ and $\phi = 0.05$. Since we wish to make contact with possible full particle simulations, we chose values of α such that the observed change in $P(t)$ is large enough to be visible in a simulation, rather than strictly adhering to the condition $\gamma \ll \omega_b$. Experience with parallel-propagating waves indicates that this approach yields qualitatively correct results in the entire range $\gamma < \omega_b$.
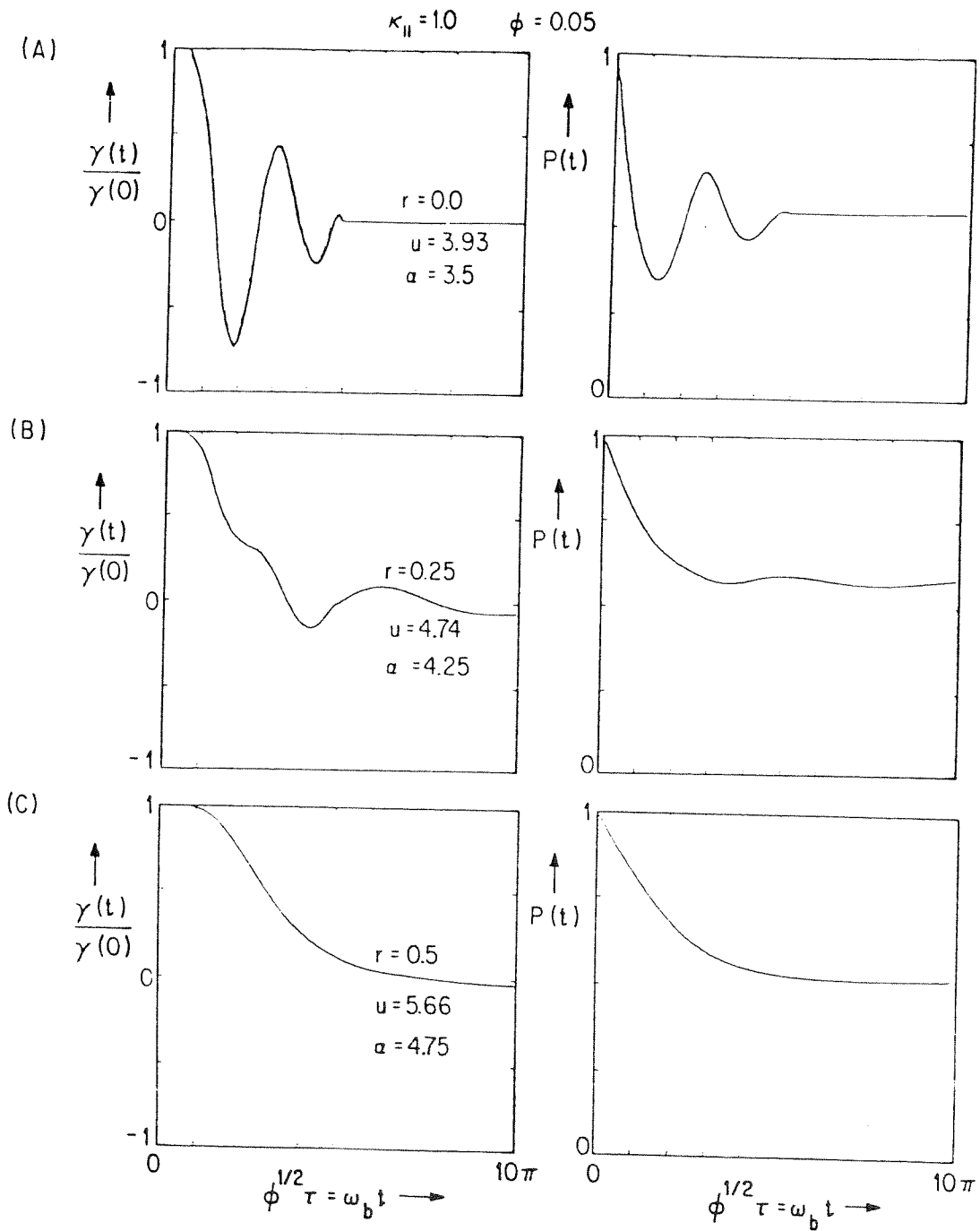
Fig. 3.2   Variation of $\gamma(t)/\gamma(0)$ and $P(t)$ with r (increasing angle).

50

The effect in which we are primarily interested, the disappearance of the amplitude oscillations, is clearly visible in Fig. 3.2. At r = 0.25, which corresponds to an angle of propagation of about 14°, the oscillations in $\gamma(t)/\gamma(0)$ are still visible, although quite reduced in comparison to the case when r = 0.0. By contrast, the oscillations in P(t) have almost disappeared. When r = 0.5, which corresponds to an angle of propagation of about 27°, virtually no oscillation in $\gamma(t)/\gamma(0)$ and P(t) can be detected. The disappearance of the amplitude oscillations with increasing r is not dependent on our choices of α because the shape of $\gamma(t)/\gamma(0)$ is essentially independent of α, as shown in Fig. 3.3.

This disappearance is not a simple phenomenon and is due to a cancellation between different resonances, as shown in Fig. 3.4, where the ratio $\gamma_n(t)/\gamma(0)$ is plotted for various values of n. Each resonance contains some averaging over different bounce frequencies, but not enough to destroy the oscillations in $\gamma_n(t)/\gamma(0)$.

Shown in Fig. 3.5 is the variation with increasing $\kappa_{\shortparallel}$ of $\gamma(t)/\gamma(0)$ and P(t). We see that as $\kappa_{\shortparallel}$ is increased, the amplitude oscillations become even more evident even though the number of resonances participating in the damping increases. Essentially, the resonances now interfere constructively. At the same time, the total damping of the wave decreases when $\kappa_{\shortparallel}$ increases because the resonances "bite" less deeply into the distribution function. It must be noted that since stochastic overlap occurs when $\kappa_{\shortparallel} > 0.25\phi^{-1/2} \simeq 1.4$, this theory is not expected to be valid for large $\kappa_{\shortparallel}$, and, in fact, as will be
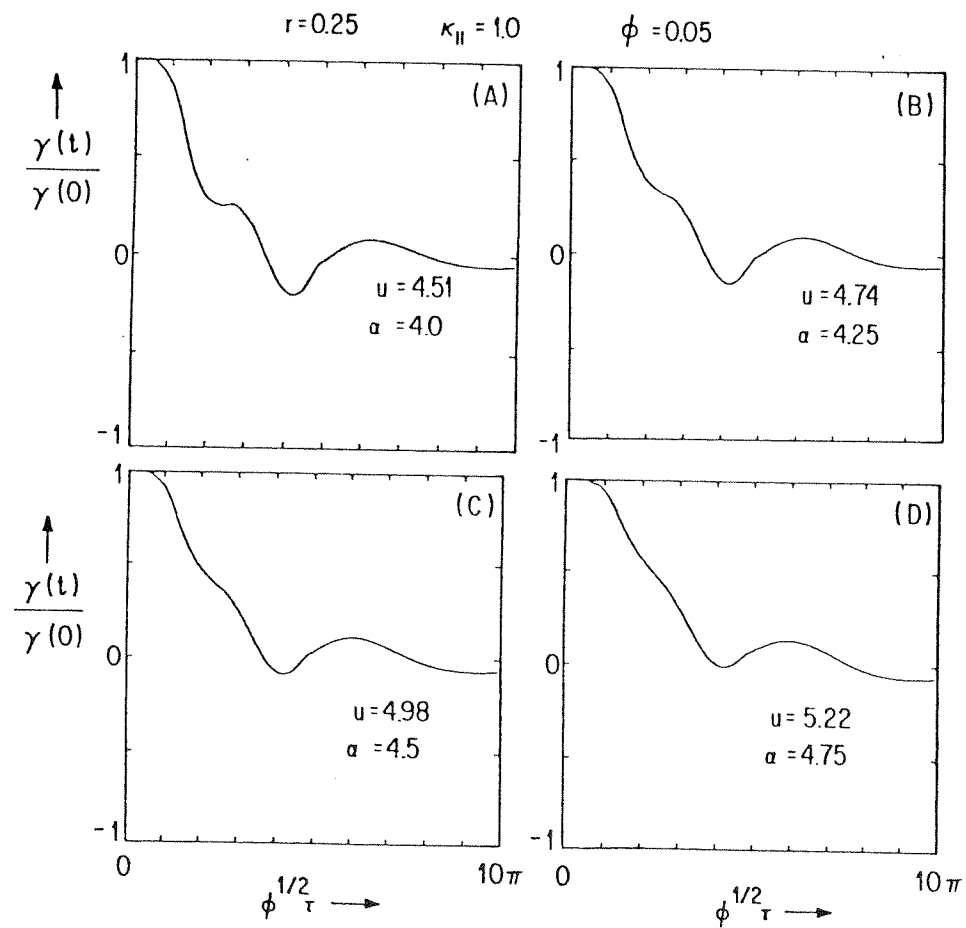
Fig. 3.3 Variation of $\gamma(t)/\gamma(0)$ with α.
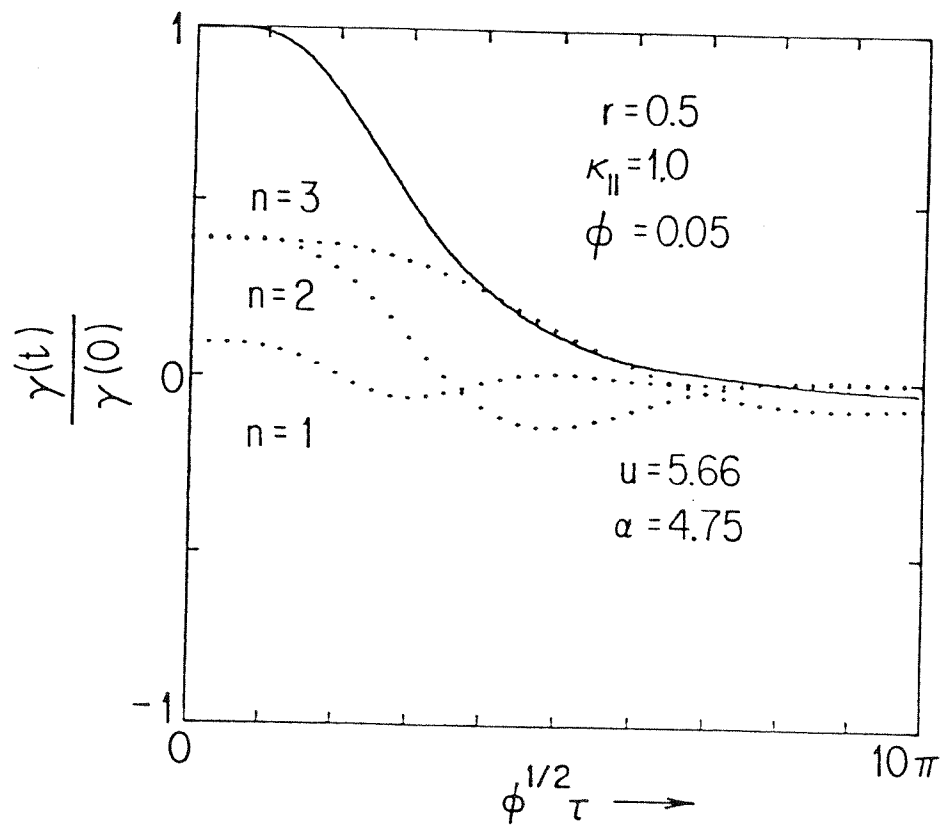
Fig. 3.4 Display of $\gamma_n(t)/\gamma(0)$ for various values of n. The oscilla-
tions of $\gamma_2(t)$ and $\gamma_3(t)$ tend to cancel each other.

53
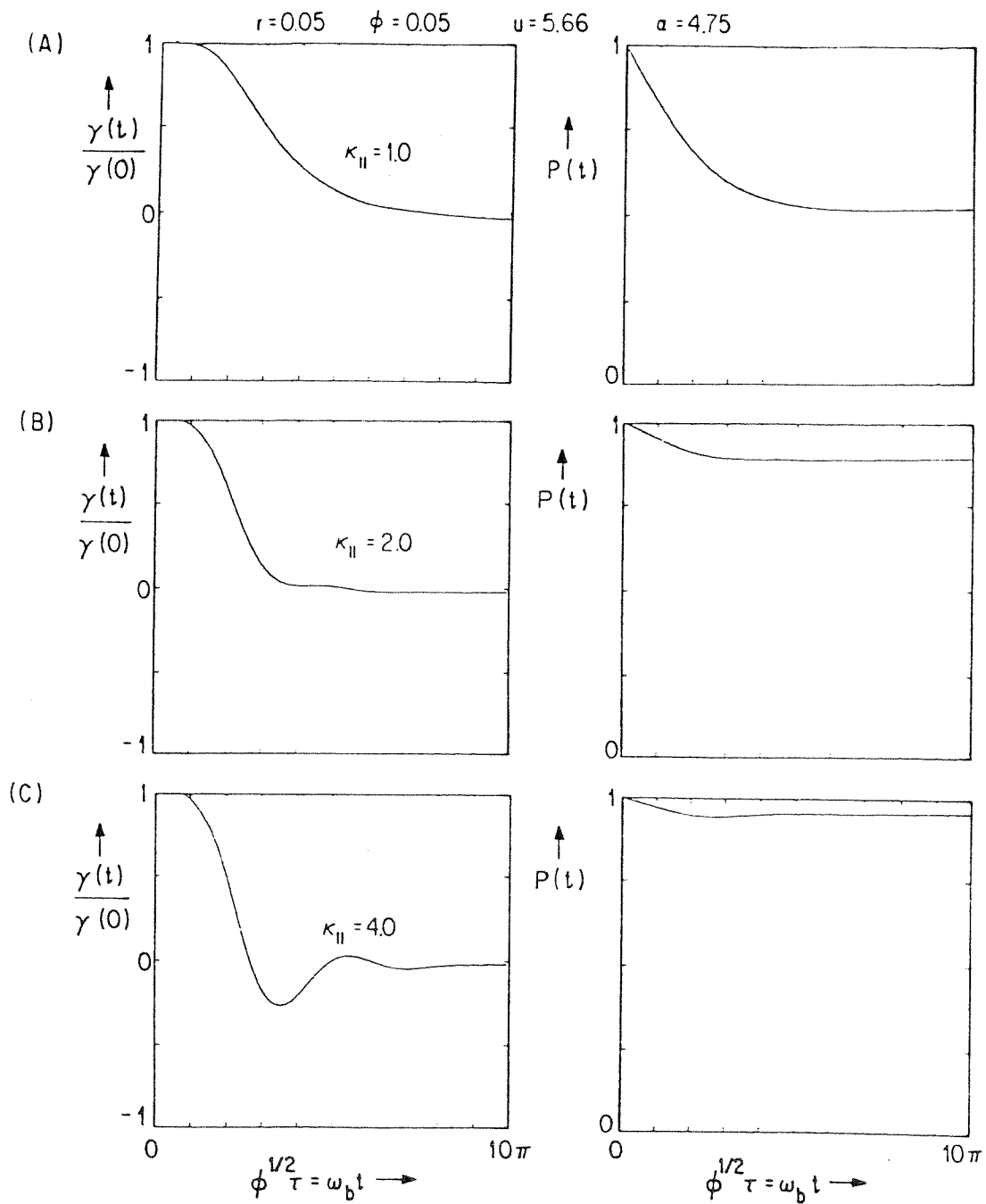
Fig. 3.5 Variation of $\gamma(t)/\gamma(0)$ with $\kappa_{\shortparallel}$.

54

shown in the next chapter, the total damping is expected to <u>increase</u> as $\kappa_{||}$ increases, beyond the point where resonance overlap occurs.

4. TRANSITION TO THE STOCHASTIC REGIME

4.1 Preliminary Discussion

The determination of when the transition between regular and stochastic motion occurs has received much attention in the last few years. Such a determination is often important because it tells us when particle motion can be treated statistically and when not. In fact, the onset of stochasticity could very well be the physical basis of the ergodic hypothesis, one of the central tenets of statistical mechanics.[6]

Most of the progress in recent years has centered about the Kolmogorov-Arnol'd-Moser theorem, which states that particle motion can be stable, i.e. local invariants of the motion can exist, even though global invariants do not. (Invariants are functions of position and momentum which confine particle motion to subspaces of lower dimensionality than the space as a whole. These invariants can apply to part of the space, in which case they are local, or to the whole space, in which case they are global.) This theorem has been verified in many numerical experiments, and Chirikov[20] has distilled the results of these numerical experiments into a simple criterion: When resonances overlap, particle motion is stochastic; when they do not, it is regular.

The numerical experiments have generally looked at situations where the six equations of motion can be reduced to four as is the case in the oblique wave problem; these four can then be reduced to two by making surface-of-section plots. One also generally examines situations

in which the motion is conservative, in which case one can determine whether the motion is stochastic or regular by simple visual inspection of the surface-of-section plots. If the motion is non-conservative, then one cannot, in general, simply examine the surface-of-section plots to determine the character of the motion, because the resonance structure is itself time-dependent. Nonetheless, the resonance overlap criterion appears to be valid in this case as well.[16]

The work done to date has focused primarily on particle motion in fixed fields and not addressed the question of how the fields change in response to the particle motion. This question is of interest in many of the applications where the transition between regular and stochastic behavior has been used. Moreover, in any basic physics experiment or simulation which would look for the transition, the change in the field would be the principal observable.

Electron motion in the transition regime $\omega_b \approx \Omega$, where overlap between the largest resonances first occurs, is quite complicated even if we assume $\gamma \ll \omega_b$. Regular and stochastic regions in phase space are pathologically interwoven, and solving for the electron motion explicitly, as we did in Chapter 3, is evidently not possible. We can, however, determine the asymptotic ($t=\infty$) change in the wave amplitude, given the assumption that the distribution function is asymptotically flattened in the resonant regions subject to the constraint that particle number is conserved. Similar approximations have been used in the past by Dawson and Shanny,[24] Stix,[12] and Smith and Kaufman.[9] This approximation allows us to treat the trapping and stochastic regimes in a unified fashion and explore the transition between the two. In

Sections 4.2 and 4.3, this model is used to show that the total damping R, i.e., the fractional decrease in the wave amplitude, significantly increases when resonance overlap occurs.

As $\kappa_{||} \equiv k_{||}v_t/\Omega$ increases (Ω decreases), and we move well into the stochastic regime, there is a region in velocity-space where resonances overlap and particle motion is expected to be stochastic. This situation is shown schematically in Fig. 4.1. The stochastic region in velocity space is symmetric about $v_z = v_p$, and its width in the v_z-direction increases as $v_\perp$ increases. Since electrons in the stochastic regime can undergo large changes in v_z, their motion is expected to dominate the wave evolution. Moreover, motion of the stochastic electrons is expected to be roughly diffusive, so that it makes sense to try using a quasi-linear type approximation to calculate the wave evolution. Unfortunately, there are two major difficulties with this approach. First, we are dealing with discrete resonances whose amplitudes vary widely from one resonance to the next. Hence, it is not clear what the diffusion coefficient should be. If we try to use quasi-linear theory with resonance broadening to calculate the diffusion coefficient, we end up with equations whose solution appears to require as much numerical work as a simulation. Second, since our distribution function is Maxwellian, most of the electrons in the stochastic region of velocity-space are actually on the edge of this region at t = 0. At the edge, large regular regions are inter-mixed with the stochastic region, and the particle motion is not simply diffusive.

These issues are discussed in Section 4.4., where the appropriate diffusion coefficient is derived using a method based on Dupree's[50]

$r = 0.25$ $\phi = 0.05$ $u = 4.98$ $\alpha = 4.5$
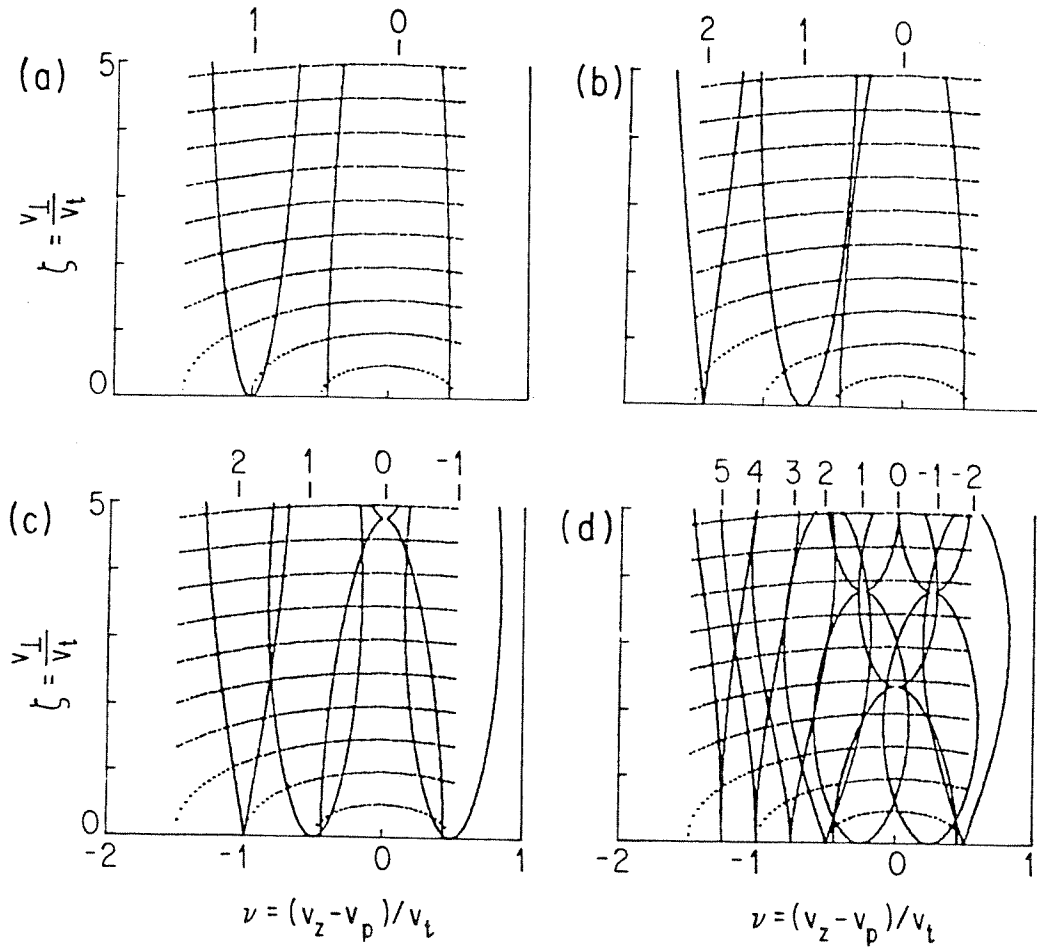
Fig. 4.1 The resonance structure at various values of $\kappa_{\shortparallel}$. The reson-
ance widths are shown in the range $3.5 < (v_z/v_t) < 5.5$,
which is important in the simulations of Chapter 5. Shown
also are the constant energy surfaces along which the distri-
bution is flattened. a) $\kappa_{\shortparallel} = 1.0$, b) $\kappa_{\shortparallel} = 1.4$, c) $\kappa_{\shortparallel} = 2.0$,
and d) $\kappa_{\shortparallel} = 4.0$.

resonance-broadening theory. In keeping with approximations that have often been made by Dupree and co-workers, we then average the diffusion coefficient, in Section 4.5, on each constant energy surface, $(v_z - v_p)^2 + v_\perp^2 =$ constant, and obtain equations which are easily soluble. Solving these equations and looking ahead to the simulations of Chapter 5, we find that this model helps us understand the important qualitative features of the true evolution, but does not yield quantitatively correct results.

4.2   Theoretical Determination of the Total Damping

To derive the total damping, we begin with the momentum relation derived in Appendix A,

$$\frac{d}{dt} \int d^3v \; m v_z \, n_o f_o \; = \; -k_{\shortparallel} \frac{\partial \varepsilon_r}{\partial \omega} \frac{d E_o^2 / 16\pi}{dt} \; , \qquad (4.1)$$

where

$$f_o(\underset{\sim}{v}, t) \; \equiv \; \int_0^{\lambda_{\shortparallel}} \frac{dz}{\lambda_{\shortparallel}} \int_0^{\lambda_\perp} \frac{dy}{\lambda_\perp} \; f(\underset{\sim}{x}, \underset{\sim}{v}, t) \; . \qquad (4.2)$$

We integrate over time to obtain the asymptotic limit,

$$\delta \int d^3v \; m v_z \, n_o f_o \; = \; -k_{\shortparallel} \frac{\partial \varepsilon_r}{\partial \omega} \; \delta \frac{E_o^2}{16\pi} \; , \qquad (4.3)$$

and noting that $E_0^2 = k^2 \varsigma^2$, we find

60

$$\delta \int d^3v \; m v_z \, n_0 f_0 \;\; = \;\; -k_\| \frac{\partial \varepsilon_r}{\partial \omega} \; \frac{k^2 T}{4} \left(\frac{T}{4\pi n_0 e^2} \right) \delta \left(\frac{e \phi}{T} \right)^2 n_0$$

$$= \;\; -k_\| \frac{\partial \varepsilon_r}{\partial \omega} \; \frac{k^2 T}{4 k_D^2} \; \delta \left(\frac{e \phi}{T} \right)^2 n_0 \; .$$

(4.4)

For the fractional charge in the wave amplitude, we obtain

$$R \equiv - \frac{\delta \phi^2}{\phi^2} = \frac{1}{k_\|} \left(\frac{\partial \varepsilon_r}{\partial \omega} \right)^{-1} \frac{4 k_D^2 \, T}{k^2 e^2} \; \delta \int d^3v \; m v_z \, n_0 f_0 \; . \qquad (4.5)$$

We can think of R as the ratio of the amount of power needed to flatten the distribution function in the resonant regions to the power initi- ally present in the wave. When R >> 1, indicating that more power is needed to flatten the distribution function than is available in the wave, experience with parallel-propagating waves indicates that the wave simply damps away.[24] If R < 1, then the fractional decrease in the wave power is approximately equal to R. In effect, we are implicitly making use of the same assumption we used in Chapter 3, where we assumed $\gamma << \omega_b$, since we use the initial wave amplitudes when calculating the resonant widths. Only when R is quite close to one will self-consistent effects be important since the resonance widths scale weakly with R, go- ing as $(1-R)^{1/4}$. Recalling that

$$\phi(t) \;\; = \;\; \phi \exp \left[- \int_0^t \gamma(t') \, dt' \right] \; , \qquad (4.6)$$

we find that for $\gamma << \omega_b$,

$$R = -\frac{\delta \Phi^2}{\Phi^2} = 2\int_0^\infty \gamma(t')\,dt' \quad, \tag{4.7}$$

so that it is related to the quantity P defined in Chapter 3 through the relation

$$P(t = \infty) = \exp(-R) \quad. \tag{4.8}$$

At $t = 0$, we assume that the electrons have a Maxwellian distribution

$$f_0(t=0) = \left(\frac{m}{2\pi T}\right)^{3/2} \exp\left[-\frac{m}{2T}(v_z^2 + v_\perp^2)\right] = \left(\frac{m}{2\pi T}\right)^{3/2} \mathscr{f}_0(t=0), \tag{4.9}$$

where, letting $\nu \equiv (v_z - v_p)/v_t$ and $\zeta \equiv v_\perp/v_t$,

$$\mathscr{f}_0(t=0) = \exp\left[-\frac{m}{2T}(v_z^2 + v_\perp^2)\right] = \exp\left\{-[\zeta^2 + (\nu + u)^2]/2\right\} \quad. \tag{4.10}$$

Then, it follows

$$R \equiv \frac{\delta \Phi^2}{\Phi^2} = \sqrt{\frac{8}{\pi}}\frac{\alpha^2 u^{\boxtimes}}{\varphi^2}\left(u\frac{\partial \varepsilon_r}{\partial u}\right)^{-1}\int d\nu\, d\zeta\,(\nu + u)\zeta$$

$$\left(\mathscr{f}_0(t=\infty) - \exp\left\{-[\zeta^2 + (\nu+u)^2]/2\right\}\right) \quad. \tag{4.11}$$

If the wave damping is neglected, energy conservation in the wave frame gives

$$\frac{1}{2}m\left[(v_z - v_p)^2 + v_\perp^2\right] + e\Phi\cos(\underset{\sim}{k}\cdot\underset{\sim}{x} - \omega t) = constant. \tag{4.12}$$

Since $\phi \equiv e\Phi/T \ll 1$, in all the case dealt with here, it follows that

62

$$\frac{1}{2} m \left[(v_z - v_p)^2 + v_\perp^2 \right] \simeq constant \, , \qquad (4.13)$$

so that electrons will move along the constant energy surfaces shown in Fig. 4.1. It is useful to change variable from (ν, ζ) to (ν, ζ_m) where

$$\zeta_m \equiv \left(\gamma^2 + \zeta^2 \right)^{1/2} = \frac{1}{v_t} \left[(v_z - v_p)^2 + v_\perp^2 \right] \, . \qquad (4.14)$$

Then, Eq. (4.11) becomes

$$R = \sqrt{\frac{8}{\pi}} \frac{\alpha^2 u}{\varphi^2} \left(u \frac{\partial \varepsilon_r}{\partial u} \right)^{-1} \int d\nu \, d\zeta_m \, (\nu + u) \, \zeta_m$$

$$\left\{ \mathscr{f}_0 \, (t = \infty) - exp \left[-(u^2 + \zeta_m^2)/2 \right] exp(-u\nu) \right\} \, . \qquad (4.15)$$

Since ζ_m is, according to Eq. 4.17, approximately constant for any given electron, the factor $\exp[-(u^2 + \zeta_m^2)/2]$ remains unaffected by the flattening of the distribution function; only the factor $\exp(-u\nu)$ is affected as the electrons change their ν-values. The resonances are located at $\nu = -n/\kappa_{\shortparallel}$ and have total widths given by

$$W_n = 4 \varphi^{1/2} \left| J_n \left(\kappa_\perp \zeta \right) \right|^{1/2} = 4 \varphi^{1/2} \left| J_n \left[\kappa_\perp \left(\zeta_m^2 - \frac{n^2}{\kappa_{\shortparallel}^2} \right)^{1/2} \right] \right|^{1/2} \, . \qquad (4.16)$$

Referring to Eq. (4.14), we see that the resonance widths cannot extend past $\nu = \pm\zeta_m$; if Eq. (4.16) yields width which extend past these limits, then the resonances are cut off there.

When the resonances do not overlap, the final distribution is approximated as being flattened over the resonant regions; when more than one resonance overlaps, the final distribution is approximated as being flattened over all of them. Letting ℓ_i and s_i be the lower and upper values of v for given values of n and ζ_m, Eq. (4.15) becomes

$$
R = \sqrt{\frac{8}{\pi}} \frac{\alpha^2}{\varphi^2} u \left(u \frac{\partial \epsilon_r}{\partial u} \right)^{-1} \exp\left(-u^2/2\right) \int_0^\infty \zeta_m \, d\zeta_m \, \exp\left(-\zeta_m^2/2\right)
$$

$$
\sum_i \left\{ \frac{(s_i - \ell_i)}{2u} \left[\exp\left(-u\ell_i\right) + \exp\left(-u s_i\right) \right] \right.
$$

$$
\left. - \frac{1}{u^2} \left[\exp\left(-u\ell_i\right) - \exp\left(-u s_i\right) \right] \right\} . \tag{4.17}
$$

where the constraint that particle number is conserved has been used.

In the case of a single small resonance, this calculation is expected to yield a result which is somewhat high since only the part of the distribution function inside the separatrix shown in Fig. 4.2 is really flattened. The result of our calculation can be compared to O'Neils,[26] which is valid in this limit, and shown to be high by nearly a factor of two. If a resonance is small, then

$$
\frac{(s_i - \ell_i)}{2u} \left[\exp\left(-u\ell_i\right) + \exp\left(-u s_i\right) \right] - \frac{1}{u^2} \left[\exp\left(-u\ell_i\right) \right.
$$

$$
\tag{4.18}
$$

$$
\left. - \exp\left(-u s_i\right) \right] = \exp\left(u n/K_{\shortparallel}\right) \frac{u}{12} \left(s_i - \ell_i\right)^3 .
$$

In the case of a parallel-propagating wave, n=0 and $s_i - \ell_i = 4\phi^{1/2}$,
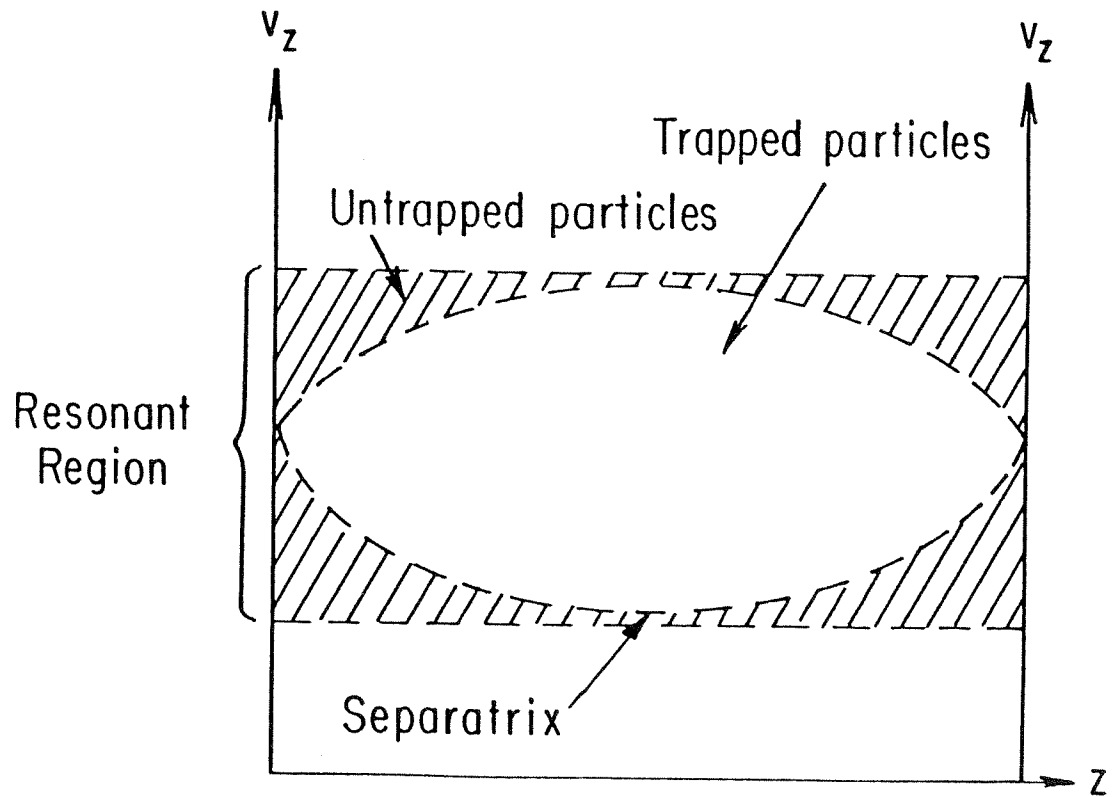
Fig. 4.2 Schematic structure of a resonant region in the trapping

regime. The distribution function does not flatten

asymptotically over the whole resonant region, shown inside

dashed lines, but only over the unshaded portion inside the

separatrix.

so that Eq. (4.17) becomes

$$R = \sqrt{\frac{8}{\pi}} \frac{\alpha^2}{\varphi^2} u \left(u \frac{\partial \mathcal{E}_r}{\partial u} \right)^{-1} \exp\left(-u^2/2\right) \left(\frac{16}{3} \varphi^{3/2} u\right)$$

$$= \frac{16}{3} \sqrt{\frac{8}{\pi}} \frac{\alpha^2}{\varphi^{1/2}} u^2 \left(u \frac{\partial \mathcal{E}_r}{\partial u} \right)^{-1} \exp\left(-u^2/2\right) \quad . \tag{4.19}$$

In O'Neil's calculation, R is

$$R_0 = 2 \int_0^\infty \gamma(t)\, dt = 2 \int_0^\infty |u_i(\tau)|\, d\tau = 2 |u_i(0)| \tau_{eff} \quad . \tag{4.20}$$

Solving the O'Neil problem numerically, we find $\tau_{eff} = 1.746\phi^{-1/2}$, and using Eq. (2.20), we conclude

$$R_0 = 1.746 \sqrt{2\pi} \frac{\alpha^2}{\varphi^{1/2}} u^2 \left(u \frac{\partial \mathcal{E}_r}{\partial u} \right)^{-1} \exp\left(-\tfrac{1}{2} u^2\right) \quad . \tag{4.21}$$

Eq. (4.19) has the same parameter dependence as Eq. (4.21) and only differs by a factor which is

$$\frac{R}{R_0} = \frac{1}{1.746} \frac{32}{3\pi} = 1.94 \quad , \tag{4.22}$$

and corresponds to a difference in the final amplitudes of a factor of 1.39

In the limit where resonances are large but non-overlapping, Eq. (4.17) is not expected to yield results which are very accurate, since in this limit neither the trapped nor untrapped electrons are treated

66

in a precisely correct fashion. Nonetheless, because the distribution function is not approximated by a Taylor series, this approximation is a significant improvement over O'Neil's. O'Neil's theory predicts that as ϕ increases, R will decrease indefinitely. However, as Dawson and Shanny[24] showed, beyond some value of ϕ, a Taylor expansion of the distribution function is not adequate, and R will increase because the number of electrons trapped by the wave is growing exponentially. This effect, called enhanced Landau damping, is contained in Eq. (4.17), as shown in Fig. 4.3, where we plot R as a function of the electrostatic amplitude for a parallel-propagating wave. To facilitate comparison with the results of Dawson and Shanny's Fig. 2, we have plotted R vs. $\phi_{DS} \equiv \phi^2/\alpha^2$. Like them, we find that we must have u > 4, in order for it to be possible that R < 1. It should be recalled, however, that our calculation of R is expected to be about a factor of two too high. Our results are somewhat different from those of Dawson and Shanny because we flatten the distribution function along the curves ζ_m = constant, rather than ζ = constant as they do.

In the limit where there are many overlapping resonances, Eq. (4.17) should yield a fairly accurate result, since electron motion will be stochastic in the entire resonant region. This contention is confirmed by the simulations of Chapter 5. However, as the results of Section 4.5 and Chapter 5 make clear, the approach to the asymptotic state is extremely slow.
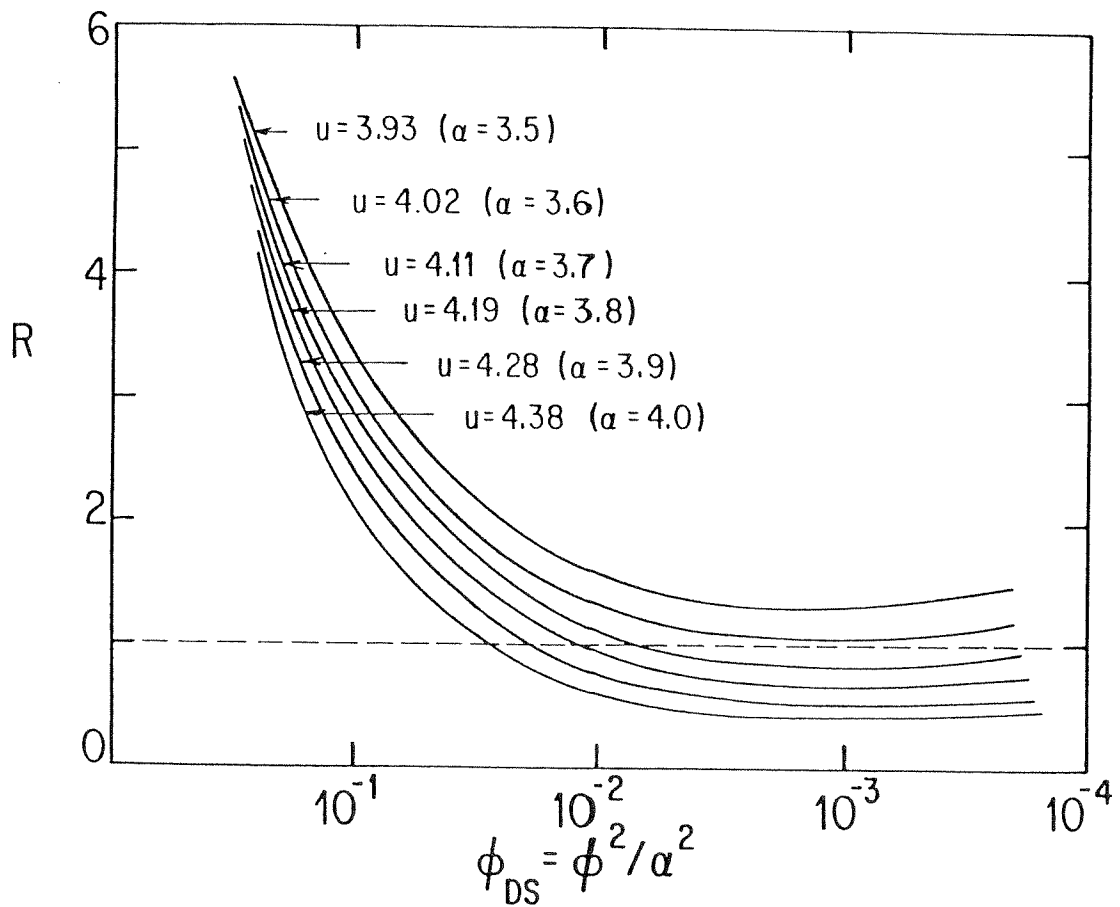
Fig. 4.3 Total damping of a parallel-propagating wave as a function of
$\phi_{DS} \equiv \phi^2/\alpha^2$. If $u \lesssim 4.0$, it is impossible to ever have
R < 1.0, due to the effect of enhanced Landau damping.

4.3 Numerical Calculations of the Total Damping and Discussion

There are two ways to make resonance overlap occur. One can increase the widths of the resonances by increasing ϕ, or one can move the resonances closer together by increasing $\kappa_{\shortparallel}$ (decreasing Ω). The second approach has two principal advantages. First, as ϕ increases, the resonances bite more deeply into the distribution function, and there is a possibility of confusing the increase in R due to resonance overlap with the increase due to enhanced Landau damping. By contrast, when $\kappa_{\shortparallel}$ is increased, the resonances with n > 0 are moved farther out on the tail of the distribution function and bite less deeply into it. As a result, R is expected to decrease until resonance overlap occurs, as shown in Fig. 3.4. Second, the resonance widths are proportional to $\kappa_{\shortparallel}\phi^{1/2}$, so that $\kappa_{\shortparallel}$ is a more sensitive parameter. In this section, we therefore concentrate primarily on discussing resonance overlap due to increasing $\kappa_{\shortparallel}$, although for completeness we have included an example of resonance overlap due to increasing ϕ as well.

The criterion for the nth and $(n+1)^{th}$ resonances to overlap at a given ζ_m is

$$2\,\phi^{1/2}\left(J_n^{1/2}\left[\left(K_\perp^2 \gamma_m^2 - n^2 r^2\right)^{1/2}\right] + J_{n+1}^{1/2}\left\{\left[K_\perp^2 \gamma_m^2 - (n+1)^2 r^2\right]^{1/2}\right\}\right)$$
$$> 1/K_{\shortparallel}\ . \qquad (4.23)$$

For each pair (n, n+1), there is a particular ζ_m where the function

$$J_n^{1/2}\left[\left(K_\perp^2 \gamma_m^2 - n^2 r^2\right)^{1/2}\right] + J_{n+1}^{1/2}\left\{\left[K_\perp^2 \gamma_m^2 - (n+1)^2 r^2\right]^{1/2}\right\}$$

has its maximum. Designating this maximum $j_{n,\,n+1}$, its numerical

69

values for n = 0, 1, 2 and r = 0.25, 0.5 are shown in Table 4.1, and given these values, we can calculate the point at which resonances first overlap. These results are also shown in Table 4.1.

Shown in Fig. 4.4 are our principal results. Since we wish to make contact with possible full particle simulations, the values of α were chosen so that R is a significant fraction of one in the regime were resonances first overlap. Shown also is the overlapping fraction, the fraction contributed to R by electrons in overlapping resonances. This overlapping fraction increases rapidly when resonance overlap first occurs and allows us to definitely correlate the observed increase in R with resonance overlap.

In all cases, R is first observed to fall as $\kappa_{||}$ is increased because the resonances are moved closer to the central resonance, and, thus, bite less deeply into the distribution. This result agrees with those of Fig. 3.5. When r = 0.25, there is a sharp rise in R which occurs at $\kappa_{||} \simeq 1.4$ when $\phi = 0.05$ and at $\kappa_{||} \simeq 1.0$ when $\phi = 0.1$. Refferring to Table 4.1, we see that this rise to due to the overlap of the n = 0, 1, and -1 resonances. At this point the overlapping fraction also rises sharply from 0 to more than 0.75, indicating that more than three-quarters of the contributions to R comes from electrons in the overlapping resonances. As the resonances move closer together, R falls again, and then rises again as more of the resonances overlap. This second rise cannot be directly correlated with the overlap of particular resonances, presumably because the resonances first overlap at high values of ζ_m, where there are few electrons, and the resonances must overlap at lower values of ζ_m before R is noticeably affected.

TABLE 4. 1

resonance pair	$j_{n,n+1}$ (r=0.25)	$\kappa_\perp \zeta_m$ (r=0.25)	$j_{n,n+1}$ (r=0.5)	$\kappa_\perp \zeta_m$ (r=0.5)
(0,1)	1.53	1.0	1.51	1.1
(1,2)	1.37	2.4	1.36	2.5
(2,3)	1.29	3.5	1.28	3.7

resonance pair	$\kappa_{\parallel}$ at overlap (r=0.25, ϕ=0.05)	$\kappa_{\parallel}$ at overlap (r=0.25, ϕ=0.1)
(0,1)	1.45	1.03
(1,2)	1.63	1.15
(2,3)	1.73	1.22
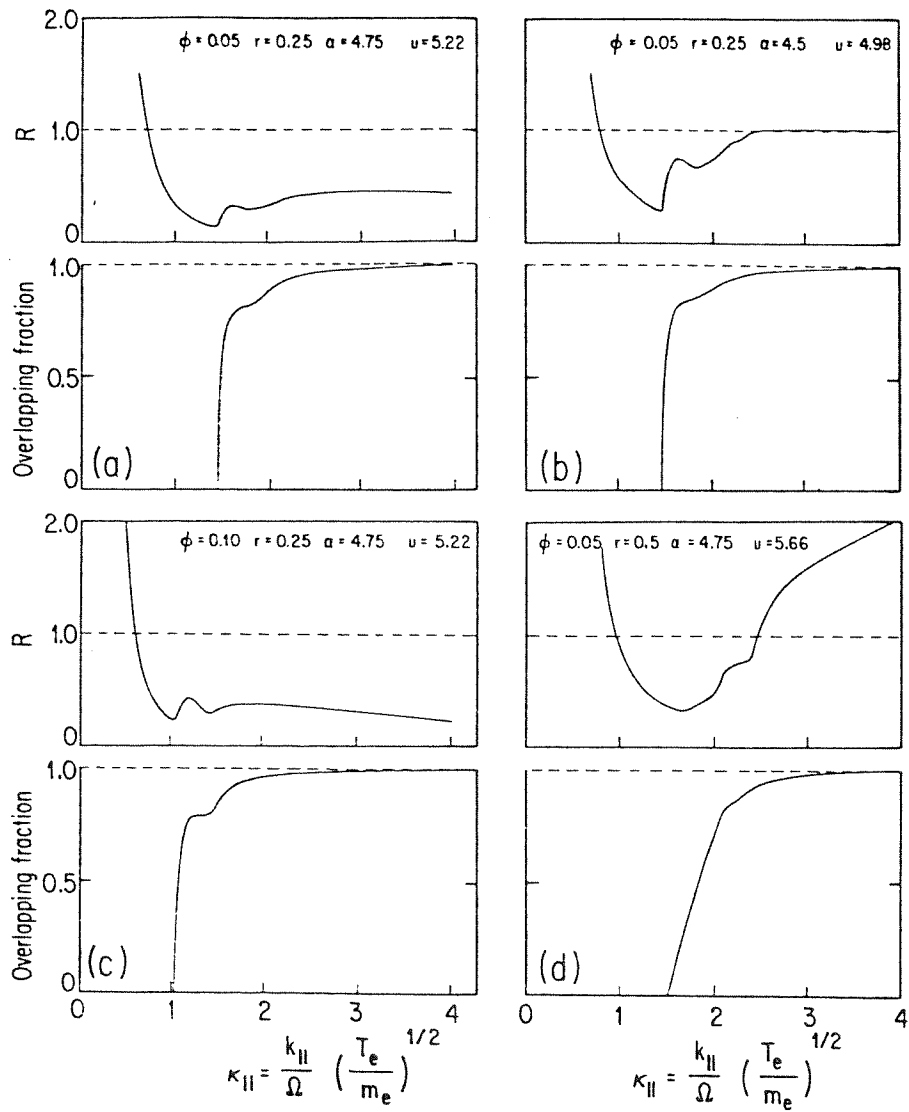
Fig. 4.4   Variation of R and the overlapping fraction as a function of

$\kappa_{\shortparallel}$.

72

In the case where r = 0.5, resonance overlap is more gradual than when r = 0.25. The overlapping fraction rises more slowly and R does not start to rise until $\kappa_{\shortparallel}$ is somewhat larger than the point at which overlap takes place. This effect presumably occurs because there is a larger contribution from the high-$|n|$ resonances when r is greater, and the effect of resonances with n > 0 moving farther out on the distribution function tail must be overcome before R can start to increase. In constrast to the cases where r = 0.25, when r = 0.5, R continues to rise as $\kappa_{\shortparallel}$ increases instead of saturating.

Comparing Fig. 4.4a to Figs. 4.4b and 4.4c, we see that the shape of $R(\kappa_{\shortparallel})$ is not very sensitive to changes in u or ϕ; whereas, comparing Figs. 4.4a to 4.4d, we see that it is quite sensitive to changes in r. That is not surprising since it is r which determines the relative strength of the different resonances at a given value of $\kappa_{\shortparallel}$. While the shape of R does not change greatly with increasing ϕ, the argument of R scales as $\phi^{-1/2}$; for example, the sharp rise in R which is visible at $\kappa_{\shortparallel} \simeq 1.4$ when $\phi = 0.05$ occurs at $\kappa_{\shortparallel} \simeq 1.0$ when $\phi = 0.1$. This $\phi^{-1/2}$ scaling should be visible in simulations and experiments and ought to be looked for as one of the signposts that the phenomenon being observed is really resonance overlap.

Shown in Fig. 4.5 is R as a function of ϕ, with $\kappa_{\shortparallel}$ fixed at 1.2. The sharp rise in both the overlapping fraction and in R when resonance overlap occurs at $\phi \simeq 0.7$ indicates that the effect of resonance overlap dominates over that of enhanced Landau damping for the values of ϕ considered.

Some discussion of the errors inherent in our approximations is

$\kappa_{||} = 1.2 \quad r = 0.25 \quad u = 4.98 \quad \alpha = 4.5$
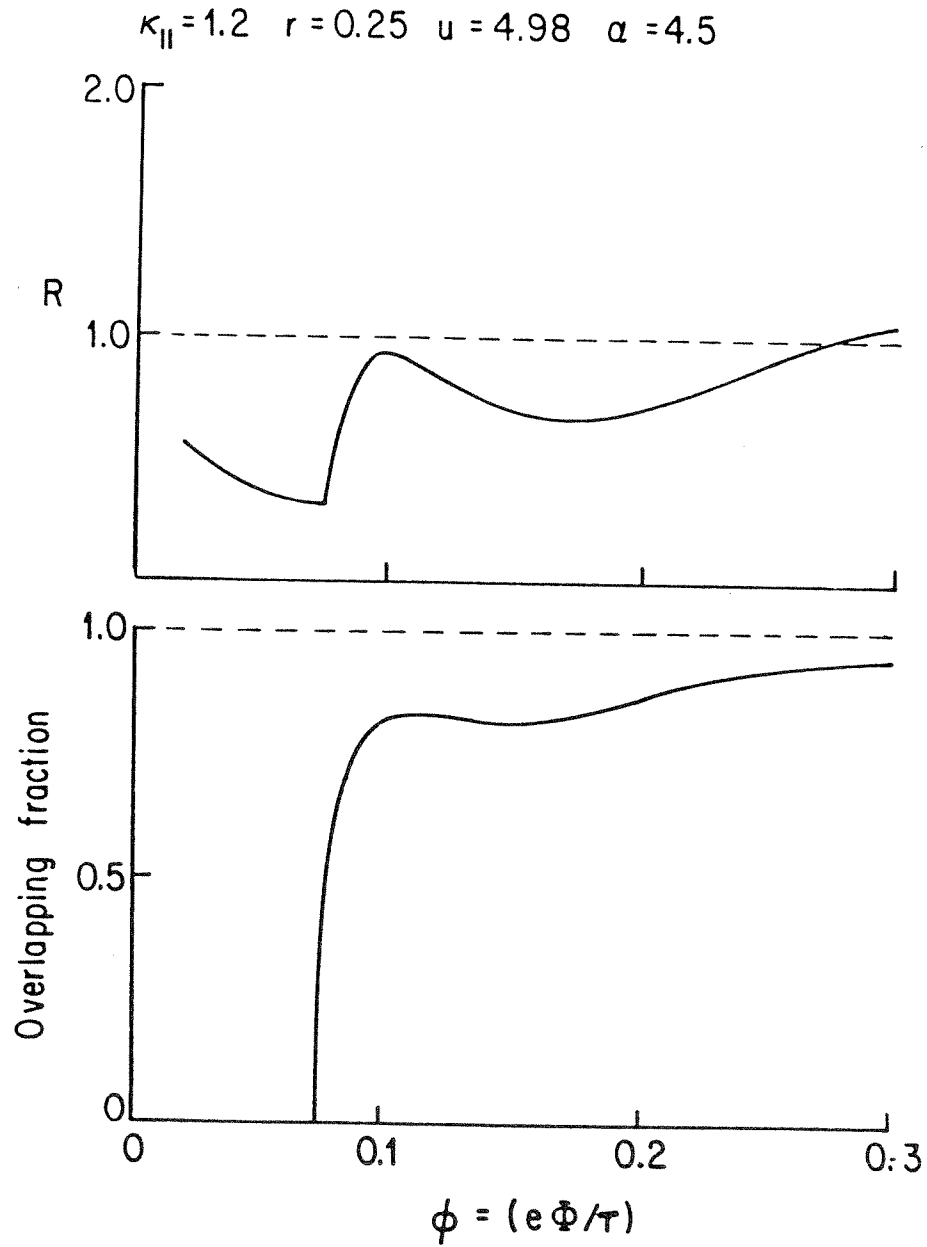
Fig. 4.5   Variation of R and the overlapping fraction with ϕ.

now appropriate. First, the assumption that the distribution will be asymptotically flattened in the resonant region yields values of R that are a factor of two too high in the trapping regime. A correct calculation of the orbits, which is found in Chapter 5, leads to an enhancement of the increased total damping observed in Fig. 4.4 when $\kappa_{\shortparallel}$ increases. However, it is shown in Chapter 5 that it takes the wave far longer to reach its asymptotic state in the stochastic regime than it does in the trapping regime, so that if a finite time is taken rather than $t = \infty$, this enhancement is decreased. Second, the assumption that the change in the field is small ($\gamma << \omega_b$) is evidently violated over some of the range in Fig. 4.4. However, we expect that since the resonance widths scale only weakly with R, as $(1-R)^{1/4}$, that until R $\simeq 1.0$, self-consistent effects make only a small difference; the results of Chapter 5 confirm this expectation. Third, the assumption that the onset of stochasticity is sudden is responsible for the sharp initial rise in R seen in Fig. 4.4 a-c. The more realistic treatment of the onset in Chapter 5 leads to a smoothing of this sharp rise, but no change in the qualitative results.

4.4 Wave Evolution in the Stochastic Regime: Quasilinear Theory with Resonance-Broadening

In the stochastic regime, the wave evolution is largely determined by electrons which move chaotically in the region of velocity space where resonances overlap. This region is symmetric about the velocity $\nu = (v_z - v_p)/v_t = 0$, and has a half-width which we will designate $w(\zeta_m)$, where $\zeta_m \equiv \nu^2 + \zeta^2$, with $\zeta \equiv v_\perp/v_t$. We consider small amplitude

fields ($e\Phi/T \equiv \phi << 1.0$), so that to good approximation electrons move along curves in veloicty space where ζ_m is constant. The stochastic character of the electron motion suggests that the distribution function evolution might be described by the diffusion equation

$$\frac{\partial f_o}{\partial t} - \frac{\partial}{\partial \underset{\sim}{v}} \underset{\approx}{D} \frac{\partial}{\partial \underset{\sim}{v}} f_o = 0 ,$$

(4.24)

where

$$\underset{\approx}{D} \equiv \int_0^\infty d\tau \; \langle \dot{v}_z (t) \, \dot{v}_z (t + \tau) \rangle \; ,$$

(4.25)

and the brackets indicate an average over initial time t and over space. This assumption is not really justified over the entire region in velocity space where resonances overlap. In this region, regular regions are pathologically interwoven with the principal stochastic region and can be quite large near its edge. Because particles tend to spend long times in the neighborhoods of the regular regions, these regions can greatly affect the motion.[20,51] Nonetheless, Eq. (4.24) provides some useful insights into the qualitative nature of the wave evolution.

Using v and ζ_m as our independent variables, and recalling that ζ_m is held constant, Eq. (4.24) reduces to the one-dimensional diffusion equation

$$\frac{\partial f_o}{\partial t} - \frac{\partial}{\partial v} \frac{D}{v_t^2} \frac{\partial}{\partial v} f_o ,$$

(4.26)

where

$$D = \int_0^\infty d\tau \; \langle \dot{v}_z(t) \; \dot{v}_z(t+\tau) \rangle \quad .$$

(4.27)

To calculate D, we begin by using standard quasilinear theory.[52] Recalling from Eqs. (2.23) and (2.24) that

$$\dot{v}_z = -(e k_{\shortparallel} \Phi / m) \sum_{h=-\infty}^{\infty} J_h(k_\perp \rho) \; \sin(k_{\shortparallel} z_0 + k_\perp y_0 + h\theta_0$$
$$+ k_{\shortparallel} v_z t + n\Omega t - \omega t) ,$$

(4.28)

we find

$$D = \left(\frac{e k_{\shortparallel} \Phi}{m}\right)^2 \frac{\pi}{2 k_{\shortparallel}} \sum_{h=-\infty}^{\infty} J_h^2(k_\perp \rho) \; \delta\left(k_n v_z + n\Omega - \omega\right) \quad .$$

(4.29)

This result, which exhibits the well-known resonance singularity of quasilinear theory, is is not quite suitable as it stands for our purposes. The problem comes about because we have taken no account of the change in v_z which occurs in the electron motion. To account for this change, we may use a simple and intuitively appealing "resonance-broadening" scheme due to Dupree.[50] If we neglect the variation of D during one electron autocorrelation time, it follows that

$$\overline{(\Delta v)^2}(t) = 2Dt ,$$

$$\overline{(\Delta z)^2}(t) = 2Dt^3/3 \quad .$$

Hence, the electrons have a correlation time approximately equal to $(3/k_{\shortparallel}^2 D)^{1/3}$, just as in the case of parallel-propagating waves. If we neglect non-linearities in $\dot{\theta}$, which should be valid since $\phi \ll 1$.

Eq. (4.29) becomes

$$D = \int_0^\infty d\tau \, \langle \dot{v}_z(t) \, \dot{v}_z(t+\tau) \rangle$$

$$= \left(\frac{e k_{\shortparallel} \Phi}{m} \right)^2 \frac{1}{2} \sum_{h=-\infty}^{\infty} J_h^2(k_\perp \rho) \, \langle \sin[k_{\shortparallel} z(t) + h\Omega t - \omega t]$$

$$\sin[k_{\shortparallel} z(t+\tau) + h\Omega(t+\tau) - \omega(t+\tau)] \rangle \, d\tau$$

(4.30)

$$\doteq \left(\frac{e k_{\shortparallel} \Phi}{m} \right)^2 \frac{1}{2} \sum_{h=-\infty}^{\infty} J_h^2(k_\perp \rho) \int_0^\infty d\tau \, \exp(-k_{\shortparallel}^2 D \tau^3 / 3) \cos[(k_{\shortparallel} v_z + h\Omega - \omega)\tau]$$

$$= \left(\frac{e k_{\shortparallel} \Phi}{m} \right)^2 \frac{1}{2} \sum_{h=-\infty}^{\infty} J_h^2(k_\perp \rho) \left(\frac{\pi}{2 D^{1/3}} \left\{ Hi\left[\frac{i(k_{\shortparallel} v_z + h\Omega - \omega)}{D^{1/3}} \right] + Hi\left[\frac{-i(k_{\shortparallel} v_z + h\Omega - \omega)}{D^{1/3}} \right] \right\} \right),$$

where Hi(x) is an Airy function.[53] In effect, we see that the delta

functions in Eq. (4.29) are broadened into resonances with widths

approximately equal to $\omega_b / k_{\shortparallel}$, consistent with the widths calculated

assuming that the resonances are well-separated.

In principal, Eqs. (4.24) and (4.30) together determine the dis-

tribution function evolution and the resultant change in the electro-

static amplitude; however, because Eq. (4.30) is an implicit equation

for D, these equations are not simple to solve. Moreover, there is

little point in doing so, since the equations are expected to be only

qualitatively valid. Instead, we approximate Eq. (4.30) at each value

of ζ_m by averaging Eq. (4.30) over the region in velocity space where

resonances overlap. This approximation leads to equations which are

simple to solve and provide insight into the physical issues involved

in the wave evolution. Similar approximations have been used by

Dupree[50] and Stix.[12]

Normalizing D by v_t^2 and averaging Eq. (4.30), we find

$$\bar{D} = \frac{1}{2w} \int_{-w}^{w} d\nu \, D = \frac{1}{v_t^2} \left(\frac{e k_{\shortparallel} \phi}{m} \right)^2 \frac{\pi}{4 k_{\shortparallel} w} \sum_n J_n^2 (k_{\perp} \rho) , \qquad (4.31)$$

where the sum of Bessel functions is over resonances in the stochastic region. Noting that almost all the resonances which make significant contributions to the sum are in this region, we find

$$\sum_{n = \infty}^{\infty} J_n^2 (k_{\perp} \rho) = 1 , \qquad (4.32)$$

and Eq. (10) becomes

$$\bar{D} = \begin{cases} (k_{\shortparallel} v_t) \dfrac{\pi \phi^2}{4 w} , & |\nu| < w \\[4mm] 0 , & |\nu| > w \end{cases} \qquad (4.33)$$

where w has been normalized to the thermal velocity. As noted previously, there are expected to be large regular regions in velocity space at the edge $\nu = -w$, where most of the electrons are initially located. These regular regions impede the distribution function evolution, and hence, the use of Eqs. (4.24) and (4.33) is certain to overestimate the rate at which the distribution function approaches saturation.

4.5 Solution of the Diffusion Equation

Given the diffusion coefficient shown in Eq. (4.33), Eq. (4.26) becomes

$$\frac{\partial f_0}{\partial t} - \bar{D} \frac{\partial^2 f_0}{\partial \nu^2} = 0 . \tag{4.34}$$

Recalling that our initial distribution has the form

$$f_0 (t = 0) = A(\gamma_m) \tilde{f} (t=0) , \tag{4.35}$$

where

$$A(\gamma_m) = \left(\frac{m}{2\pi T}\right)^{3/2} \exp\left[-(u^2 + \gamma_m^2)/2\right] , \tag{4.36a}$$

$$\tilde{f} (t=0) = \exp(-\nu u) . \tag{4.36b}$$

Eq. (4.34) becomes

$$\frac{\partial \tilde{f}}{\partial t} - \bar{D} \frac{\partial^2 \tilde{f}}{\partial \nu^2} = 0 . \tag{4.37}$$

The general solution of Eq. (4.37) may be written in the form

$$\tilde{f} = a_0 + \sum_{n=1}^{\infty} a_n \exp\left(-\gamma_n^{(1)}(t)\right) \cos(A_n \nu)$$

$$+ \sum_{n=1}^{\infty} b_n \exp\left(-\gamma_n^{(2)}(t)\right) \sin(B_n \nu) . \tag{4.38}$$

The coefficients A_n and B_n have to be chosen to satisfy the boundary condition

$$\frac{\partial \tilde{f}}{\partial \nu}\bigg|_{y = \pm w} = 0 , \qquad (4.39)$$

whence

$$A_n = \frac{n\pi}{w} , \qquad B_n = \frac{(2n-1)\pi}{2w} . \qquad (4.40)$$

Substituting Eq. (13) into Eq. (12), we find

$$\gamma_n^{(1)} = \frac{n^2 \pi^2}{w^2} \bar{D} , \qquad \gamma_n^{(2)} = \frac{(2n-1)^2 \pi^2}{4 w^2} \bar{D} . \qquad (4.41)$$

It only remains now to calculate the coefficients a_n and b_n. Fourier decomposing Eq. (4.36b), we conclude

$$a_0 = \frac{1}{2uw} \left[\exp(uw) - \exp(-uw) \right] ,$$

$$a_n = \frac{(-1)^{(n-1)}}{w} \frac{u}{u^2 + \frac{n^2 \pi^2}{w^2}} \left[\exp(uw) - \exp(-uw) \right] , \qquad (4.42)$$

$$b_n = \frac{(-1)^n}{w} \frac{u}{u^2 + \frac{(2n-1)^2 \pi^2}{4w^2}} \left[\exp(uw) + \exp(-uw) \right] .$$

In order to determine the change in the wave amplitude, we must calculate the change in the distribution function's momentum, which can be done conveniently in the wave frame. The cosine components carry no

81

momentum since they are symmetric about the point $\nu = 0$; only the sine components contribute to the momentum change. Noting that

$$P_h = \int_{-w}^{w} \nu \sin\left[\frac{(2h-1)\pi}{2w}\nu\right] d\nu = (-1)^{h-1} 8 \left[\frac{w}{(2h-1)\pi}\right]^2 , \qquad (4.43)$$

the momentum as a function of time may be written

$$p(t) = \sum_{h=1}^{\infty} b_h P_h \exp(-\gamma_h t) = -\frac{8wu}{\pi^2} \sum_{h=1}^{\infty} \frac{1}{(2h-1)^2} \frac{\exp(-\gamma_h t)}{u^2 + \frac{(2h-1)^2 w^2}{4\pi^2}} , \quad (4.44)$$

where the superscript (2) has been dropped from γ_n. At $t = 0$, the series may be explicitly summed, using a method described by Morse and Feshbach,[54] to yield

$$p(o) = -\frac{w}{u}\left[\exp(wu) + \exp(-wu)\right] + \frac{1}{u^2}\left[\exp(wu) - \exp(-wu)\right] , \qquad (4.45)$$

whence

$$\delta p(t) = p(t) - p(o) = \frac{w}{u}\left[\exp(wu) + \exp(-wu)\right]$$

$$-\frac{1}{u^2}\left[\exp(wu) - \exp(-wu)\right] - \frac{8wu}{\pi^2} \sum_{h=1}^{\infty} \frac{1}{(2h-1)^2} \frac{\exp(-\gamma_h t)}{u^2 + \frac{(2h-1)^2 w^2}{4\pi^2}} . \qquad (4.46)$$

Recalling the momentum equation

$$k_{\parallel}\left(\frac{\partial \varepsilon_r}{\partial \omega}\right) \frac{d E_0^2 / 16\pi}{dt} = \frac{d}{dt}\int d^3\nu \, n_0 m \nu_z f_0(\underset{\sim}{\nu}, t) , \qquad (4.47)$$

82

and the form of the distribution function shown in Eqs. (4.35) and (4.36), we conclude

$$R(t) = \frac{\delta \varphi^2(t)}{\varphi^2} = \sqrt{\frac{8}{\pi}} \frac{\alpha^2}{\varphi^2} u \left(u \frac{\partial \varepsilon_r}{\partial u}\right)^{-1} \exp(-u^2/2)$$

$$\int_0^\infty \zeta_m \, d\zeta_m \, \exp(-\zeta_m^2/2) \, \delta p(t) \, , \tag{4.48}$$

where $\phi \equiv \phi(t = 0)$.

The solution to Eq. (4.48) is quite simple to calculate numerically, but, before doing so, it is worthwhile to discuss some of its qualitative features. Recalling from Eqs. (4.33) and (4.41) that

$$\gamma_h t = \frac{(2h-1)^2 \pi^2}{4 w^2} \bar{D} t = \frac{(2h-1)^2 \pi^3 \varphi^2}{16 w^3} (k_\shortparallel v_t) t \, , \tag{4.49}$$

and noting that the bounce frequency ω_b may be written

$$k_\shortparallel (e \Phi/m)^{1/2} = (k_\shortparallel v_t) \varphi^{1/2} \, ,$$

we find

$$\gamma_h t = \frac{(2h-1)^2 \pi^3 \varphi^{3/2}}{16 w^3} (\omega_b t) \, . \tag{4.50}$$

We observe that the diffusion time depends strongly on w, increasing rapidly as w increases. One power of w is due to the decrease of the power in the individual Bessel functions as w increases, and the other two powers are due to the greater distance that electrons have to diffuse in velocity space. Noting that w increases with increasing ζ_m as shown in Fig. 4.6a, we conclude that the diffusion time should

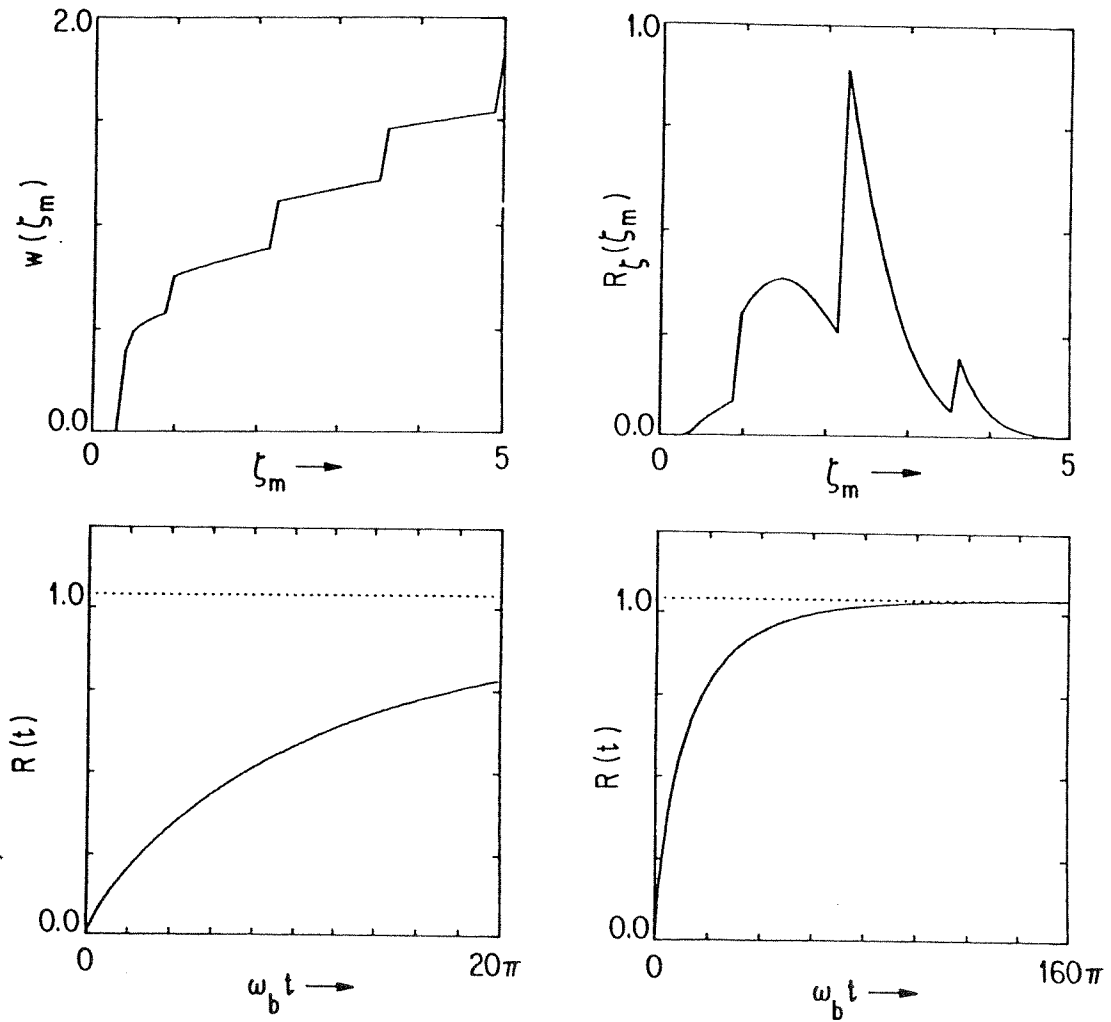83

Fig. 4.6   Quantities relating to   the calculation of R(t).   a)   the

width of the stochastic region vs. ζ_m, b) R_ζ vs. ζ_m,

c) R(t) between t = 0 and t = $10\tau_b$, and d) R(t) between t = 0

and t = $80\tau_b$.

increase rapidly with increasing ζ_m. This result is confirmed in the simulations in Chapter 6. We further note that the diffusion time scales as ϕ^{-2}; whereas, the bounce time scales as $\phi^{-1/2}$. Since we are interested in the limit $\phi \leq 0.1$, it follows that the diffusion time will be long compared to the bounce time. Shown in Fig. 4.6d is R_ζ, where $R_\zeta d\zeta_m$ is the contribution of electrons between ζ_m and $\zeta_m + d\zeta_m$ to R.

$$ R_\zeta = \sqrt{\frac{\pi}{8}} \frac{\alpha^2 u}{\varphi^2} \left(u \frac{\partial \varepsilon_r}{\partial u} \right)^{-1} exp \left[-\left(u^2 + \zeta_m^2 \right) / 2 \right] $$

$$ \left\{ \frac{w}{u} \left[exp(wu) + exp(-wu) \right] - \frac{1}{u^2} \left[exp(wu) - exp(-wu) \right] \right\} . \tag{4.51} $$

We see that R_ζ peaks at about $\zeta_m = 2.3$, at which point $w \simeq 1.2$. Substituting this value of w into Eq. (4.50), along with $\phi = 0.05$, we find that the time for the n = 1 contribution to R(t) to go through two e-folds, at which point R(t) should be close to saturation, is $\omega_b t = 92$, which is about 15 bounce periods. The saturation time calculated here is a lower limit, and the simulation results in Chapter 6 indicate that the saturation time is actually much longer. By comparison, the saturation time in the trapping regime is at most about five bounce periods.

The solution to Eq. (4.48) is shown in Figs. 4.6c and 4.6d for ten bounce periods and 80 bounce periods. We see that R(t) rises monotonically with an ever-decreasing slope. This smooth rise is confirmed in the simulations in Chapter 6, and is in marked contrast to the results in the trapping regime.

5. NUMERICAL SIMULATIONS

5.1 Description of the Method

In order to test various aspects of the theory presented in this thesis, as well as to determine the time evolution of the wave in the stochastic regime with greater accuracy than was done in Section 4.5, we have run a series of "mini-simulations;" electrons in a small region of velocity space are followed numerically, while elsewhere in velocity space, the electrons are assumed to respond linearly to the wave and are treated analytically. This approach has been used before in studying the beam-plasma problem[38] and the parallel-propagating wave.[33,39] In both these cases, there is only one resonant velocity, so that the division into resonant and non-resonant regions is fairly simple. In the case of the obliquely propagating wave studied here, there are infinitely many resonances, and this division is considerably more delicate.

In this chapter, we discuss two types of simulations. The first is non-self-consistent: The amplitude of the wave is kept fixed at its initial value when determining the particle trajectories, and the change in the field is determined from the momentum equation derived in Appendix A,

$$-k_{\parallel} \frac{\partial \varepsilon_r}{\partial \omega} \, \delta \frac{E_o^2}{16\pi} = \delta P_z \ , \tag{5.1}$$

where P_z is the z-momentum of the simulation electrons. This approach mirrors the theory of Chapters 3 and 4, where the field was also held at its initial value in determining the distribution function evolution, and is useful for examining the validity of the assumption made in Chapter 4 that the distribution function is asymptotically flattened in the resonant regions. Since the field is held fixed, separate regions in velocity space (and in fact individual particles) have no influence on one another, and the total $\delta\phi^2$ is just the sum of the contributions to $\delta\phi^2$ from the separate regions. We can thus determine the electron response in the region surrounding an individual resonance without the necessity of following electrons from other regions, allowing us to make a resonance-by-resonance comparison with the trapping regime calculations.

The second approach used is self-consistent. The change in momentum is used to modify the field amplitude at every time step. This approach differs from a full particle simulation in that the possibility that new modes are generated is ignored. In non-self-consistent simulations, the linear part in the momentum change of the simulation particles is zero, because the change in the field experienced by the particles is zero. By contrast, in self-consistent simulations, there is a linear part in the momentum change of simulation particles which must be compensated for. So, as discussed in Appendix A, the momentum equation becomes

$$-k_{\parallel}\left(\frac{\partial \varepsilon_r}{\partial \omega} - \frac{\partial \chi_{ir}}{\partial \omega}\right)\delta\frac{E_0^2}{16\pi} = \delta P_z \quad , \tag{5.2}$$

87

where χ_{1r} is the real part of the linear susceptibility in the region of velocity-space being simulated. In order to use this approach, it must be possible to include in the region of velocity-space being simulated all parts of the distribution function which contribute significantly to the non-linear wave evolution. As the region to be simulated increases, noise due to our use of a finite number of particles, rather than a Vlasov fluid, will eventually overwhelm the effects we wish to observe, placing a limit on the size of the region which can be simulated. In the trapping regime, it turns out that the important resonances are spread throughout the distribution function, and the fraction of the distribution function that would have to be kept in a self-consistent simulation is too large to be feasible using a mini-simulation technique. However, in the stochastic regime, the important resonances are clustered in the neighborhood of the phase velocity, and self-consistent simulations are feasible. By comparing the self-consistent simulation results to those of the non-self-consistent calculations, we can determine the extent to which self-consistent effects reduce the total damping of the wave.

In order to compare the results of this chapter directly with those of Chapter 4, we define a quantity $R(t) \equiv \delta\phi^2/\phi^2$, where $\phi \equiv \phi(t = 0)$. For the non-self-consistent simulations, Eq. (5.1) yields

$$R(t) \approx \frac{2\alpha^2 u}{\phi^2} \left(u \frac{\partial \varepsilon_r}{\partial u} \right)^{-1} \delta p_z \ ,$$

(5.3)

and for the self-consistent simulations, Eq. (5.2) yields

$$R(t) = \frac{2\alpha^2 u}{\varphi^2} \left(u \frac{\partial \varepsilon_r}{\partial u} - u \frac{\partial \chi_{1r}}{\partial u} \right)^{-1} \delta p_z \; , \tag{5.4}$$

where $p_z \equiv P_z / mv_t$ is the normalized momentum calculated in the simulations.

As noted at the beginning of Chapter 3, an electron's position and velocity are specified by four independent variables, which are chosen here to be $\psi \equiv k_{||}z + k_{\perp}y$, $\theta \equiv \tan^{-1}(-v_x/v_y)$, $\zeta \equiv v_{\perp}/v_t$, and $\nu \equiv (v_z - v_p)/v_t$. Thus, we have a four dimensional phase space to fill, in contrast to the parallel-propagating wave problem, where phase space is only two dimensional. In this latter problem, it has been found that about four thousand particles must be used to obtain good results, and if we directly scaled this result to four dimensions, we would conclude that we need sixteen million particles, well beyond the capacity of most modern simulations. Of course, we can do much better than this simple scaling suggests by suitably randomizing the initial particle locations, but phase space granularity and the resultant noise remains a problem. The technique we have used of loading particles into only a small region of velocity space allows us to reduce this noise considerably.

The initial coordinates of the particles to be simulated were chosen as follows: First, we select the number of different values in each dimension, N_ψ, N_θ, $N_\perp$, and $N_{||}$. The total number of particles, N, equals $N_\psi N_\theta N_\perp N_{||}$. Values for ν and ζ are chosen using one of two

algorithms. The first uses an equal weight scheme in which we first

pick the boundaries, $\ell \equiv v_{zi}/v_t$ and $s \equiv v_{zf}/v_t$, where v_{zi} and v_{zf} are

respectively the lower and upper z-velocities of the region in vel-

ocity-space to be simulated. Since we wish to approximate a Maxwel-

lian distribution, we choose the $N_{\shortparallel}$ values of ν, namely $\nu = \nu_h$, $h = 1$,

$2,\ldots,$ $N_{\shortparallel}$ such that

$$
\frac{\displaystyle\int_{\ell-u}^{\nu_h} d\nu \, \exp\left[-\tfrac{1}{2}(\nu+u)^2\right]}{\displaystyle\int_{\ell-u}^{s-u} d\nu \, \exp\left[-\tfrac{1}{2}(\nu+u)^2\right]} = \frac{\mathrm{erf}\left(\frac{u+\nu_h}{\sqrt{2}}\right) - \mathrm{erf}\left(\frac{\ell}{\sqrt{2}}\right)}{\mathrm{erf}\left(\frac{s}{\sqrt{2}}\right) - \mathrm{erf}\left(\frac{\ell}{\sqrt{2}}\right)} = \frac{h-1}{N_{\shortparallel}} \, . \tag{5.5}
$$

This choice spaces the particles in ν such that each simulation par-

ticle represents the same fraction of real electrons. Similarly, we

choose the $N_{\perp}$ values ζ_i of ζ, $i = 1$, $2,\ldots,$ $N_{\perp}$ such that

$$
\frac{\displaystyle\int_{0}^{\gamma_i} \gamma d\gamma \, \exp\left(-\tfrac{1}{2}\gamma^2\right)}{\displaystyle\int_{0}^{\infty} \gamma d\gamma \, \exp\left(-\tfrac{1}{2}\gamma^2\right)} = \exp\left(-\tfrac{1}{2}\gamma_i^2\right) = \frac{2i-1}{2N_{\perp}} \, . \tag{5.6}
$$

At each time, to calculate p_z, we use

$$
p_z = \frac{\left[\,\mathrm{erf}\left(\frac{s}{\sqrt{2}}\right) - \mathrm{erf}\left(\frac{\ell}{\sqrt{2}}\right)\,\right]}{N} \sum_{h=1}^{N} \nu_h(t) \quad , \tag{5.7}
$$

where ν_n is the ν-value of the nth particle at time t; the fraction

of the distribution function being simulated is $[\mathrm{erf}(s/\sqrt{2}) - \mathrm{erf}(\ell/\sqrt{2})]$,

so that the fraction of the distribution contributed by each simulation

particle is $[\mathrm{erf}(s/\sqrt{2}) - \mathrm{erf}(\ell/\sqrt{2})]/N$. The second algorithm is a Max-

wellian weight scheme. As before, we first pick the boundaries s and

ℓ. We then choose the ν and ζ-values such that

$$\nu_h = (\ell - u) + \left(\frac{h-1}{N_{\parallel}-1}\right)(s-\ell),$$

$$\zeta_i = \left(\frac{2i-1}{2N_{\perp}}\right)5,$$

(5.8)

where the value 5 is chosen as the upper bound for the ζ_i's because beyond $5v_t$, the electron distribution function is quite small. Additionally, we define a particle weight

$$W_{hi} = \sqrt{\frac{2}{\pi}}\,\zeta_i\,\exp\left\{-\left[\zeta_i^2 + (\nu_h + u)^2\right]\right\},$$

(5.9)

and, in accordance with the trapezoidal rule, multiply this weight by one-half if $h = 1$ or $h = N_{\parallel}$. The momentum is then calculated at each time step using the formula

$$p_z = \frac{N_{\parallel}}{N_{\parallel}-1}\,\frac{5(s-\ell)}{N}\,\sum_h W_h \nu_h(t).$$

(5.10)

No matter which algorithm we use, the θ-values are chosen so that

$$\theta_j = \frac{2\pi(j-1)}{N_\theta} + \frac{\theta_{hi}}{N_\theta}$$

(5.11)

where $j = 1, 2, \ldots, N_\theta$ and θ_{hi} is a random number chosen between 0 and 2π for each h,i combination. Similarly, the ψ-values are chosen so that

$$\psi_k = \frac{2\pi(k-1)}{N_\psi} + \frac{\psi_{hij}}{N_\psi},$$

(5.12)

where ψ_{hij} is a random number chosen between 0 and 2π for each h,i,j combination.

The final answer should not depend on the particle initialization, assuming that velocity space is filled densely enough to adequately simulate a Maxwellian distribution, and to verify this, we ran many of the results presented in this chapter with different initializations, i.e., with different choices of $N_{||}$, $N_{\perp}$, N_{θ}, and N_{ψ} and with the two different weighting schemes. All the simulations were run with 4096 particles, and a standard leapfrog algorithm was used to advance the particle coordinates. The simulations were run in the wave-frame, so that the shortest fundamental time appearing is $\min[\Omega^{-1}, |k_{||}v_{zi}-\omega|^{-1}, |k_{||}v_{zf}-\omega|^{-1}]$, where the second and third elements are respectively the time for particles at the lower and upper boundaries to pass through one wavelength. We chose our time-step such that $\Delta\tau = (k_{||}v_t)\Delta t = 0.2 \min[\kappa_{||}^{-1}, |\ell-u|^{-1}, |s-u|^{-1}]$. There are two sources of noise in these simulations. The first is the phase space granularity mentioned previously. The noise is strongest at a frequency near $\omega - k_{||}v_{zi}$ because particles are concentrated near this boundary in the equal weight simulation or are heavily weighted near this boundary in the Maxwellian weight simulation. As v_{zi}, or equivalently ℓ, is lowered, the fraction of the distribution function included in the simulation increases rapidly and so does the noise, setting an effective lower limit of $\ell = 3.0$. A second source of noise is the transient which occurs at $t = 0$ when the field is "turned on." Because only part of the plasma is being simulated, the transient phase mixes slowly relative to full particle simulations and is strongly visible in the simu-

lation of Landau damping shown in Fig. 5.1. The transient's frequency

of oscillation is approximately equal to $\omega - k_{\parallel}v_{zi}$, just like the noise

due to granularity. This transient is evidently a major perturbation

on the short time scale of Landau damping; on the long time scales of

the non-linear phenomena in which we are interested, it fortunately

turns out not to have much importance, except for a spurious initial

jump which it causes in $R(t)$.

Since the noise fluctuations occur at frequencies much higher

than those of the non-linear phenomena, we were able to almost com-

pletely eliminate these fluctuations by filtering our simulation data.

We Fourier-transformed the data, multiplied it by a Gaussian

$\exp(-\omega^2/\omega_0^2)$, and then inverse-transformed; this procedure is equiva-

lent to convolving our unfiltered data with a Gaussian. The cutoff

frequency ω_0 must evidently be chosen with case in each particular

case, so as not to affect the phenomena in which we are interested.

The effectiveness of this filtering is evident in Fig. 5.2, where we

have simulated the amplitude oscillations of a parallel-propagating

wave. There is excellent agreement between the filtered data in Fig.

5.2.c and the theoretical results in Fig. 5.2.a; whereas, the unfil-

tered data in Fig. 5.2.b looks quite different from the theory. The

results of a filtered, self-consistent simulation are shown in Fig.

5.2.d; both the expected decrease in the peak of $R(t)$ and increase

in the period of oscillation are observed.

Another example of this filtering is shown in Fig. 5.3 for an

obliquely propagating wave in the stochastic regime. The dotted line

shows $R(t)$ calculated from linear theory, which should be the same as
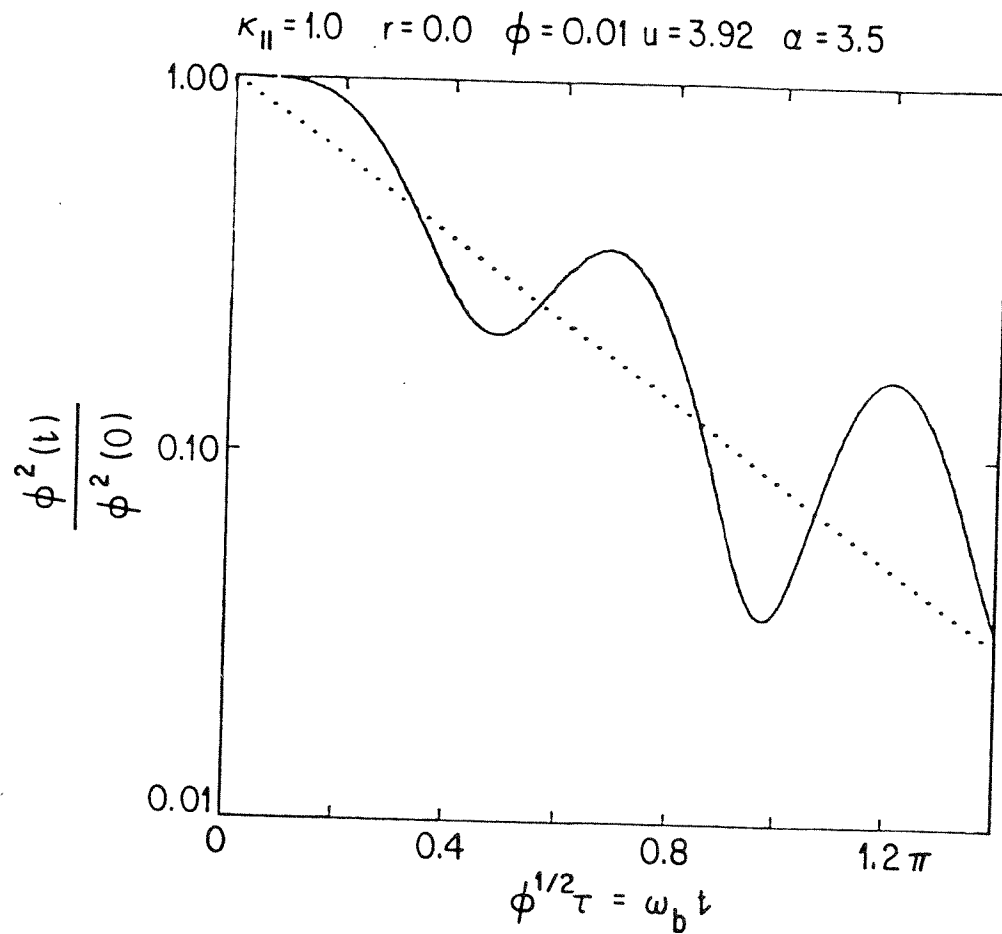
Fig. 5.1 A linearly damping wave plotted on a log scale vs. time.
The solid line shows the simulation results and the dashed
line the usual theoretical result.

$\kappa_\parallel = 1.0$ $r = 0.0$ $\phi = 0.05$ $u = 3.92$ $\alpha = 3.5$
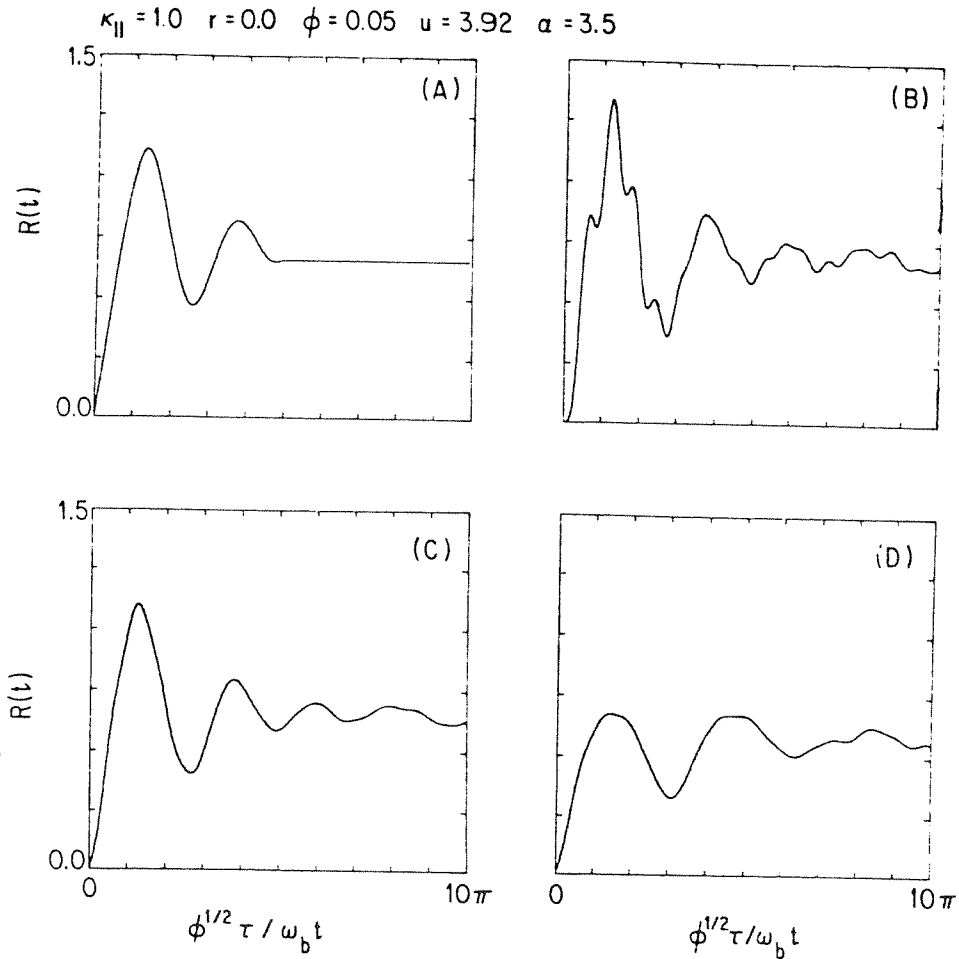
Fig. 5.2   Wave variation in the trapping regime.   The effect of fil-
           tering is shown.   a) theoretical result, b) unfiltered
           simulation result, c) filtered simulation result, d) result
           of a filtered, self-consistent simulation.

95

$\kappa_\parallel = 3.0$ $r = 0.05$ $u = 4.98$ $\alpha = 4.5$
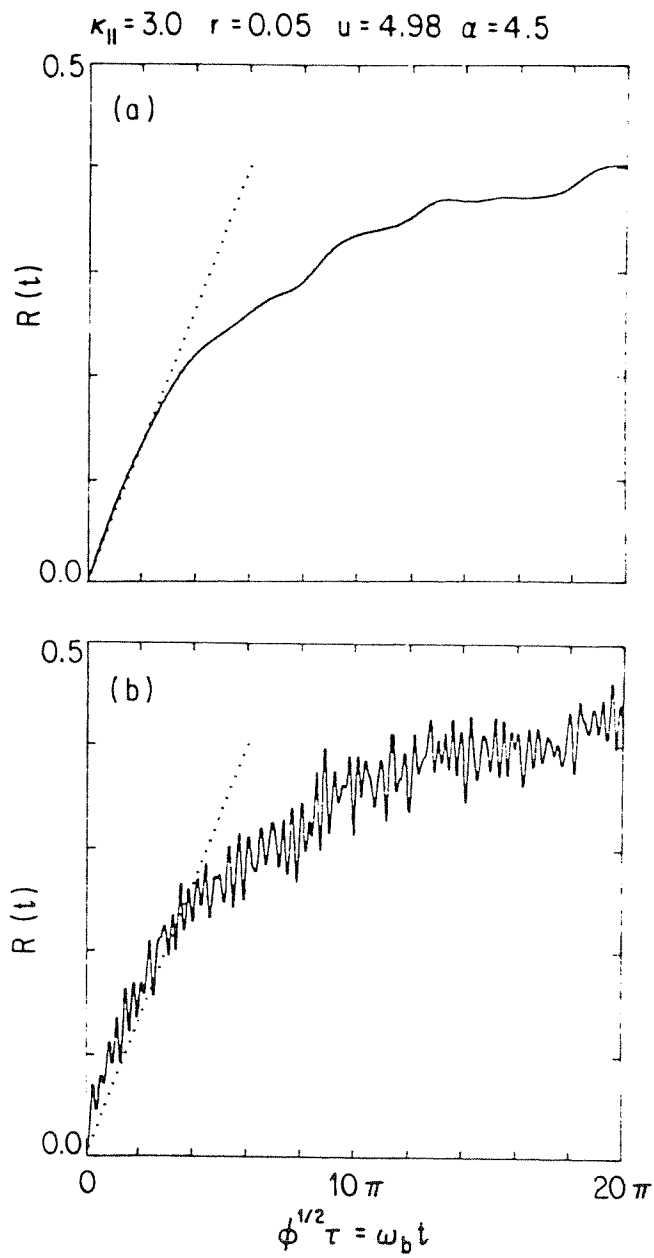
Fig. 5.3 Wave variation in the stochastic regime. a) filtered, b) unfiltered. The dotted line shows the linear variation.

the R(t) observed in the simulation near t = 0. Before filtering, the two results look different because of the transient at t = 0, but, after filtering, they appear quite similar.

5.2 Results

In this chapter, we are primarily interested in checking the theoretical results of Chapters 3 and 4, and accurately determining the time evolution in the stochastic regime. One result is already apparent in Fig. 5.3. Saturation of R(t) occurs on a long time scale. R(t) is still increasing even after ten bounce periods, $10\tau_b$; whereas, we recall from Chapter 3 that in the trapping regime, the wave saturates after about $5\tau_b$. We also see that R(t) continues to rise monotonically, at an ever-decreasing rate; whereas, in the trapping regime R(t) varies much less smoothly and at times actually decreases.

In all the cases discussed in this section, we set r = 0.25, ϕ = 0.05, and u = 4.98 (α = 4.5) and varied $\kappa_{_{11}}$. The results of calculating R $\equiv$ R(∞) for these cases, using Eq. (4.17), are shown in Fig. 4.4b and are repeated as the solid line in Fig. 5.4. All our self-consistent simulations were done with the boundaries set at ℓ = 3.5 and s = 5.5. If we calculate R using Eq. (4.17) but only keeping resonances within these boundaries, we obtain the result shown with a dashed line in Fig. 5.4; the jump shown at $\kappa_{_{11}}$ = 1.33 is due to the n = 2 resonance crossing into the region being considered. Comparing the solid and dashed lines, we see that in the stochastic regime almost the entire contribution to R comes from inside the region being simulated, and it is reasonable to assume that particle behavior is
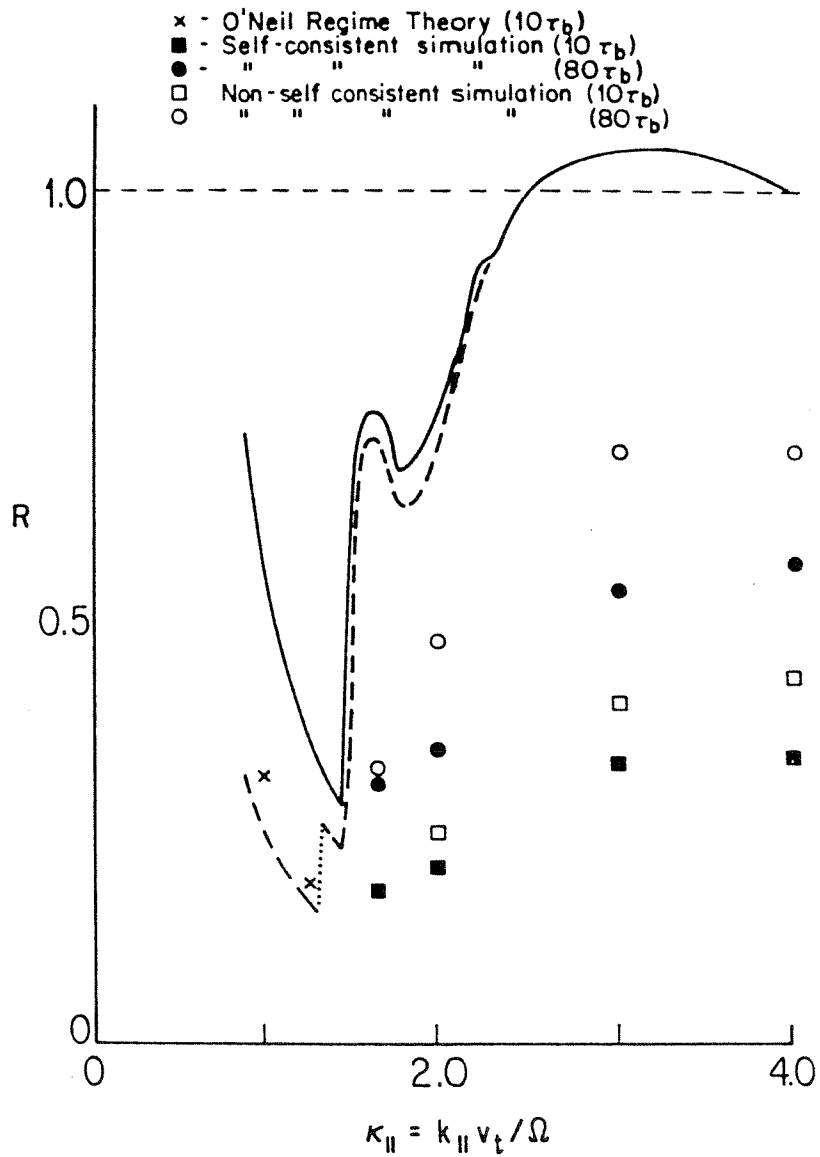
Fig. 5.4 $R \equiv R(\infty)$ vs. $\kappa_{\shortparallel}$. The solid line shows the asymptotic total damping keeping all resonances and is the same as Fig. 4.4b. The dashed line shows the contribution to R from resonances in the range $3.5 < v_z/v_t < 5.5$. The points show the results of particular simulations.

is nearly linear outside this region, allowing us to do self-consistent

simulations. In the trapping regime, significant contributions to R

come from outside the region $\ell < \nu < s$, and self-consistent simulations

are not possible. Non-self-consistent simulations, however, give useful

information in this regime.

The points in Fig. 5.4 summarize the results of a number of simu-

lations of various lengths, both self-consistent and non-self-consistent,

which are described in detail in the following paragraphs.

Shown in Fig. 5.5 are the results when $\kappa_{||} = 1.0$. Fig. 5.5.a shows

the theoretically calculated total damping, as well as the amounts which

the separate resonances contribute to it. Fig. 5.5.b shows the resonance

structure when $\kappa_{||} = 1.0$. Shown in the first half of Fig. 5.5.c is $R_0(t)$,

the theoretically calculated contributions of the $n = 0$ resonance to $R(t)$

using the methods of Chapter 3; shown in the second half is a simulation

in which the boundaries were taken at $\ell = 4.5$ and $s = 5.5$, so that only

the $n = 0$ resonance contributes. The theoretical and simulation results

compare quite well, except that the non-linear phase-mixing of the amp-

litude oscillations occurs considerably more slowly than the trapping

regime theory predicts, due to our having cut off the boundaries at

finite values rather than at infinity. In Fig. 5.5.d, the theoretical

and simulation values of $R_1(t)$ are compared. Once again, there is little

difference except for the slow phase-mixing of the simulation results.

Shown in Fig. 5.6 are similar results with $\kappa_{||} = 1.25$. The simu-

lation results for $R_0(t)$ were calculated with $\ell = 4.6$ and $s = 5.4$, and

the simulation results for $R_1(t)$ were calculated with $\ell = 3.8$ and $s =$

4.6. The tightness of the boundaries have affected the results for

Fig. 5.5   Contribution of specific resonances to R(t) when $\kappa_{\shortparallel} = 1.0$.

a)   contribution of four of the resonances to R(t), b) resonance structure, c) the theoretical and simulation calculations of $R_0(t)$, and d) the theoretical and simulation calculation of $R_1(t)$.
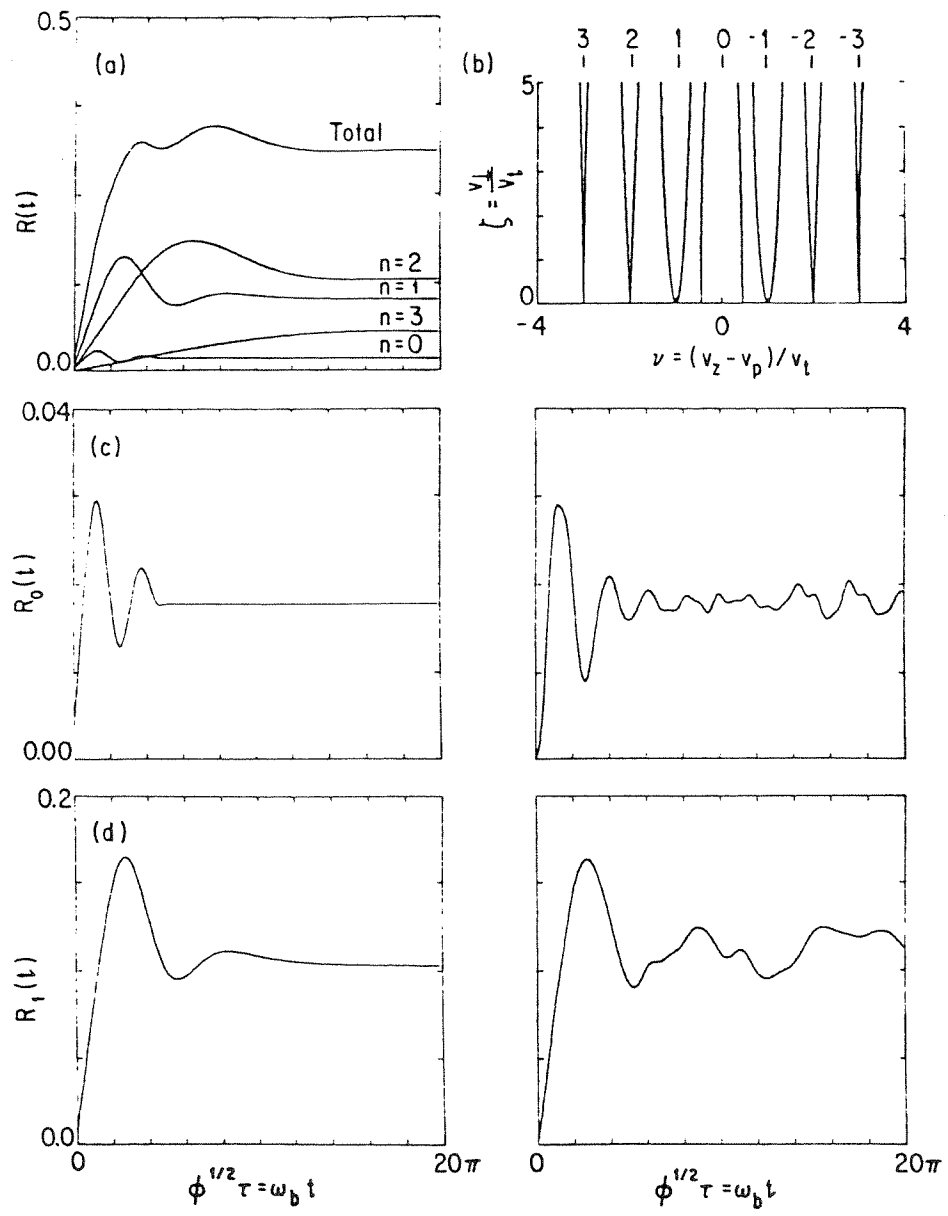
Fig. 5.6   Contribution of specific resonances to R(t) when $\kappa_{||}$ = 1.25

a)   contribution of four of the resonances to R(t), b)

resonance structure, c) the theoretical and simulation

calculations of $R_0(t)$, and d) the theoretical and simula-

tion calculation of $R_1(t)$.

$R_0(t)$ quite a bit, leading to a decrease in the amplitude oscillations as well as slow phase-mixing, but there is still no sign, such as an increase in $R_1(t)$ due to diffusive particle motion, that stochasticity has set in. By contrast, when $\kappa_{\shortparallel} = 1.67$ the onset of stochasticity is quite apparent in Fig. 6.7 where the simulated $R_1(t)$ continually rises as opposed to the theoretical $R_1(t)$ which has saturated by $5\tau_b$.

For $\kappa_{\shortparallel} = 1.67$, Fig. 5.4 indicates that we may run self-consistent simulations with the boundaries set at $\ell = 3.5$ and $s = 5.5$ since the total damping obtained by just including resonances within these boundaries (dashed curve) is almost the same as the total damping including all resonances (solid curve). Figure 5.8 shows the results of running both self-consistent and non-self-consistent simulations with these boundaries. In this case, R(t) is always small enough so that self-consistant effects make little difference in the final results. In addition to the simulations of length $10\tau_b$, we ran simulations of length $80\tau_b$. Eighty bounce periods is far too long to be observed in present-day experimental devices, as discussed in Chapter 7, but it could be observed in some full particle simulations. Even after this large amount of time, R(t) still has not saturated, and its derivative with time is still steadily decreasing, if statistical fluctutations are ignored. It should be noted that at $10\tau_b$, R(t) is already about one-and-a-half times as the O'Neil theory prediction shown in Fig. 5.7.a, indicating a significant increase in total damping due to the onset of stochasticity.

In Figs. 5.9-11, similar results are shown for $\kappa_{\shortparallel} = 2.0$, 3.0, 4.0. Comparing Figs. 5.8-11, we see that at any given time R(t) increases monotonically with $\kappa_{\shortparallel}$ from $\kappa_{\shortparallel} = 1.67$ to $\kappa_{\shortparallel} = 3.0$ but it unchanged as $\kappa_{\shortparallel}$ goes from 3.0 to 4.0, indicating a saturation with respect to $\kappa_{\shortparallel}$.
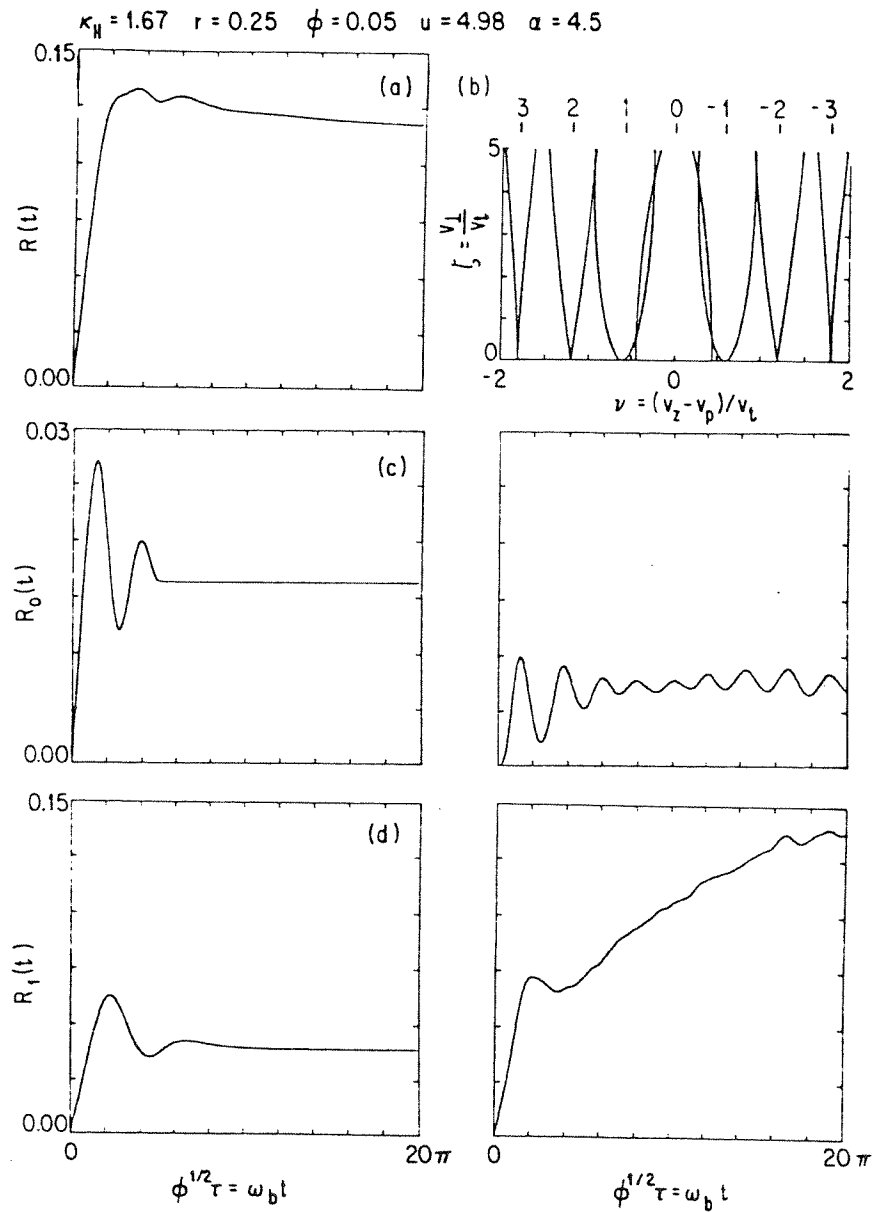
Fig. 5.7 Contribution of specific resonances to R(t) when $\kappa_{\shortparallel} = 1.67$.
a) R(t) vs. time, b) resonance structure, c) the theoretical
and simulation calculations of $R_0(t)$, and d) the theoretical
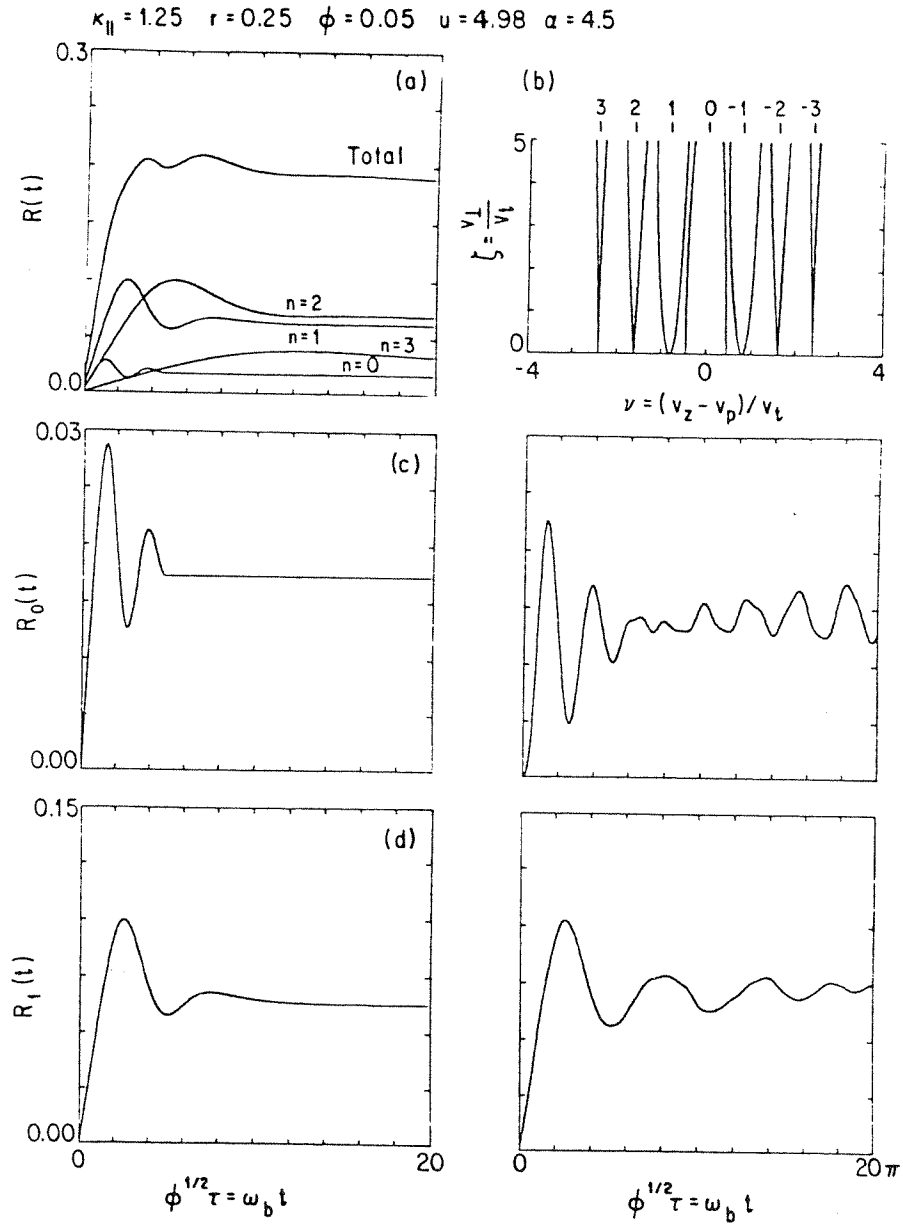and simulations calculations of $R_1(t)$.
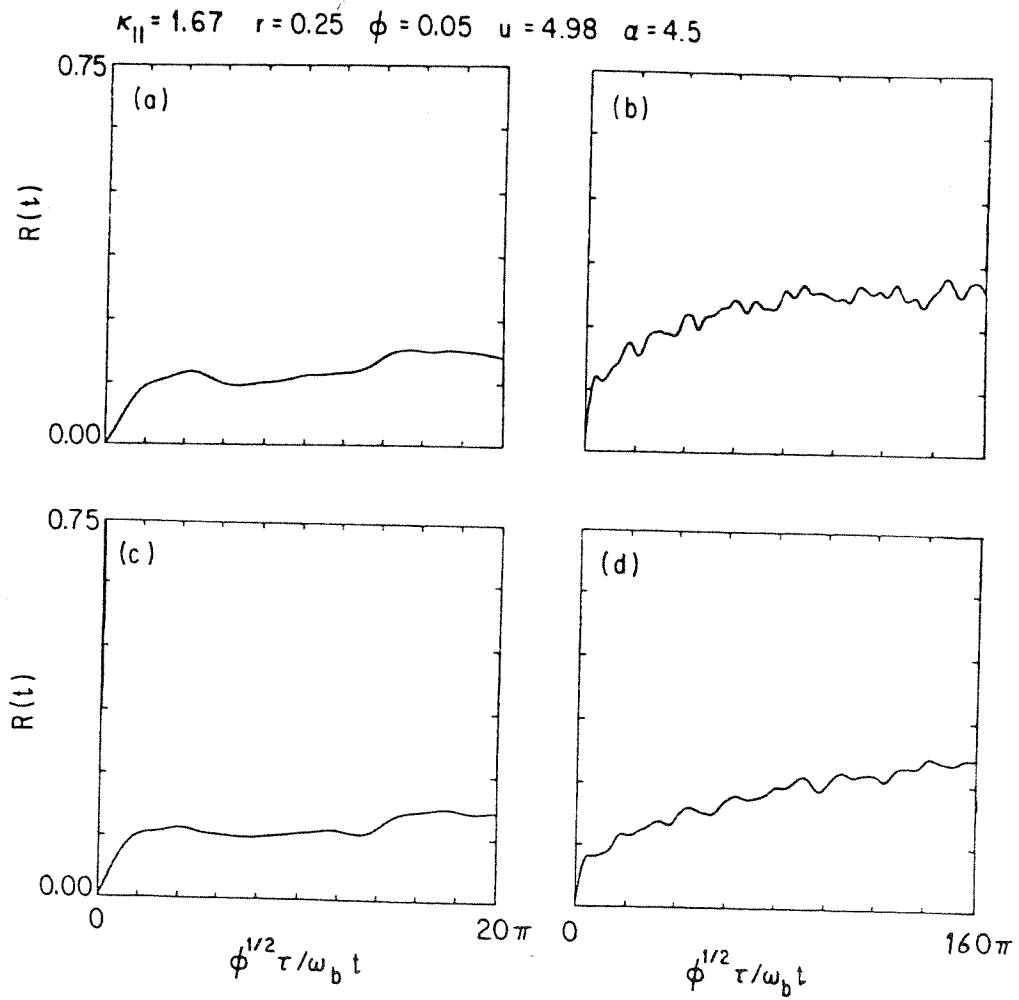
Fig. 5.8 Variation of the total damping when $\kappa_{II} = 1.67$. a) non-self-consistent simulation ($10\tau_b$), b) non-self-consistent simulation ($80\tau_b$), c) self-consistent simulation ($10\tau_b$), and d) self-consistent simulation ($80\tau_b$).
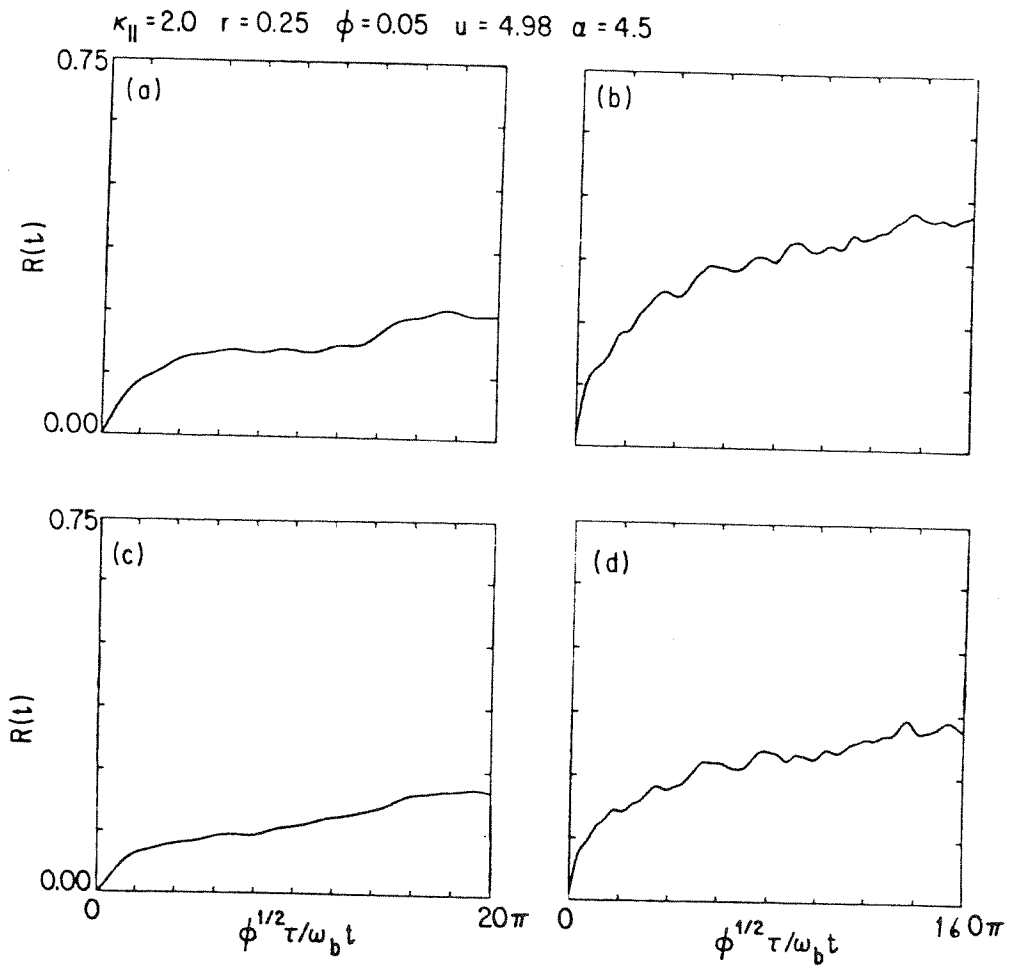
Fig. 5.9 Variation of the total damping when $\kappa_{\shortparallel} = 2.0$. a) non-self-consistent simulation ($10\tau_b$), b) non-self-consistent simulation ($80\tau_b$), c) self-consistent simulation ($10\tau_b$), and d) self-consistent simulation ($80\tau_b$).
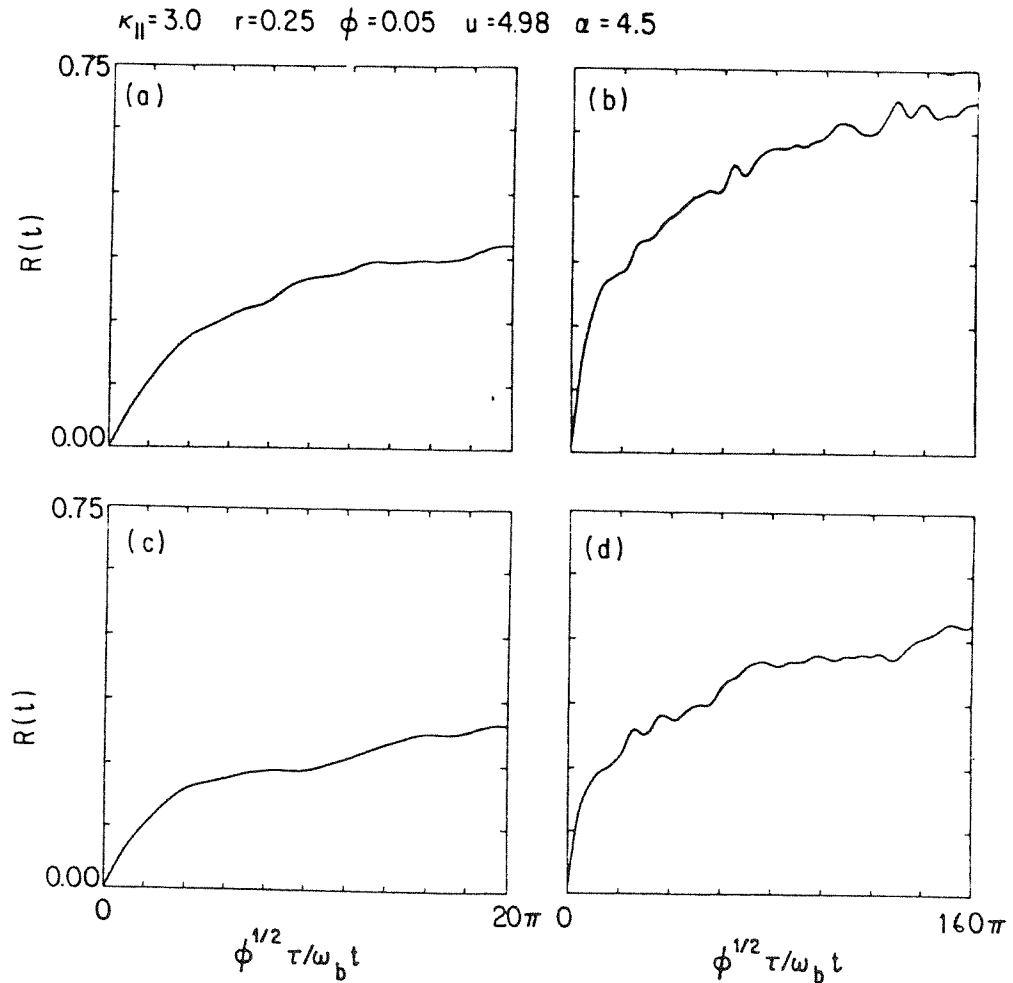
Fig. 5.10 Variation of the total damping when $\kappa_{\shortparallel}$ = 3.0. a) non-self-consistent simulation ($10\tau_b$), b) non-self-consistent simulation ($80\tau_b$), c) self-consistent simulation ($10\tau_b$), and d) self-consistent simulation ($80\tau_b$).

$\kappa_{\parallel} = 4.0$ $r = 0.25$ $\phi = 0.05$ $u = 4.98$ $\alpha = 4.5$
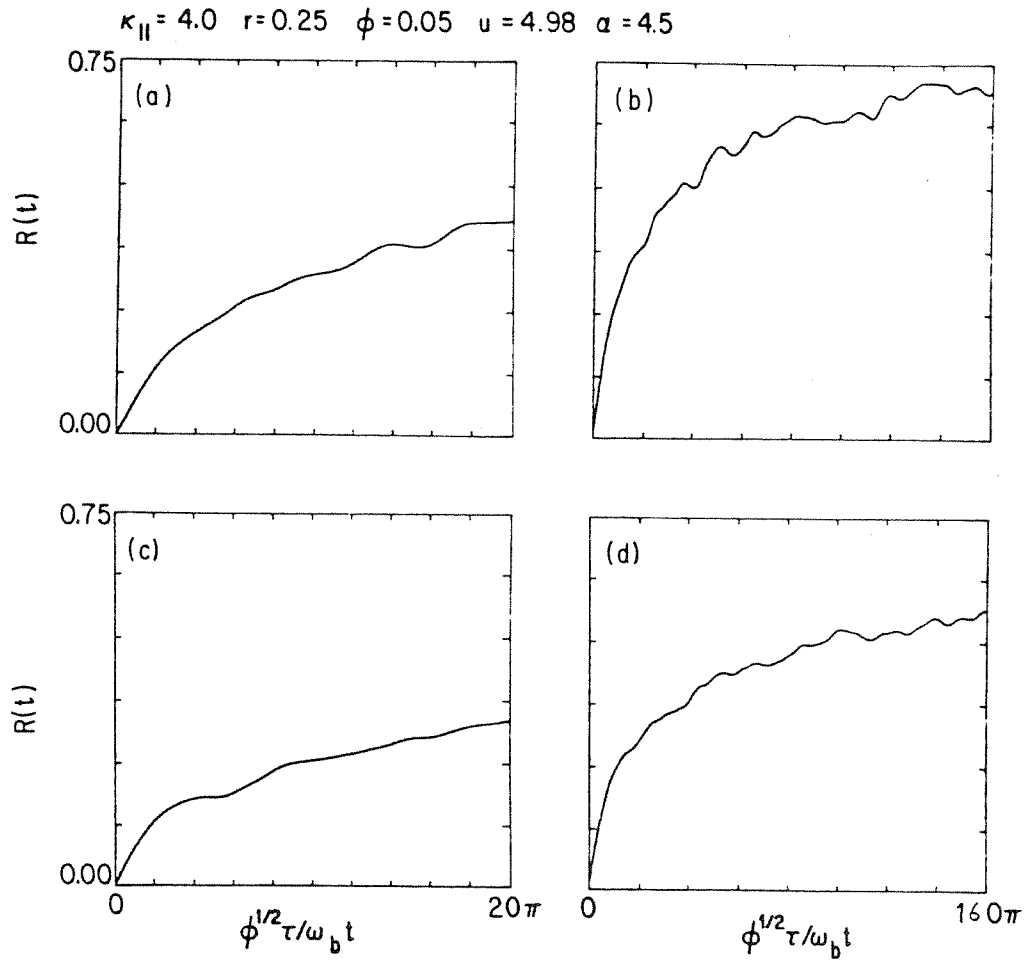
Fig. 5.11 Variation of the total damping when $\kappa_{\parallel} = 4.0$. a) non-self-consistent simulation $(10\tau_b)$, b) non-self-consistent simulation $(80\tau_b)$, c) self-consistent simulation $(10\tau_b)$, and d) self-consistent simulation $(80\tau_b)$.

107

The results of Figs. 5.5-11 for $R(10\tau_b)$ and $R(80\tau_b)$ are summarized in Fig. 5.4. We see that the increase in total damping observed in the simulations when resonances overlap is not quite as rapid as predicted by the asymptotic theory of Chapter 4, but it is still fairly rapid. At a fixed time of $10\tau_b$, the theoretically predicted value of R is roughly a factor of two higher than that obtained numerically in both the trapping and stochastic regimes. The factor of two appears in the trapping regime, because, as discussed in detail in Chapter 4, the distribution function is not really flattened over the whole resonant region, but only over the portion inside the separatrices; in the stochastic regime, as we have noted $R(t)$ converges towards its asymptotic value very slowly, and at $t = 10\tau_b$ has only attained half the theoretical value of R. However, the principal qualitative result of Chapter 4 is confirmed; there is an increase in the total damping, correlated with the transition between the trapping and stochastic regimes, and this increased total damping should be observable in both experiments and full particle simulations. Moreover, we find a qualitative difference in the wave's behavior in the two regimes. In the trapping regime, the wave has essentially saturated after about $5\tau_b$, while in the stochastic regime, the wave amplitude continues to decrease for as long as can be observed.

From a theoretical point of view, it is interesting to determine whether or not $R(t)$ ever reaches the theoretically calculated value of R. To explore this question, we have run one non-self-consistent simulation extending to $1500\tau_b$, with the results shown in Fig. 5.12. We find that the theoretically calculated value of R is reached and
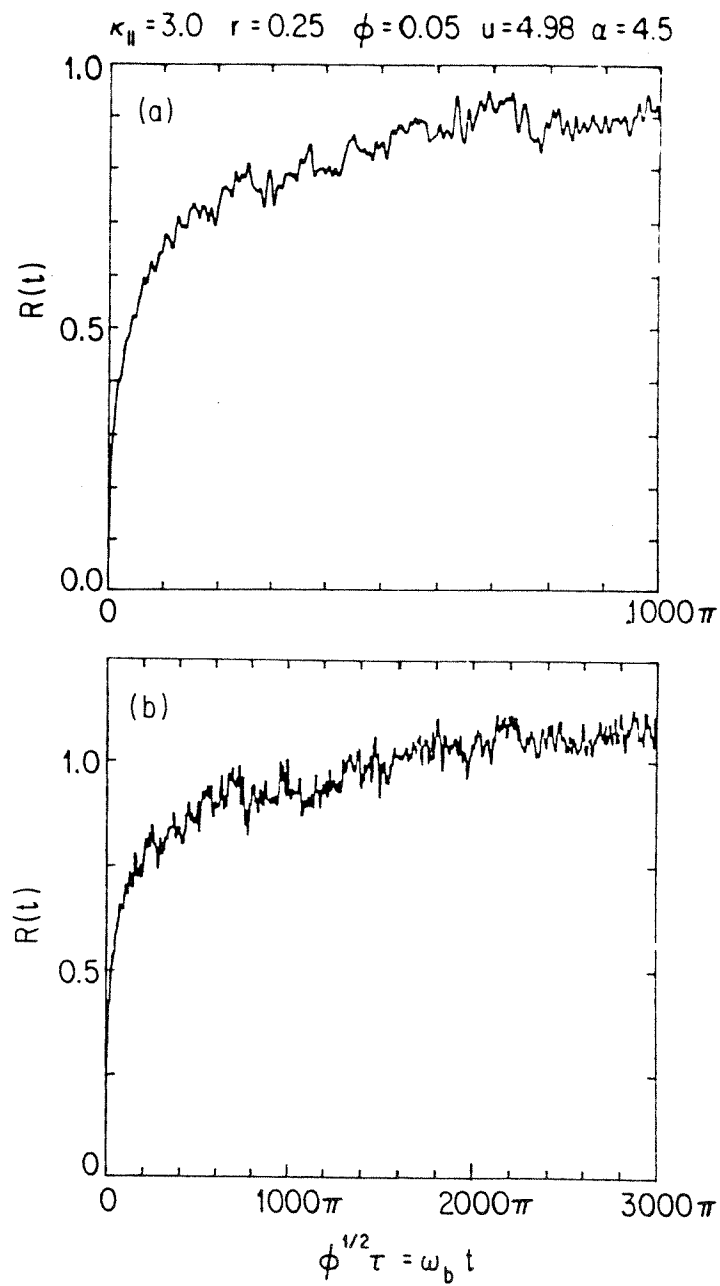
Fig. 5.12 Long time variation of the total damping. a) simulation

length $500\tau_b$, and b) simulation length of $1500\tau_b$.

even slightly surpassed. To check that no obvious numerical drifts were introduced over the long time scale of this simulation, we verified that non-stochastic particles remained bound in phase space.

In order to get a better feeling for the time-evolution of the distribution function, we ran non-self-consistent simulation with $N_{\shortparallel} = N_{\perp} = N_{\theta} = N_{\psi} = 8$. Thus, at $t = 0$ there are 64 particles with different θ and ψ-values at each initial velocity pair (v_h, ζ_i). At subsequent times, we can calculate

$$\overline{v_{hi}} = \frac{1}{N_{\theta} N_{\psi}} \sum_{j=1}^{N_{\theta}} \sum_{k=1}^{N_{\psi}} v_{hijk} \quad,$$

(5.13)

$$\overline{\zeta_{hi}} = \frac{1}{N_{\theta} N_{\psi}} \sum_{j=1}^{N_{\theta}} \sum_{k=1}^{N_{\psi}} \zeta_{hijk} \quad,$$

where v_{hijk} and ζ_{hijk} are the v and ζ-values of particular particles and $\overline{v}_{hi}$ and $\overline{\zeta}_{hi}$ are the ensemble-averaged v and ζ-values of all the particles which initially begin with the same v and ζ. Plots of $(\overline{v}_{hi}, \overline{\zeta}_{hi})$ with $\kappa_{\shortparallel}$ set equal to 3.0 are shown in Fig. 5.13. Since the resonance structure is symmetric about $v = 0$, stochastic particles should on the average tend toward $v = 0$, as is seen. Stochastic particles with low initial values of $\zeta_m \equiv (v^2 + \zeta^2)^{1/2}$ diffuse rapidly, and their $\overline{v}$-values rapidly approach zero, but as ζ_m increases, the diffusion rate decreases sharply, in part because of the falloff of the effective wave amplitude and in part because the particles have farther in velocity space to diffuse, as discussed in Section 4.5

Knowing how the particles diffuse allows us to understand the time development of R(t) in the stochastic regime. At short times, particles

$\kappa_\parallel = 3.0$ $r = 0.25$ $\phi = 0.05$ $u = 4.98$ $a = 4.5$

(a)

$\tau = 0$

(b)

$\tau = 0.5 t_b$

(c)

$\tau = 2 t_b$

(d)

$\tau = 10 t_b$

(e)

$\tau = 30 t_b$

(f)

$\tau = 80 t_b$

$\zeta = \dfrac{v_\perp}{v_t}$

$\nu = (v_z - v_p)/v_t$
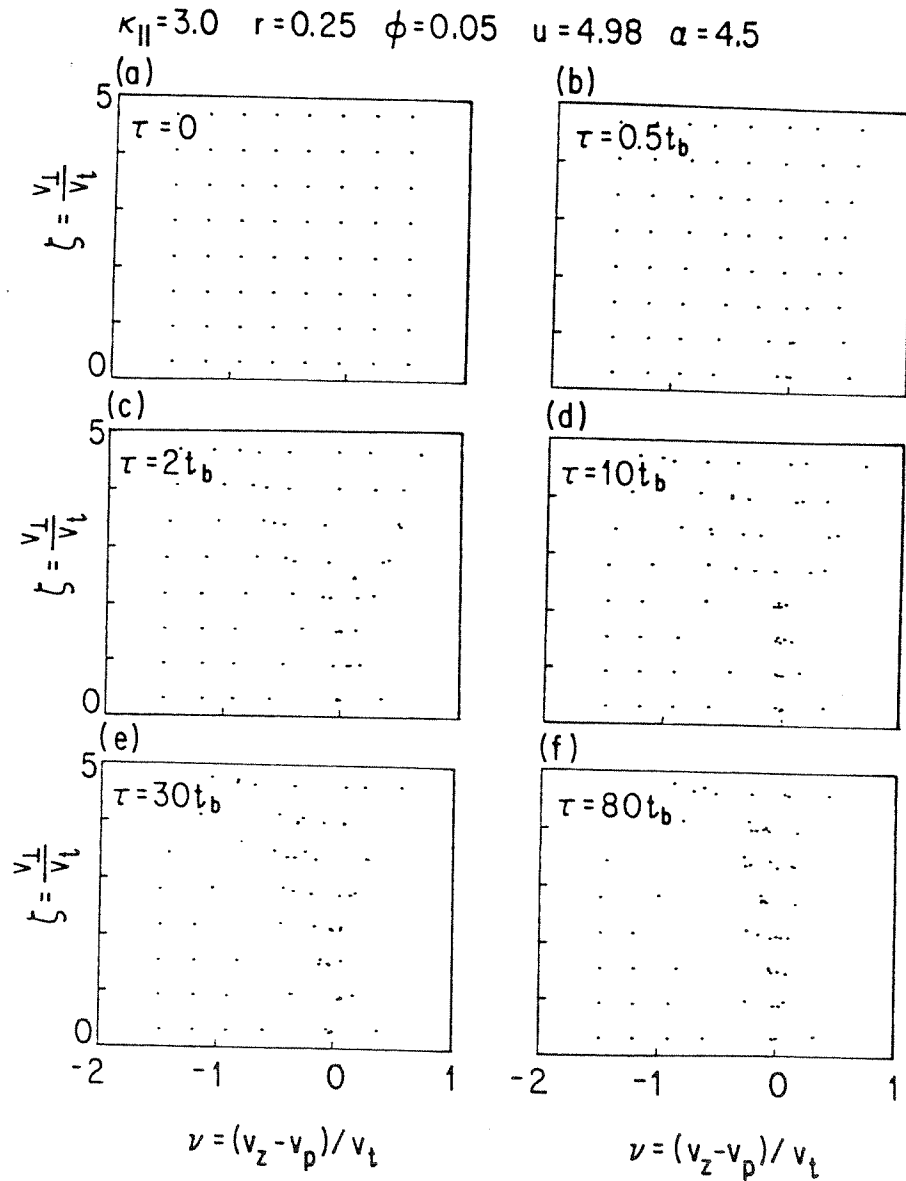
Fig. 5.13 Variation of the ensemble -averaged velocities in the stochastic regime.

with low ζ_m-values, which diffuse rapidly, contribute to the initially sizeable value of $dR(t)/dt$. The contribution of these particles then saturates, and the principal contribution to $dR(t)/dt$ then comes from particles with slightly higher values of ζ_m, which diffuse more slowly, leading to a slightly lower value of $dR(t)/dt$. After a bit more time, the contribution of these new particles saturates, and the process repeats itself indefinitely, leading to a continually decreasing value of $dR(t)/dt$.

In order to exhibit the correlation of the diffusive particle behavior with the overlap of resonances, we have plotted in Fig. 5.14 the average particle velocities at $t = 0$ and $t = 80\tau_b$ with the resonance structure superimposed. The only particles which diffuse are those in the regions of velocity space where overlap occurs; outside these regions, the particles are bound. As further corroboration, we show in Fig. 5.15 a similar plot for $\kappa_{\shortparallel} = 1.0$, where there is no resonance overlap. We see that the particles are bound, and the average velocity plots look the same at $20\tau_b$ as they did at $5\tau_b$.

$\kappa_{\parallel} = 3.0$ $r = 0.25$ $\phi = 0.05$ $u = 4.98$ $\alpha = 4.5$
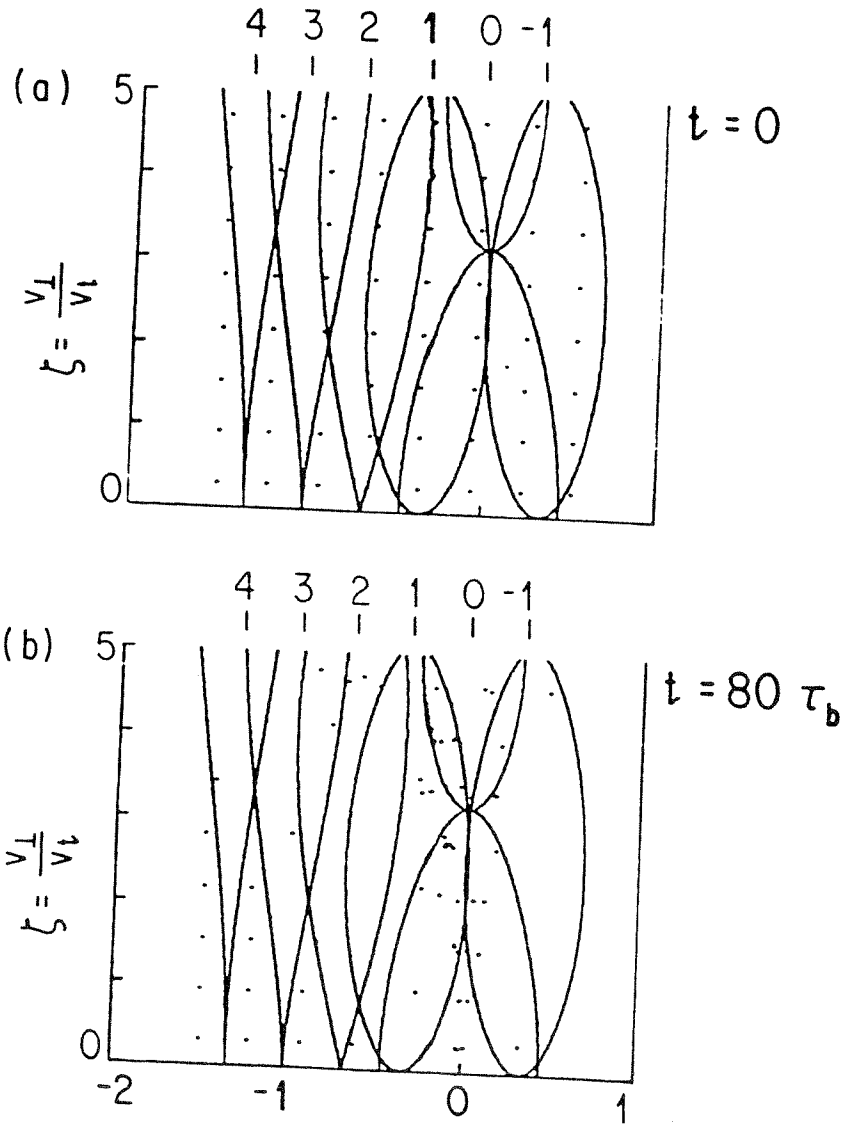
Fig. 5.14 Variation of the ensemble -averaged velocities with the resonance structure super-imposed.

$\kappa_{\parallel} = 1.0$ $r = 0.25$ $\phi = 0.05$ $u = 4.98$ $\alpha = 4.5$

(a) $\tau = 0$

(b) $\tau = 5\tau_b$

(c) $\tau = 10\tau_b$

(d) $\tau = 20\tau_b$

$\zeta = \dfrac{v_{\perp}}{v_t}$

$\nu = (v_z - v_p)/v_t$
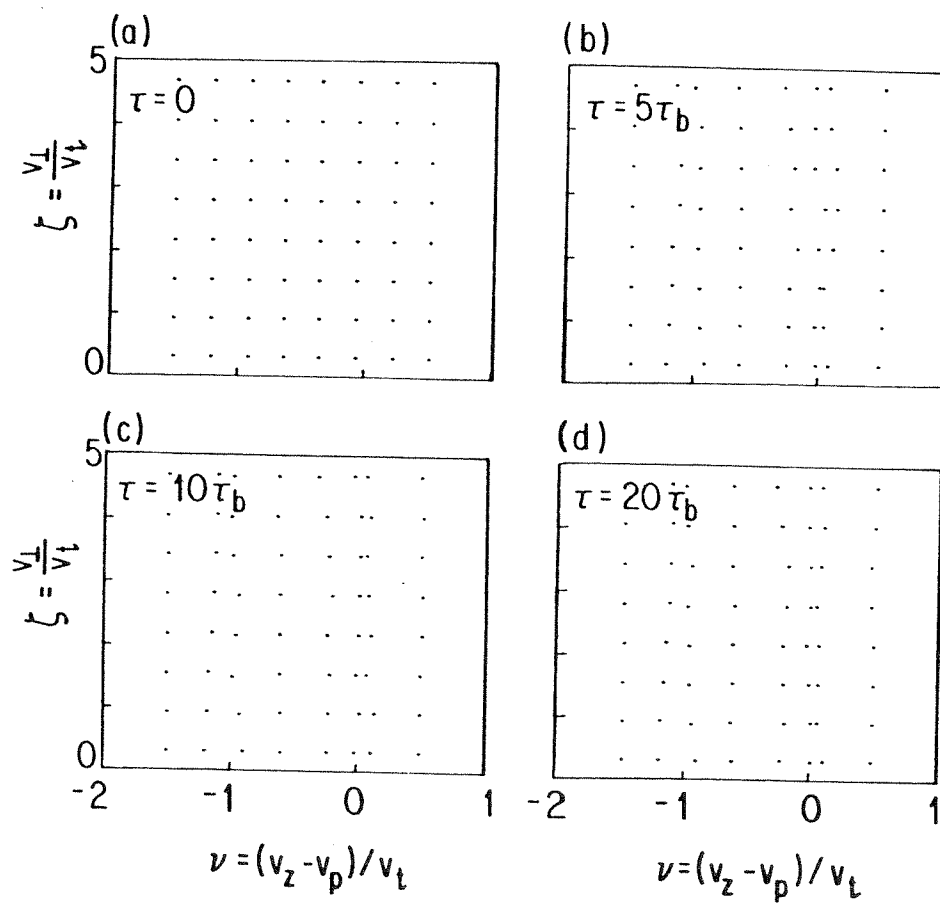
Fig. 5.15 Variation of the ensembled-averaged velocities in the trapping regime.

6. BOUNDARY-VALUE PROBLEM

Up to this point, we have considered the initial-value problem, since it is the simplest to treat conceptually. Moreover, it is the problem dealt with in simulations. In experiments, however, waves are launched from a grid at fixed ω and evolve spatially, and it is therefore necessary to solve the boundary-value problem.

In this chapter, we consider a dipolar, phased array immersed in the plasma, oriented perpendicular to the magnetic field, as shown schematically in Fig. 6.1. The phased array fixes ω and $k_\perp$, and the plasma then fixes $k_{||}$, which may vary spatially due to nonlinear effects. The quantity $k_{||}$ is in general complex and may be written in the form

$$k_{||} = k_{||0} + \delta k_{||} + i \gamma_z ,$$
(6.1)

where $k_{||0}$ is the solution of the dispersion relation $\varepsilon_r(k_{||0}, k_\perp, \omega) = 0$, $\delta k_{||}$ is the real wave-number shift, and γ_z is the spatial damping rate. The wave variation may now be written quite generally as

$$\Phi(\underset{\sim}{r}, t) = \Phi \exp\left[-\int_0^z \gamma_z(z') \, dz'\right]$$

$$\sin\left[k_{||0} z + \int_0^z \delta k_{||}(z') \, dz' + k_\perp y - \omega t\right] ,$$
(6.2)

The problem of determining the wave evolution in the boundary-value
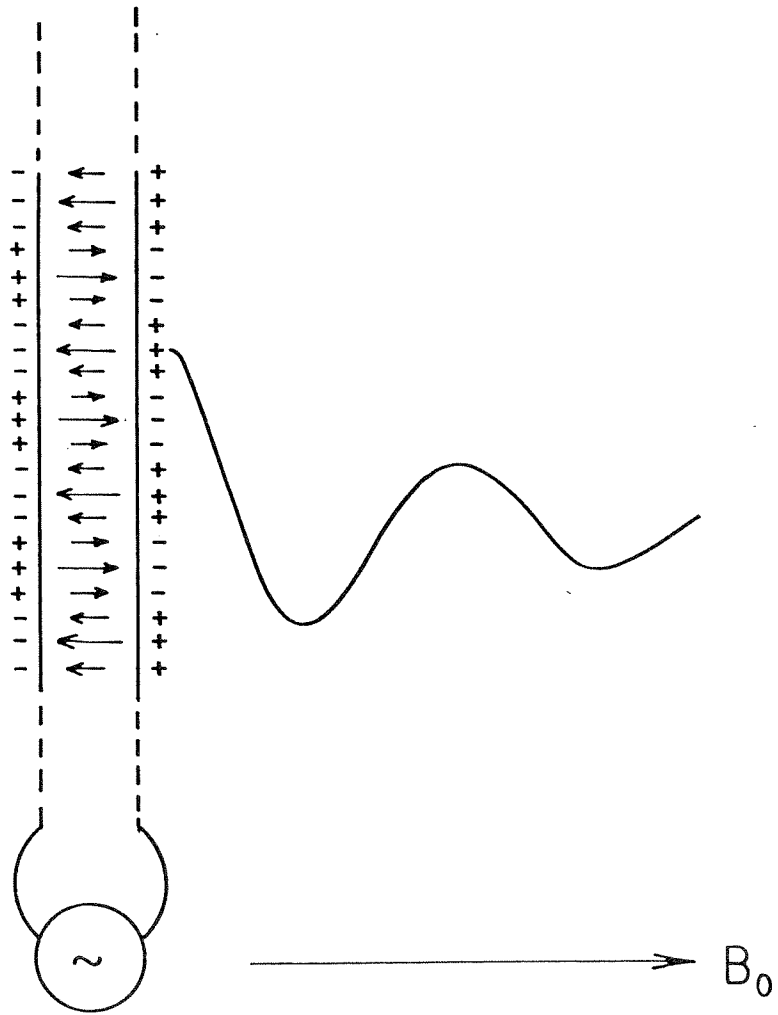
Fig. 6.1 Schematic drawing of a dipolar, phased array.

problem is just the problem of determining $\gamma_z(z)$ and $\delta k_{,,}(z)$, a problem analogous to that of determining $\gamma(t)$ and $\delta\omega(t)$ in the initial-value problem. We concentrate here on the determination of the change in the wave amplitude with z, which is given by $\gamma_z(z)$. This question has been treated for the case of a parallel-propagating wave by Lee and Schmidt.[29] They found that the spatial evolution in the boundary-value problem is self-similar to the time evolution in the initial-value problem, but that the total damping as a function of z,

$$R_z(z) \equiv 2 \int_0^z \gamma(z') \, dz' , \tag{6.3}$$

is a factor of v_p/v_g larger than $R(t = z/v_p)$ in the corresponding initial-value problem.

Eq. (6.3) is derived in both Section 6.2 and in Appendix A from somewhat different points-of-view. Physically, this self-similarity exists because all the resonant electrons move with $v_z \simeq v_p$. Hence, the momentum change that the electrons have undergone in going from $z = 0$ to $z = Z$ is the same as the momentum change we calculate in the initial-value problem for electrons going from $t = 0$ to $t = Z/v_p$. By contrast, this self-similarity breaks down in the oblique wave problem because electrons trapped in different resonances move at different velocities, $v_z = v_n = (\omega - n\Omega)/k_{,,}$. As a result, electrons trapped in the different resonances take different amounts of time to get from $z = 0$ to $z = Z$, and an exact correspondence between time and space can no longer be made.

Nonetheless, as we show in the remainder of this chapter, the primary qualitative effects in which we are interested still persist. First, in the trapping regime, super-phase-mixing of the electron motion due to the many bounce frequencies leads to disappearance of the amplitude oscillations. Second, in making the transition between the trapping and stochastic regimes, increased total damping of the wave is observed. While R_z is not related to R by exactly a factor of v_p/v_g, except in the case of parallel-propagation, we still expect this factor to be approximately correct since the low-$|n|$ resonances are the principal contributors to R. As we shall see in Section 6.3, this approximation gives the correct answer within a factor of two. Because v_p/v_g tends to be rather large in the cases of interest (>10), we must use values of α higher than those used in the initial-value problem in order to be in the non-linear regimes.

6.1 Linear Regime

The real variables α, $\kappa_{||}$, r, and u which have been used thus far, all involve $k_{||}$, and are not, strictly speaking appropriate for describing a situation in which $k_{||}$ has an imaginary part. To circumvent this difficulty, we redefine these variables to include only the real part of $k_{||}$. At this point, we restate the relation of these parameters with the physical parameters ω, $k_\perp$, Ω, n_0, and T, which are set experimentally and $k_{||}$ which is determined through the dispersion relation. Since the four dimensionless parameters are determined from the six physical ones, two of the latter may be considered as specifying the length and time scales. We can fix any two of the physical parameters

save for $k_{\parallel}$, which is fixed through the dispersion relation, and, by varying the others obtain all possible values of the four dimensionless parameters. In general, T is fixed experimentally, and we shall consider it to be fixed here. We shall also consider n_0 to be fixed, although one can imagine cases where it is far more convenient experimentally to fix $k_{\perp}$ and vary n_0. Fixing n_0 and T fixes k_D and ω_p and, thus, fixes our length and time scales. Recalling the definitions of α, $\kappa_{\parallel}$, r, and u,

$$\alpha \equiv k_D / k \,, \qquad \kappa_{\parallel} \equiv k_{\parallel} v_t / \Omega \,,$$

$$r \equiv k_{\perp} / k_{\parallel} \,, \qquad u \equiv \omega / k_{\parallel} v_t \,,$$

$$\text{(6.4)}$$

we may write our physical variables in terms of the dimensionless parameters as

$$\Omega = \frac{1}{\kappa_{\parallel} \, \alpha \, (1 + r^2)^{1/2}} \, \omega_p \,, \tag{6.5a}$$

$$k_{\perp} = \frac{r}{\alpha \, (1 + r^2)^{1/2}} \, k_D \,, \tag{6.5b}$$

$$\omega = \frac{u}{\alpha \, (1 + r^2)^{1/2}} \, \omega_p = \left(1 + \frac{3}{2 \alpha^2} \right) \omega_p \,, \tag{6.5c}$$

where the asymptotic approximation to the Bohm-Gross dispersion relation has been used in Eq. (6.2c). We showed in Chapter 2 that this

dispersion relation is quite accurate for a homogeneous, infinite

plasma when $\kappa_{\shortparallel} \gtrsim 1.0$. However, because a real experimental device is

not infinite and not necessarily homogeneous, the dispersion relation

may, in general, be altered significantly, as was the case in the

experiments on parallel-propagating waves,[23,41] and must be determined

for the particular experimental device.

We continue throughout this chapter to use the dimensionless

parameters. To convert these to physical variables, Eq. (6.5) should

be used. From an experimental point of view, Eq. (6.5) yields the

values of the physical parameters which are necessary to generate

desired values of α, $\kappa_{\shortparallel}$, r, and u.

Linear theory in the boundary-value problem is not as simple as

linear theory in the initial-value problem; the presence of the grid

is an inevitable complicating factor. Close to the grid, there will

be a complex near field which does not vary exponentially with distance,

and, in the limit far away from the grid, there is, in principle, a far

field, due to the ballistic contributions, whose variation with distance

is slower than exponential.[40] Nonetheless, in between these two limits,

the field variation is given by the "least-damped" root of the disper-

sion relation and is exponential with distance. In this chapter, we

concentrate on this intermediate regime in z.

The asymptotic solution to the dispersion relation is determined

much as in the initial-value problem. For an infinite, homogeneous

plasma, the real part is given by the asymptotic approximation to the

Bohm-Gross dispersion relation, and the imaginary part is given by

dividing the dispersion relation into the real and imaginary parts and

noting that

$$\frac{\partial \varepsilon_r}{\partial k_{\parallel}} \gamma_z = - \varepsilon_i \quad . \tag{6.6}$$

Recalling that

$$\frac{\partial \varepsilon_r}{\partial \omega} \gamma = \varepsilon_i \quad , \tag{6.7}$$

and noting that

$$v_g = \frac{d\omega}{dk_{\parallel}} = - \frac{(\partial \varepsilon_r / \partial k_{\parallel})}{(\partial \varepsilon_r / \partial \omega)} \quad , \tag{6.8}$$

we obtain the well-known result

$$\frac{\gamma_z}{\gamma} = \frac{1}{v_g} \quad . \tag{6.9}$$

The group velocity is parallel to the magnetic field because we have
fixed $k_{\perp}$. Using Eq. (2.21), which gives us the expression for ε_i and
using Eq. (6.6), we find

$$K_{\parallel i} \equiv \frac{\gamma_z v_t}{\Omega} = - \sqrt{\frac{\pi}{2}} \alpha^2 u K_{\parallel} \left(K_{\parallel} \frac{\partial \varepsilon_r}{\partial K_{\parallel}} \right)^{-1}$$

$$\sum_{n=-\infty}^{\infty} \Lambda_n (K_{\perp}^2) \exp\left[-\frac{1}{2} \left(u - \frac{n}{K_{\parallel}} \right)^2 \right] \quad , \tag{6.10}$$

where

$$K_{\shortparallel} \frac{\partial \mathcal{E}_r}{\partial K_{\shortparallel}} \equiv k_{\shortparallel} \frac{\partial \mathcal{E}_r}{\partial k_{\shortparallel}} = - \frac{6\alpha}{(\alpha^2+3)^2 (1+r^2)} \cdot \qquad (6.11)$$

The number of oscillations a wave makes before damping to 1/e of its initial value is $N_t \equiv |\omega/2\pi\gamma|$ in the initial-value problem and $N_z \equiv |k_{\shortparallel}/2\pi\gamma_z|$ in the boundary-value problem. Using Eq. (6.9), we find that the ratio of N_t and N_z is

$$\frac{N_t}{N_z} = - \frac{\omega}{k_{\shortparallel}} \frac{(\partial \mathcal{E}_r/\partial\omega)}{(\partial \mathcal{E}_r/\partial k_{\shortparallel})} = \frac{v_p}{v_g} \cdot \qquad (6.12)$$

This ratio is a measure of the relative lifetime, in the initial-value and boundary-value problems, of the wave measured in units of oscillations. This quantitative difference between the two problems carries over to the non-linear regimes where, as shown in Appendix A, the total damping is increased in the boundary-value problem by a factor of approximately v_p/v_g. In the case of an infinite, homogeneous plasma, this ratio becomes

$$\frac{v_p}{v_g} = \frac{(\alpha^2+3)^3 (1+r^2)}{3\alpha^4} , \qquad (6.13)$$

which is shown in Fig. 6.2. This ratio is quite large, greater than ten in the region of interest, and must be overcome by an increase in u. Because increasing u leads to an exponential decrease in the total damping, a large increase is not needed.
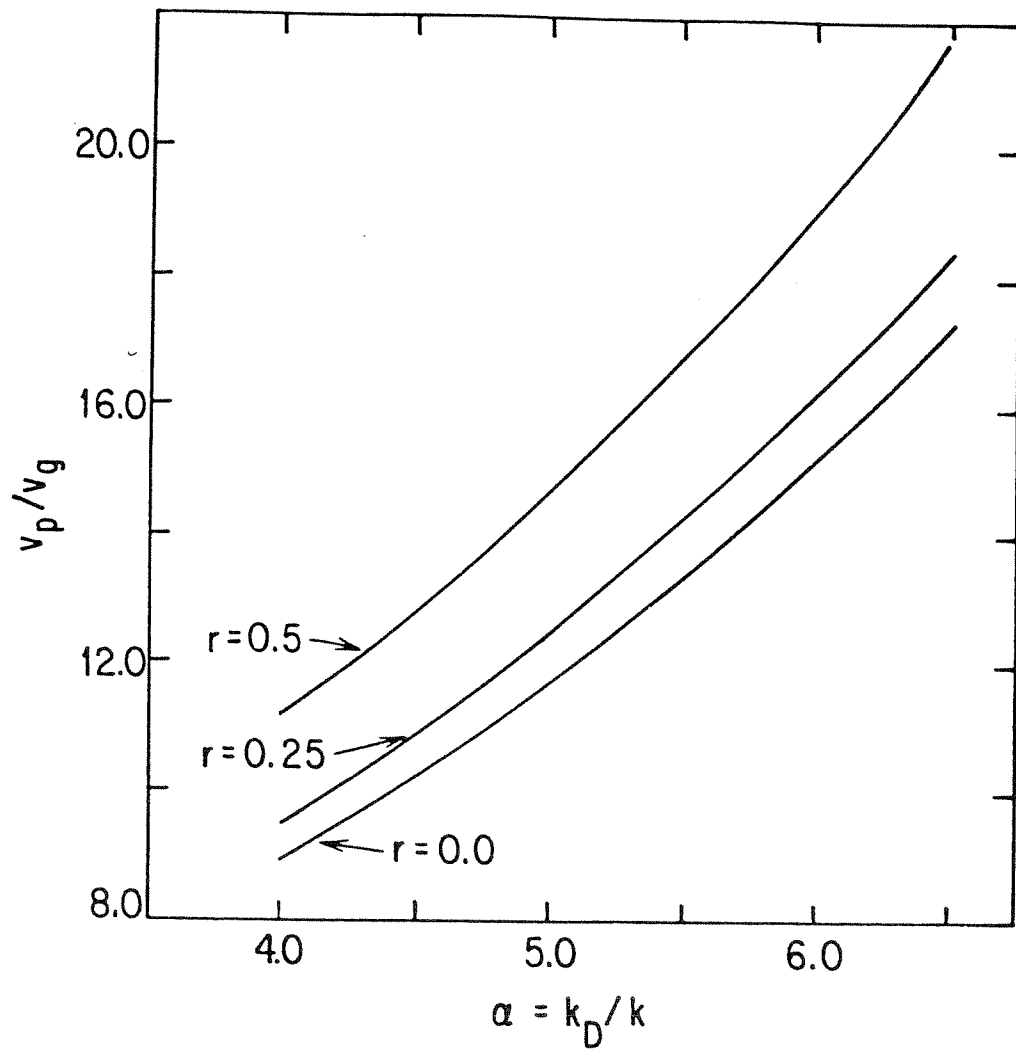
Fig. 6.2 Variation of v_p/v_g with $\alpha \equiv k_D/k$.

123

6.2 Trapping Regime

The field strength in the trapping regime is bounded on the upper end by the condition that $\omega_b = k_{||}(e\Phi/m)^{1/2} < \Omega$, so that the resonances are far apart. This limit is the same as in the initial-value problem. On the lower end, the condition is $\gamma_z < \omega_b/v_p$, which can be understood as follows. In the wave frame (i.e. in a frame moving with velocity v_p) the wave amplitude appears to damp temporally at a rate $\gamma_z v_p$, and this must exceed ω_b if the trapped or nearly trapped electrons are to have many bounces before the wave decays. Recalling Eq. (6.9), we see that this condition is a factor of v_p/v_g more restrictive than in the initial-value problem.

We begin, just as in the initial-value problem, by subtracting the real part of the linear plasma response from the full plasma response to obtain, where $\delta k_{||c}$ is the complex wavenumber shift,

$$ i k \left(\frac{\partial \varepsilon_r}{\partial k_{||}} \right) \delta k_{||c} \, E_{k_\perp, \omega} = -4\pi n_o e \int d^3 v \left(f_{k_\perp, \omega} - f_{k_\perp, \omega r} \right), \tag{6.14} $$

which is analogous to Eq. (3.19). Since we are in the limit where $(\gamma_z/k_{||}) \ll 1$, it is legitimate to define $f_{k_\perp, \omega}$

$$ f_{k_\perp, \omega} = \int_o^T \frac{dt}{T} \int_o^{\lambda_\perp} \frac{dy}{\lambda_\perp} \exp\left[-i\left(k_{||} z + k_\perp y - \omega t \right) \right] f , \tag{6.15} $$

where $T \equiv 2\pi/\omega$.

Our development now proceeds in a manner exactly analogous to that of Chapter 3. We change variables from y, v_y, x, and v_x to X, Y, θ, and $v_\perp$ and expand the distribution in a Taylor series about each of the resonant locations to obtain

$$k^2 \left(\frac{\partial \varepsilon_r}{\partial k_{\parallel}} \right) \frac{\gamma_z}{2} \Phi = 4 \pi e n_0 \sum_{n=-\infty}^{\infty} \int 2\pi v_\perp \, dv_\perp \; J_n (k_\perp \rho)$$

$$\int_0^T \frac{dt}{T} \int_{-\infty}^{\infty} dv_z \; \sin(\omega t) \left(\frac{\partial f_0}{\partial \underset{\sim}{v}} \right) \cdot \Delta \underset{\sim}{v}_n \; .$$

(6.16)

where $\Delta \underset{\sim}{v}_n$ is the deviation $\underset{\sim}{v}_0 - \underset{\sim}{v}$ in the neighborhood of the nth resonance. The equations of motion from which we determine $\Delta \underset{\sim}{v}_n$ are the same as before

$$\dot{v}_z = - \frac{e k_{\parallel} \Phi}{m} J_n (k_\perp \rho) \sin (k_{\parallel} z) ,$$

$$\dot{v}_\perp = \frac{n \Omega}{k_{\parallel} v_\perp} \dot{v}_z \; .$$

(6.17)

Integrating these equations of motion formally, we have

$$z = v_n t + \int_0^t \underset{\sim}{e}_z \cdot \Delta \underset{\sim}{v}_n (t') \, dt' ,$$

(6.18)

where $v_n = (\omega - n\Omega)/k_{\parallel}$. Since the resonances are small, we have, to lowest order in Φ,

$$z \approx v_n t .$$

(6.19)

The remainder of the discussion of the boundary-value problem is just like that for the initial-value problem. We solve Eq. (6.17),

substitute the results into Eq. (6.16) and use Eq. (6.19) to replace t with z. We then integrate over z and v_z to finally obtain

$$\gamma_z(z) = \pi \frac{\omega_p^2}{k^2} \left(\frac{\partial \varepsilon_r}{\partial k_{\shortparallel}}\right)^{-1} \sum_{n=-\infty}^{\infty} \int_0^{\infty} 2\pi v_\perp \, dv_\perp$$

(6.20)

$$\left(\frac{\partial f_0}{\partial v_z} + \frac{n\Omega}{k_n v_\perp} \frac{\partial f_0}{\partial v_\perp}\right) J_n^2(k_\perp \rho) \, \sigma_0 \left(\frac{\omega_b z}{v_n}\right).$$

We know from our study of the linear theory that the contribution of the backward-going resonances is negligible, and they are ignored in Eq. (6.20).

Because of the different v_n's which appear in Eq. (6.20), there is generally, as noted earlier, no simple relation between γ and γ_z. The exception is the case of parallel propagation, where, comparing Eqs. (3.49) and (6.20), we conclude

$$\gamma_z(z) = \frac{1}{v_g} \gamma\left(\frac{z}{v_p}\right).$$

(6.21)

The total damping in the case of the boundary-value problem is exactly a factor of v_p/v_g greater than in the initial value problem.

Shown in Fig. 6.3 is the solution of Eq. (6.20) for a Maxwellian distribution. This figure is analogous to Fig. 3.2, and we chose values of α such that the total damping would be significant but not overwhelming. Because of the v_p/v_g factor, higher values of α are needed in the boundary-value problem to get approximately the same total damping as in the initial-value problem. Also, the shape of the curves for $r \neq 0.0$ are somewhat different in the two problems; nonetheless, in both cases we find that super-phase-mixing causes

126
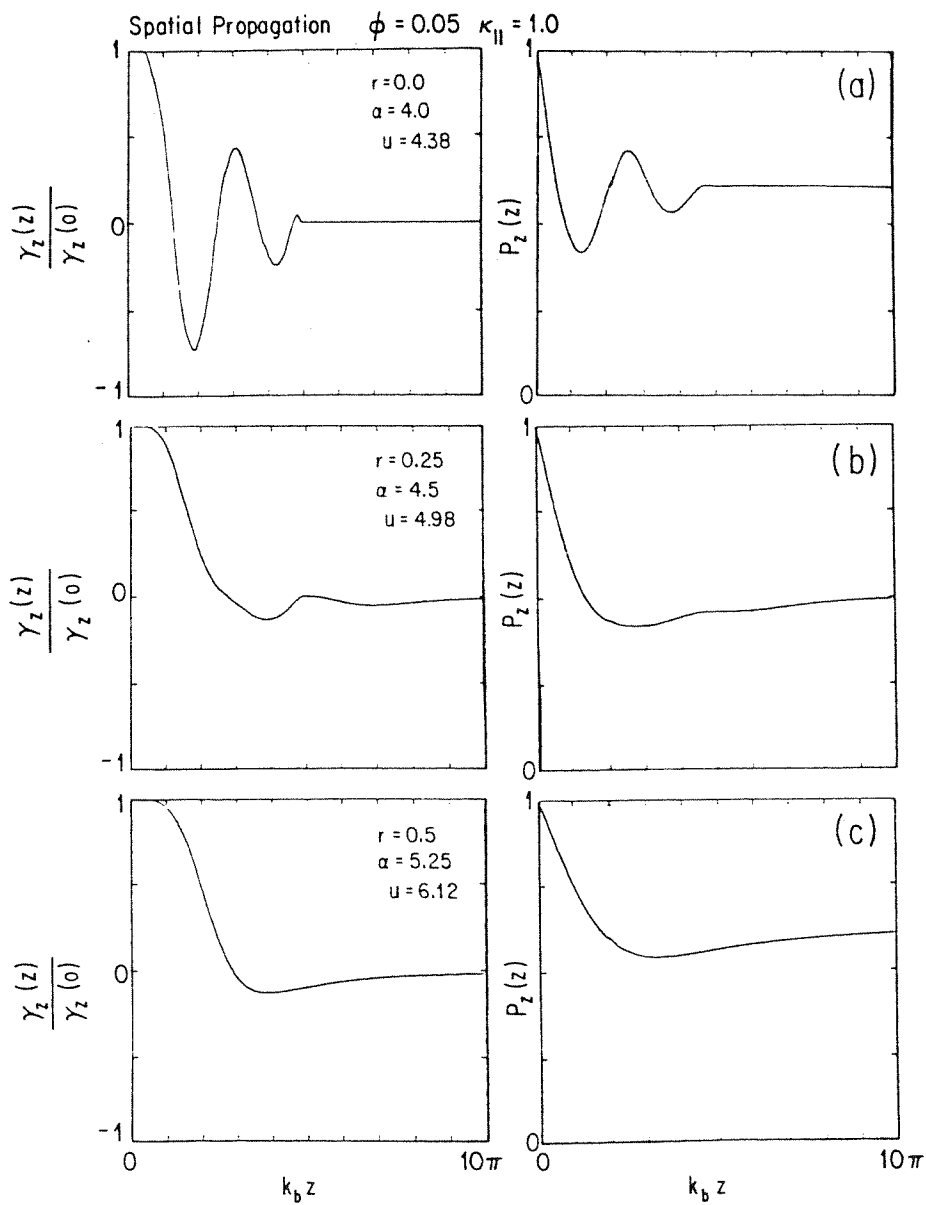
Fig. 6.3   Variation of $\gamma_z(z)/\gamma_z(0)$ and $P_z(z)$ with z.

127

the amplitude oscillations to vanish when $r > 0.25$, i.e. when the

angle of propagation with respect to the magnetic field is greater

than $14°$.

6.3 Transition to the Stochastic Regime

We begin with the momentum equation which is derived in Appendix

A for the boundary-value problem

$$\frac{d}{dz} \int d^3v \; m v_z^2 \, n_0 f_0 \;=\; k_{\shortparallel} \frac{\partial \varepsilon_r}{\partial k_{\shortparallel}} \; \frac{d \, E_0^2 / 16\pi}{dz} \, . \tag{6.22}$$

If we assume that all the electrons which are contributing to the non-

linear wave response move with $v_z \simeq v_p$, then Eq. (6.22) becomes

$$v_p \frac{d}{dz} \int d^3v \; m v_z \, n_0 f_0 \;=\; k_{\shortparallel} \frac{\partial \varepsilon_r}{\partial k_{\shortparallel}} \; \frac{d \, E_0^2 / 16\pi}{dz} \, , \tag{6.23}$$

as was shown in Appendix A. Eq. (6.23) may be integrated to yield

$$v_p \, \delta \int d^3v \; m v_z \, n_0 f_0 \;=\; k_{\shortparallel} \frac{\partial \varepsilon_r}{\partial k_{\shortparallel}} \; \delta \left(\frac{E_0^2}{16\pi} \right) \, . \tag{6.24}$$

Developing Eq. (6.24) in exactly the same manner as we developed Eq.

(4.3) in Chapter 4, we conclude

$$R_z = -\frac{\delta \varphi^2}{\varphi^2} = \frac{v_p}{v_g} R = \sqrt{\frac{8}{\pi}} \frac{\alpha^2}{\varphi^2} u \left(K_\parallel \frac{\partial \varepsilon_r}{\partial K_\parallel}\right)^{-1} exp\,(-u^2/2)$$

$$\int_0^\infty \mathcal{Y}_m\, d\mathcal{Y}_m\, exp\,(-\mathcal{Y}_m^2/2) \sum_i \left\{ \frac{(s_i - \ell_i)}{2u} \left[exp\,(-u\,\ell_i) \right.\right. \qquad (6.25)$$

$$\left.\left. + exp\,(-u\,s_i) \right] - \frac{1}{u^2} \left[exp\,(-u\,\ell_i) - exp\,(-u\,s_i) \right] \right\} \;.$$

A more accurate result can be obtained through the direct use of Eq.
(6.22), which upon integration, leads to

$$\delta \int d^3v\; m v_z^2 n_0 f_0 = k_\parallel \frac{\partial \varepsilon_r}{\partial k_\parallel} \delta \left(\frac{E_0^2}{16\pi}\right)\;. \qquad (6.26)$$

We assume that the distribution is asymptotically flattened subject
to the constraint that particle flux is conserved,

$$\delta \int d^3v\; v_z n_0 f_0 = 0, \qquad (6.27)$$

as discussed in Appendix A. We then find, developing Eq. (6.28) in a
manner analogous to that of Eqs. (4.3) and (6.24),

$$R_z = \sqrt{\frac{8}{\pi}} \frac{\alpha^2}{\varphi^2} u \left(K_\parallel \frac{\partial \varepsilon_r}{\partial K_\parallel}\right)^{-1} exp\,(-u^2/2) \int_0^\infty \mathcal{Y}_m\, d\mathcal{Y}_m\, exp\,(-\mathcal{Y}_m^2/2)$$

$$\sum_i \left(\frac{(s_i - \ell_i)}{2u} \left\{ 1 + \frac{(s_i + \ell_i)}{2u} + \frac{2}{u^2} - \frac{(s_i - \ell_i)^2}{3\left[4u^2 - (s_i + \ell_i)^2\right]} \right\} \right. \qquad (6.28)$$

$$\left[exp\,(-u\,\ell_i) + exp\,(-u\,s_i) \right]$$

129

$$-\frac{1}{u^2}\left\{1 + \frac{(s_i - \ell_i)}{2u} + \frac{2}{u^2} + \frac{(s_i - \ell_i)^2}{6} - \frac{(s_i - \ell_i)^2}{3\left[4u^2 - (s_i + \ell_i)^2\right]}\right\}$$

$$\left[\exp(-u\ell_i) - \exp(-u s_i)\right]\Bigg).$$

Eqs. (6.25) and (6.28) can be solved in the same manner in which we solved Eq. (4.17), and their limits of validity are expected to be the same. The results as a function of $\kappa_{\shortparallel}$ are shown in Fig. 5.4 and should be compared with Fig. 4.4d, since, in both cases $r = 0.5$. The quantity α was chosen so that R_z would be significant but less than one over the range of $\kappa_{\shortparallel}$ where resonance overlap first occurs. As a result of the v_p/v_g factor, the value of u went up from 5.66 to 6.45 in the boundary-value problem. We see that the result obtained from Eq. (6.28) is about a factor of two lower than that of Eq. (6.25).
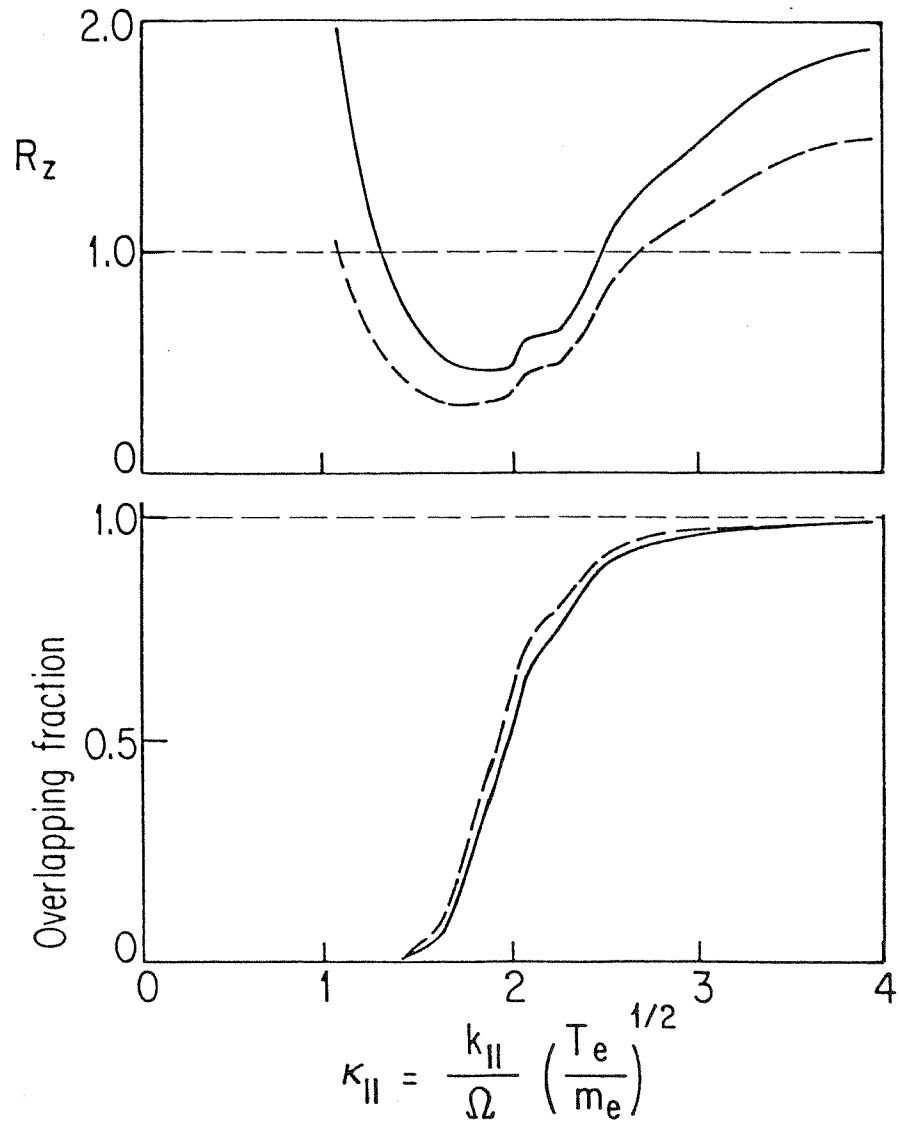
Fig. 6.4 Variation of R_z and the overlapping fraction with $\kappa_{\shortparallel} \equiv k_{\shortparallel} v_t / \Omega$. The plasma parameters are $\phi = 0.05$, $r = 0.5$, $u = 6.45$ ($\alpha = 5.5$), and $v_p / v_g = 16.7$.

131

7. CONCLUSIONS

The transition between regular and stochastic particle motion which occurs when resonances overlap is believed by many researchers to play an important role in several areas of fusion research and basic plasma physics. As a result, this transition has been subjected to intensive scrutiny, by examining the single-particle motion in a wide variety of situations, and is now fairly well understood. However, there has been little effort to understand how an ensemble of particles being influenced by a given wave feeds back on the wave to affect its evolution. In particular, it has not been shown that there is any observable difference between the wave evolution in the regime where particle motion is primarily regular and the regime where particle motion is primarily stochastic. This determination is important because, generally speaking, it is waves and not individual particles which are the primary observables in experiments and simulations.

To explore this question in the simplest possible realistic context, we studied electrostatic electron waves in a Maxwellian plasma with a uniform magnetic field. Electrons are resonant with these waves whenever $v_z = (\omega - n\Omega)/k_{\shortparallel}$, where n is any integer. These resonances can be made to overlap by either increasing the electrostatic amplitude or by decreasing Ω, which moves the resonances closer together. To keep the wave amplitude as small as possible, the phase velocity large enough to avoid overwhelming the non-linear effects by Landau damping, and the v_z separation of the resonances small enough to allow resonance

overlap, we were led to consider obliquely propagating Langmuir waves in weakly magnetized, warm plasmas. We have shown that in this case the full plasma dispersion relation reduces to good approximation to the asymptotic Bohm-Gross dispersion relation.

An obliquely propagating Langmuir wave has three distinct evolution regimes. When $\omega_b < \gamma$, the wave is in the linear regime, and damps away. When $\gamma < \omega_b < \Omega$, the wave is in the trapping regime, and its evolution is dominated by regular particle motion. Finally, when $\gamma < \Omega < \omega_b$, the wave is in the stochastic regime, and its evolution is dominated by stochastic particle motion.

When the conditions for the wave to be in the trapping regime are well satisfied, $\gamma \ll \omega_b \ll \Omega$, electrons are influenced by at most one resonance, and execute trapped particle oscillations when $v_z \simeq (\omega - n\Omega)/k_{\shortparallel}$. In this regime, the wave evolution can be treated in a fashion analogous to O'Neil's treatment of the parallel-propagating wave. We find that when the angle of propagation with respect to the magnetic field is increased from 0° to about 14°, the trapped-particle oscillations disappear because electrons in different resonances have different bounce frequencies, leading to a "super-phase-mixing" of the amplitude oscillations.

When the condition for the wave to be in the stochastic regime are well satisfied, $\gamma \ll \Omega \ll \omega_b$, the electron motion is nearly diffusive in the stochastic region of velocity space where resonances overlap. In this case, it is justified to treat the wave evolution using a quasi-linear theory with resonance broadening similar to Dupree's. This theory predicts a slower approach to the asymptotic state in the sto-

133

chastic regime than was found in the trapping regime. It also predicts that the asymptotic state is approached monotonically with an ever-decreasing slope, and that the diffusion rate decreases with increasing $v_\perp$. These predictions are all borne out by the simulations of Chapter 5; however, the simulations find that the wave approaches its asymptotic state considerably more slowly than the theory predicts. This discrepancy presumably occurs because most of the electrons are initially at the edge of the stochastic region, and in this region of velocity space the motion of the stochastic electrons is not expected to be truly diffusive.

In the transition regime between regular and stochastic motion, the electron motion is extremely complicated and cannot be simply treated. However, we can approximately determine the asymptotic $(t = \infty)$ total damping of the wave by assuming that the distribution function is asymptotically flattened over each resonant region, and that, if two or more resonances overlap, the distribution is flattened over all of them. Using this model, we find that the total damping of the wave significantly increases when a transition is made between the regular and stochastic regimes.

In all this theoretical work, the field amplitude is held fixed in determining the distribution function evolution, and the amplitude evolution is then determined through Poisson's equation. In this sense, our approach is non-self-consistent, and is strictly valid only the limit $\gamma \ll \omega_b$, where the amplitude change is small compared to the initial amplitude. Nonetheless, these calculations are a significant improvement over earlier works which study primarily single-particle

motion and hence provide little information about the wave evolution.

In order to check our theoretical results concerning the asymptotic wave amplitude and also to accurately determine the time evolution in the stochastic regime, we ran a series of "mini-simulations," in which the trajectories of the resonant electrons were followed numerically, and the bulk of the plasma was treated as a background linear dielectric. Using this method, we were able to confirm the result that increased total damping takes place when resonance overlap occurs. In the stochastic regime, we were also able to run self-consistent simulations in which the electrostatic field amplitude was updated at each time step. The amplitude evolution occured somewhat more slowly than in the non-self-consistent calculations, since the self-consistent decrease in the field amplitude led to a decreased damping rate. However, the qualitative nature of the evolution was unaffected.

To make contact with possible experiments, we have also considered an idealized boundary-value problem in which there is a phased array which fixes ω and $k_\perp$, allowing the plasma to determine $k_\parallel$. The wave then evolves spatially rather than temporally. We found that the total damping is increased with respect to the initial-value problem for a given set of plasma parameters by a factor approximately equal to v_p/v_g. In the limit of parallel propagation, this approximation becomes exact. Despite this difference, the essential qualitative results obtained from our study of the initial-value problem are confirmed.

We restate the principal qualitative results: First, in the trapping regime, the amplitude oscillations which occur for a parallel-

propagating wave disappear due to super-phase-mixing as the propagation angle is increased. Second, when a transition is made from the trapping to the stochastic regime, a significant increase in total damping is observed.

There appears to be no fundamental barrier to testing these results experimentally. As an example, we consider a plasma frequency of 500 Mhz (ω_p = 3.1 x 10^9 sec^{-1}, n_o = 3.1 x 10^9 cm^{-3}) and a plasma temperature of 10 e.v., which are close to where past experiments have been done. If we set α = 5, $k_{\shortparallel}$ < 4, and r > 0.5, we find from Eq. (6.5), B_o > 8 gauss, $\lambda_{\perp}$ > 3 cm. Hence, there should be no problem in obtaining the necessary magnetic field strength and in constructing a phased array which can produce the necessary perpendicular wavelengths. Finally, if we set ϕ > 0.05, and demand a total device length equal to $20\pi(v_p/\omega_b)$, ie., ten bounce periods, we find that the device length should be less than or equal to about 300 cm, which is long but not impossibly so. Smaller lengths are obtained at larger values of ϕ.

This thesis leaves open many possibilities for future work. One of these is to determine what other waves are generated in the plasma as a result of the wave we launch. In the case of the parallel-propagating wave, the well-known sideband instabilities are generated, and it is reasonable to expect something similar to occur for an obliquely propagating wave in the trapping regime. But what happens in the stochastic regime? One cannot say for sure, but it is reasonable to speculate that broadband instabilities are generated which are resonant with the region in velocity-space where electron motion is stochastic.

In that case, quasilinear theory with resonance broadening might well be appropriate to describe the multi-wave and distribution function evolution and could possibly yield excellent results.

Moreover, it seems likely that the methods of this thesis can be applied to a wide variety of problems where the transition between regular and stochastic motion is important. Applications can be made to ion waves and electromagnetic waves. It is possible that even unstable waves can be treated in a similar fashion. Hence, many questions are left for future exploration.

REFERENCES

1. D. Ruelle and F. Takens, Comm. Math. Phys. 20, 167 (1971).

2. B. A. Huberman and J. P. Crutchfield, Phys. Rev. Lett. 43, 1743 (1979).

3. H. Lashinsky in Intrinsic Stochasticity in Plasmas, edited by G. Laval and D. Gresillon (l'Ecole Polytechnique, Paris, 1979).

4. J. M. Wersinger, J. M. Finn, and E. Ott, Phys. Rev. Lett. 44, 453 (1980).

5. M. J. Feigenbaum, Los Alamos Science (Summer, 1980).

6. J. Ford in Advances in Chemical Physics, Vol. 24, edited by I. Prigogine and S. A. Rice (John Wiley, New York, 1973), p. 155-85.

7. H. Poincaré, Les méthodes nouvelles de la mécanique céleste (Gauthier-Villars, Paris, 1982).

8. M. Henon and C. Heiles, Astron. J. 69, 73 (1964).

9. G. R. Smith and A. N. Kaufman, Phys. Fluids 21, 2230 (1978).

10. A. Fukuyama, H. Momota, R. Itatani, and T. Takizuka, Phys. Rev. Lett. 38, 70 (1977).

11. C. F. F. Karney, Phys. Fluids 21, 1584 (1978).

12. T. Stix, PPPL Report Number 1539 (1979).

13. M. N. Rosenbluth, Phys. Rev. Lett. 29, 408 (1972).

14. A. V. Timofeev, Nucl. Fusion 14, 165 (1974).

15. G. R. Smith, J. A. Byers, and L. L. LeDestro, Phys. Fluids 23, 278 (1980).

16. C. R. Menyuk and Y. C. Lee, Phys. Fluids, 23, 2225 (1980).

17. A. Rechester and M. N. Rosenbluth, Phys. Rev. Lett. 40, 38 (1978).

18. S. P. Hirschman and K. Molvig, Phys. Rev. Lett. _42_, 648 (1979).

19. See, e.g., C. Mira and J. Gusnowski, <u>Dynamique Chaotique</u> (Cepadues Editions, Paris, 1980).

20. B. V. Chirikov, Phys. Reports _52_, 263 (1979).

21. See, e.g., R. Z. Sagdeev and A. A. Galeev, <u>Nonlinear Plasma Theory</u> (Benjamin, N.Y., 1969); R. C. Davidson, <u>Methods in Non-Linear Plasma Theory</u> (Academic, N. Y., 1972).

22. V. K. Decyk, Ph.D. thesis (UCLA, 1977).

23. T. H. Malmberg and C. B. Wharton, Phys. Rev. Lett. _19_, 775 (1967).

24. J. M. Dawson and R. Shanny, Phys. Fluids _11_, 1506 (1968).

25. R. K. Mazitov, Zh. Prikl. Mekhan. Tekh. Fiz. _1_, 27 (1965).

26. T. O'Neil, Phys. Fluids _8_, 2225 (1965).

27. W. M. Mannheimer and R. W. Flynn, Phys. Fluids _14_, 2393 (1971).

28. G. J. Morales and T. O'Neil, Phys. Rev. Lett. _28_, 417 (1972).

29. A. Lee and G. Schmidt, Phys. Fluids _13_, 2546 (1970).

30. V. L. Bailey, Jr., and J. Denavit, Phys. Fluids _13_, 451 (1970); R. Sugihara and T. Kamimura, J. Phys. Soc. Japan _33_, 206 (1972).

31. G. Pocobelli, Phys. Rev. Lett. _43_, 1865 (1979).

32. P. J. Vidmar, J. H. Malmberg, and T. P. Starke, Phys Fluids, _19_, 32 (1976).

33. S. T. Tsai, J. Plasma Physics _11_, 213 (1974).

34. A. Lee and G. Pocobelli, Phys. Fluids _16_, 1964 (1973).

35. Y. Matsuda and R. W. Crawford, Phys. Fluids _18_, 1345 (1975).

36. P. J. Palmadesso, Phys. Fluids _15_, 2006 (1972).

37. T. H. Stix, <u>The Theory of Plasma Waves</u> (McGraw-Hill, New York, 1962), Chap. 8.

38. T. M. O'Neil, J. H. Winfrey, and J. H. Malmberg, Phys. Fluids 14, 1204 (1971).

39. B. D. Fried, C. S. Liu, and R. Z. Sagdeev, Bull. Am. Phys. Soc. 14, 1034 (1968).

40. L. Landau, J. Phys. (U.S.S.R.) 10, 25 (1946).

41. See J. H. Malmberg and C. B. Wharton, Phys. Rev. Lett. 13, 184 (1964) and references cited therein.

42. J. Dawson, Phys. Fluids 5, 445 (1962).

43. B. D. Fried and S. D. Conte, The Plasma Dispersion Function (Academic, New York, 1961).

44. J. Dawson, Phys. Fluids 4, 869 (1961); F. F. Chen, Introduction to Plasma Physics (Plenum, New York, 1974), Chap. 7.5.

45. J. E. McCune, Phys. Fluids 10, 2082 (1967).

46. C. R. Menyuk, Sherwood Meeting: Theoretical Aspects of Controlled Thermonuclear Research (April, 1980).

47. L. D. Landau and E. M. Lifshitz, Electrodynamics of Continuous Media (Pergamon, New York, 1975), p. 253-6.

48. L. M. Milne-Thomson in Handbook of Mathematical Functions, edited by M. Abramowitz and I. A. Stegun, National Bureau of Standards Applied Mathematic Series no. 55 (U. S. Government Printing Office, Washington, D. C., 1964), Chap. 16.1.

49. I. S. Gradshteyn and I. M. Ryzhik, Table of Integrals, Series, and Products (Academic, New York, 1965), Chap. 8.146.

50. T. H. Dupree, Phys. Fluids 9, 1773 (1966).

51. A. B. Rechester, R. B. White, and M. N. Rosenbluth, Phys. Rev. A 23, 2664 (1981).

52. C. F. Kennel and F. Engelmann, Phys. Fluids $\underline{9}$, 2377.

53. H. Antosiewicz, in <u>Handbook of Mathematical Functions</u>, edited by M. Abromowitz and I. A. Stegun, National Bureau of Standards Applied Mathematics Series no. 55 (U. S. Government Printing Office, Washington, D. C., 1964), Chap. 10.4.

54. P. M. Morse, and H. Feshbach, <u>Methods of Theoretical Physics, Part I</u>, (McGraw-Hill, New York, 1953), p. 413-4.

Within this appendix, the basic equations of Chapters 3-6 are derived, using a method similar in spirit to a calculation by Landau and Lifshitz.[47] The basic assumption we use is that the non-linear phenomena occur on a time-scale which is long compared to the wave's period of oscillation in the laboratory frame $T = 2\pi/\omega_0$. This time is also roughly the time-scale on which phase-mixing occurs.

We begin by assuming a field of the form

$$\underset{\sim}{E}(t) = \underset{\sim}{E}_0(t) \sin\left[\underset{\sim}{k}\cdot\underset{\sim}{x} - \omega_0 t - \eta(t)\right]$$

$$= \underset{\sim}{E}_{\underset{\sim}{k}}(t) \exp\left[i(\underset{\sim}{k}\cdot\underset{\sim}{x} - \omega_0 t)\right] + \underset{\sim}{E}_{\underset{\sim}{k}}^{*}(t) \exp\left[-i(\underset{\sim}{k}\cdot\underset{\sim}{x} - \omega_0 t)\right],$$

(A.1)

where

$$\eta(t) = \int_0^t \delta\omega(t')\,dt',$$

(A.2)

$$\underset{\sim}{E}_{\underset{\sim}{k}}(t) = \frac{\underset{\sim}{E}_0(t)}{2i} \exp\left[-i\int_0^t \delta\omega(t')\,dt'\right].$$

Noting that we may quite generally write

$$\underset{\sim}{E}_0(t) = E_0 \exp\left[-\int_0^t \gamma(t')\,dt'\right],$$

(A.3)

we conclude

$$\underset{\sim}{E}_{\underset{\sim}{k}}(t) = \frac{\underset{\sim}{E}_0}{2i} \exp\left[-i\int_0^t \delta\omega_c(t')\,dt'\right],$$

(A.4)

where

$$\delta \omega_c = \delta \omega - i\gamma \quad . \tag{A.5}$$

From Poisson's equation

$$\nabla \cdot \underset{\sim}{E} = 4\pi\rho , \tag{A.6}$$

it follows that

$$i\underset{\sim}{k} \cdot \underset{\sim}{E}_{\underset{\sim}{k}}(t) = 4\pi\rho_{\underset{\sim}{k}}(t) , \tag{A.7}$$

where

$$\rho = \rho_{\underset{\sim}{k}}(t) \exp\left[i\left(\underset{\sim}{k}\cdot\underset{\sim}{x}-\omega_0 t\right)\right] + \rho_{\underset{\sim}{k}}^{*}(t) \exp\left[-i\left(\underset{\sim}{k}\cdot\underset{\sim}{x}-\omega_0 t\right)\right] \tag{A.8}$$

is the electron charge which generates $\underset{\sim}{E}$.

It is useful in our work to Fourier transform $E_{\underset{\sim}{k}}(t) \exp (-i\omega_0 t)$ and $\rho_{\underset{\sim}{k}}(t) \exp (-i\omega_0 t)$. Doing so, we may write

$$\underset{\sim}{E}_{\underset{\sim}{k}}(t) = \int_{-\infty}^{\infty} d\omega' \, \underset{\sim}{E}_{\underset{\sim}{k}}(\omega') \exp\left[-i\left(\omega'-\omega_0\right)t\right] ,$$

$$\rho_{\underset{\sim}{k}}(t) = \int_{-\infty}^{\infty} d\omega' \, \rho_{\underset{\sim}{k}}(\omega') \exp\left[-i\left(\omega'-\omega_0\right)t\right] , \tag{A.9}$$

where $E_{\underset{\sim}{k}}(\omega')$ and $\rho_{\underset{\sim}{k}}(\omega')$ are respectively the transforms of $E_{\underset{\sim}{k}}(t) \exp (-i\omega_0 t)$ and $\rho_{\underset{\sim}{k}}(t) \exp (-i\omega_0 t)$. In general, $\rho_{\underset{\sim}{k}}(\omega')$ can be divided into a linear portion $\rho_{\underset{\sim}{k\ell}}(\omega')$ and a non-linear portion $\rho_{\underset{\sim}{kn\ell}}(\omega')$. The

linear portion $\rho_{k\ell}(\omega')$ is related to $\underset{\sim}{E}_k(\omega')$ through the usual suscepti-

bility tensor

$$-i \underset{\sim}{k} \cdot \underset{\approx}{\chi} \cdot \underset{\sim}{E}_k(\omega') = 4\pi \rho_{k\ell}(\omega'), \tag{A.10}$$

which is calculated in linear theory. The quantity $\rho_{k\ell}(\omega')$ can be

further divided into two portions, $\rho_{kr}(\omega')$ which is related $\underset{\sim}{E}_k(\omega')$ by

the real part of $\underset{\sim}{\chi}$, $\underset{\sim}{\chi}_r$, and $\rho_{ki}(\omega')$ which is related to $\underset{\sim}{E}_k(\omega')$ by the

imaginary part, $\underset{\sim}{\chi}_i$.

$$-i \underset{\sim}{k} \cdot \underset{\approx}{\chi}_r \cdot \underset{\sim}{E}_k(\omega') = 4\pi \rho_{kr}(\omega'),$$

$$\tag{A.11}$$

$$-i \underset{\sim}{k} \cdot \underset{\approx}{\chi}_i \cdot \underset{\sim}{E}_k(\omega') = 4\pi \rho_{ki}(\omega').$$

The portion $\rho_{kr}(\omega')$, which is 90° out of phase with $\underset{\sim}{E}_k(\omega')$, is

responsible for supporting the wave, and $\rho_{ki}(\omega')$, which is in phase

with $\underset{\sim}{E}_k(\omega')$, is responsible for the usual linear damping. Finally, it

is useful to define an auxilliary (real dielectric) field, such that

$$\underset{\sim}{D}_{kr}(\omega') \equiv \underset{\sim}{E}_k(\omega') + \underset{\approx}{\chi}_r \cdot \underset{\sim}{E}_k(\omega') = \underset{\approx}{\varepsilon}_r \cdot \underset{\sim}{E}_k(\omega'), \tag{A.12}$$

where $\underset{\sim}{\varepsilon}_r$ is the usual real dielectric tensor. Using Eq. (A.7) and

(A.11), we find

$$i \underset{\sim}{k} \cdot \underset{\sim}{D}_{kr}(\omega') = 4\pi \left[\rho_k(\omega') - \rho_{k\ell}(\omega') \right]. \tag{A.13}$$

144

We can determine the time-varying quantities, $\rho_{kr}(t)$ and $D_{kr}(t)$ by inverse transforming $\rho_{kr}(\omega')$ and $D_{kr}(\omega')$ in analogy with Eq. (A.6),

$$\rho_{kr}(t) = \int_{-\infty}^{\infty} d\omega' \; \rho_k(\omega') \; \exp\left[-i(\omega'-\omega_0)t\right],$$

$$D_{kr}(t) = \int_{-\infty}^{\infty} d\omega' \; D_k(\omega') \; \exp\left[-i(\omega'-\omega_0)t\right],$$

(A.14)

and the Eq. (A.13) becomes

$$i\underset{\sim}{k} \cdot D_{kr}(t) = 4\pi\left[\rho_k(t) - \rho_{kr}(t)\right].$$

(A.15)

As a result of our assumption that $E_k(t)$ varies slowly, we conclude that $E_k(\omega')$ is sharply peaked near $\omega' = \omega_0$, allowing us to Taylor expand $\varepsilon_r(k,\omega')$ in the neighborhood $\omega' = \omega_0$. Using Eqs. (A.12) and (A.14), and noting that $\varepsilon_r(k, \omega_0) = 0$, we have

$$D_{kr}(t) = \int_{-\infty}^{\infty} d\omega' \; \varepsilon_r(\underset{\sim}{k}, \omega') \cdot E_k(\omega') \exp\left[-i(\omega'-\omega_0)t\right]$$

$$= \int_{-\infty}^{\infty} d\omega' \; \frac{\partial \varepsilon_r}{\partial \omega} \; (\omega'-\omega_0) \cdot E_k(\omega') \exp\left[-i(\omega'-\omega_0)t\right]$$

(A.16)

$$= i \; \frac{\partial \varepsilon_r}{\partial \omega} \cdot \frac{d E_k(t)}{dt}.$$

substituting Eqs. (A.4) and (A.5) in (A.16), and using Eq. (A.13), we finally conclude

145

$$\underset{\sim}{k} \cdot \frac{\partial \underset{\sim}{\varepsilon} r}{\partial \omega} \, \delta \omega_c \cdot \underset{\sim}{E}_{\underset{\sim}{k}}(t) \; = \; 4\pi \left[\rho_{\underset{\sim}{k}}(t) - \rho_{\underset{\sim}{k}r}(t) \right]$$

$$= \; -4\pi n_0 \, e \int_{-\infty}^{\infty} d^3v \left(f_{\underset{\sim}{k}} - f_{\underset{\sim}{k}r} \right) , \qquad \text{(A.17)}$$

where $f_k(v, t)$ and $f_{kr}(v, t)$ are the contributions of electrons moving
at a given velocity to ρ_k and ρ_{kr}. Up until now, we have not explicitly
specialized our results to the case of electrostatic waves. Doing so,
we find

$$i k \, \frac{\partial \varepsilon_r}{\partial \omega} \, \delta \omega_c \, E_{\underset{\sim}{k}}(t) \; = \; -4\pi n_0 \, e \int d^3v \left(f_{\underset{\sim}{k}} - f_{\underset{\sim}{k}r} \right) , \qquad \text{(A.18)}$$

where $\varepsilon_r \equiv \underset{\sim}{k} \cdot \underset{\sim}{\varepsilon}_r \cdot k/k^2$. Eq. (A.18) is just the subtraction formula
used in Chapter 3.

We note that the procedure we have followed of only subtracting
the real part of ρ_{kr} from both sides of Eq. (A.7) has resulted in the
use of a dielectric function ε_r which is explicitly real. By using
this procedure, we have also effectively included with the non-linear
response on the right-hand side of Eq. (A.17), the portion of the
linear response which contributes to Landau damping. We could have,
if we had wished, subtracted the whole linear response. Since our

146

Fourier transform technique requires expansion about the real frequency ω_0, we would have found, to lowest order in the Taylor expansion

$$4\pi \left(\rho_{\underset{\sim}{k}} - \rho_{\underset{\sim}{k}\ell} \right) = ik \left(\frac{\partial \varepsilon_r}{\partial \omega} \delta\omega_c + \varepsilon_i \right) E_{\underset{\sim}{k}}$$

$$= ik \frac{\partial \varepsilon_r}{\partial \omega} \left(\delta\omega_c + \gamma_L \right) E_{\underset{\sim}{k}} \, , \tag{A.19}$$

where γ_L is the usual linear (Landau) damping rate.

The momentum equation used in Chapter 4, as well as the corresponding energy equation, may be derived in a similar manner starting from Poisson's equation,

$$\nabla \cdot \underset{\sim}{E} = 4\pi\rho \, ,$$

$$\frac{\partial \underset{\sim}{E}}{\partial t} = -4\pi \underset{\sim}{j} \, , \tag{A.20}$$

where the current $\underset{\sim}{j}$ is determined by the continuity relation

$$\frac{\partial \rho}{\partial t} + \nabla \cdot \underset{\sim}{j} = 0 \, . \tag{A.21}$$

The charge ρ is related through Eq. (A.8) to $\rho_{\underset{\sim}{k}}$, we may similarly define

$$\rho_r = \rho_{\underset{\sim}{k}r}(t) \, exp\left[i \left(\underset{\sim}{k} \cdot \underset{\sim}{x} - \omega_0 t \right) \right] + \rho_{\underset{\sim}{k}r}^*(t) \, exp\left[-i \left(\underset{\sim}{k} \cdot \underset{\sim}{x} - \omega_0 t \right) \right],$$

$$\tag{A.22}$$

$$\underset{\sim}{D}_r = \underset{\sim}{D}_{\underset{\sim}{k}r}(t) \, exp\left[i \left(\underset{\sim}{k} \cdot \underset{\sim}{x} - \omega_0 t \right) \right] + \underset{\sim}{D}_{\underset{\sim}{k}r}^*(t) \, exp\left[-i \left(\underset{\sim}{k} \cdot \underset{\sim}{x} - \omega_0 t \right) \right] \, .$$

The charge $\underset{\sim}{j}_r$ can be obtained directly from ρ_r through the continuity relation. We then find

$$\nabla \cdot \underset{\sim}{D}_r = 4\pi (\rho - \rho_r),$$

$$\frac{\partial \underset{\sim}{D}_r}{\partial t} = -4\pi (\underset{\sim}{j} - \underset{\sim}{j}r),$$

(A.23)

where $\rho - \rho_r$ is the total charge minus the charge that supports the wave, i.e., the charge due to non-linear effects and Landau damping; $j - j_r$ is the corresponding current. Hence, when we multiply both sides of Eq. (A.23) by $\underset{\sim}{E}$, we conclude

$$\frac{1}{4\pi} \underset{\sim}{E} \nabla \cdot \underset{\sim}{D}_r = (\rho - \rho_r) \underset{\sim}{E} = \frac{d \underset{\sim}{P}}{dt},$$

$$-\frac{1}{4\pi} \underset{\sim}{E} \cdot \frac{\partial \underset{\sim}{D}_r}{\partial t} = (\underset{\sim}{j} - \underset{\sim}{j}r) \cdot \underset{\sim}{E} = \frac{dU}{dt},$$

(A.24)

where P and U are the momentum and energy per unit volume taken from the wave due to non-linear effects and Landau damping. Using the relation from Eq. (A.16)

$$\underset{\sim}{D}_{kr}(t) = i \frac{\partial \underset{\sim}{\varepsilon}_r}{\partial \omega} \cdot \frac{d \underset{\sim}{E}_k(t)}{dt},$$

(A.25)

Eq. (A.1), Eq. (A.22), and the reality of $\underset{\sim}{\varepsilon}_r$, we find

148

$$\nabla \cdot \underset{\sim}{D}_r = -\underset{\sim}{k} \cdot \frac{\partial \underset{\approx}{\varepsilon}_r}{\partial \omega} \exp\left[i(\underset{\sim}{k} \cdot \underset{\sim}{x} - \omega_0 t)\right] \cdot \frac{d\,\underset{\sim}{E}_{\underset{\sim}{k}}(t)}{dt}$$

$$-\underset{\sim}{k} \cdot \frac{\partial \underset{\approx}{\varepsilon}_r}{\partial \omega} \exp\left[-i(\underset{\sim}{k} \cdot \underset{\sim}{x} - \omega_0 t)\right] \cdot \frac{d\,\underset{\sim}{E}_{\underset{\sim}{k}}^{*}(t)}{dt} \quad ,$$

(A.26)

$$\frac{\partial \underset{\sim}{D}_r}{\partial t} = i\,\frac{\partial \underset{\approx}{\varepsilon}_r}{\partial \omega} \exp\left[i(\underset{\sim}{k} \cdot \underset{\sim}{x} - \omega_0 t)\right] \cdot \frac{d\,\underset{\sim}{E}_{\underset{\sim}{k}}(t)}{dt}$$

$$-i\,\frac{\partial \underset{\approx}{\varepsilon}_r}{\partial \omega} \exp\left[-i(\underset{\sim}{k} \cdot \underset{\sim}{x} - \omega_0 t)\right] \cdot \frac{d\,\underset{\sim}{E}_{\underset{\sim}{k}}^{*}(t)}{dt} \quad .$$

Recalling

$$\underset{\sim}{E}_{\underset{\sim}{k}} = \frac{\underset{\sim}{E}_0(t)}{2i} \exp\left[-i\,\eta(t)\right] = \frac{\underset{\sim}{E}_0(t)}{2i} \exp\left[-i\int_0^t \delta\omega(t')\,dt'\right],$$

we obtain

$$\nabla \cdot \underset{\sim}{D}_r = -\underset{\sim}{k} \cdot \frac{\partial \underset{\approx}{\varepsilon}_r}{\partial \omega} \sin\left[\underset{\sim}{k} \cdot \underset{\sim}{x} - \omega_0 t - \eta(t)\right] \cdot \frac{d\underset{\sim}{E}_0}{dt}$$

$$+ \underset{\sim}{k} \cdot \frac{\partial \underset{\approx}{\varepsilon}_r}{\partial \omega} \cos\left[\underset{\sim}{k} \cdot \underset{\sim}{x} - \omega_0 t - \eta(t)\right] \cdot \delta\omega\,\underset{\sim}{E}_0 \;,$$

(A.27)

$$\frac{\partial \underset{\sim}{D}_r}{\partial t} = (\omega_0 + \delta\omega)\,\frac{\partial \underset{\approx}{\varepsilon}_r}{\partial \omega} \sin\left[\underset{\sim}{k} \cdot \underset{\sim}{x} - \omega_0 t - \eta(t)\right] \cdot \frac{d\underset{\sim}{E}_0}{dt}$$

$$- (\omega_0 + \delta\omega)\,\frac{\partial \underset{\approx}{\varepsilon}_r}{\partial \omega} \cos\left[\underset{\sim}{k} \cdot \underset{\sim}{x} - \omega_0 t - \eta(t)\right] \cdot \delta\omega\,\underset{\sim}{E}_0 \qquad \text{(A.28)}$$

$$+ \frac{\partial \underset{\approx}{\varepsilon} r}{\partial \omega} \cos \left[\underset{\sim}{k} \cdot \underset{\sim}{x} - \omega_0 t - \eta(t) \right] \cdot \frac{d^2 \underset{\sim}{E}_0}{dt^2}$$

$$+ \frac{\partial \underset{\approx}{\varepsilon} r}{\partial \omega} \sin \left[\underset{\sim}{k} \cdot \underset{\sim}{x} - \omega_0 t - \eta(t) \right] \cdot \frac{d}{dt} \left(\delta\omega \, \underset{\sim}{E}_0 \right) .$$

Substituting Eqs. (A.27) and (A.28) into Eq. (A.24), and averaging over one wavelength, we conclude

$$- k_{\|} \frac{\partial \varepsilon_r}{\partial \omega} \frac{d E_0^2 / 16\pi}{dt} = \frac{d \overline{P_z}}{dt}$$

$$= \frac{d}{dt} \int \frac{dy}{\lambda_\perp} \int \frac{dz}{\lambda_\|} \int d^3 v \, n_0 \, m \, v_z \left(f - f_r \right) ,$$

<div align="right">(A.29)</div>

$$- \frac{\partial \varepsilon_r}{\partial \omega} \frac{d \left(\omega_0 + 2\delta\omega \right) E_0^2 / 16\pi}{dt} = \frac{d \overline{U}}{dt}$$

$$= \frac{d}{dt} \int \frac{dy}{\lambda_\perp} \int \frac{dz}{\lambda_\|} \int d^3 v \, n_0 \, \frac{m}{2} \left(v_z^2 + v_\perp^2 \right) \left(f - f_r \right) ,$$

where $\overline{P}_z$ and $\overline{U}$ are the average z-momentum and energy. If we use a non-self-consistent approach to calculate the right-hand side of Eq. (A.20), as is the case in Chapter 4, then it follows that f_r is zero when averaged over one wavelength and can be dropped from Eq. (A.29) to yield

$$- k_{\|} \frac{\partial \varepsilon_r}{\partial \omega} \frac{d E_0^2 / 16\pi}{dt} = \frac{d}{dt} \int d^3 v \, n_0 \, m \, v_z \, f_0(\underset{\sim}{v}, t) , \qquad \text{(A.30.a)}$$

$$-\frac{\partial \varepsilon_r}{\partial \omega} \frac{d(\omega_0 + 2\delta\omega) E_0^2/16\pi}{dt}$$

$$= \frac{d}{dt} \int d^3v \; n_0 \; \frac{m}{2} (v_z^2 + v_\perp^2) f_0(\underset{\sim}{v}, t), \qquad \text{(A.30.b)}$$

where

$$f_0(\underset{\sim}{v}, t) = \int \frac{dy}{\lambda_\perp} \int \frac{dz}{\lambda_{||}} f \; . \qquad \text{(A.31)}$$

Physically, there is no contribution from f_r because it is proportional to $\underset{\sim}{E}$, and if $\underset{\sim}{E}$ is held fixed, as is the case in the non-self-consistent calculations of Chapters 4 and 5, then f_r must be fixed as well. However, if $\underset{\sim}{E}$ is allowed to vary as is the case in the self-consistent calculations of Chapter 6, then f_r will vary, and its change must be accounted for.

In Chapter 4, we make the approximation

$$[(v_z - \omega_0/k_{||})^2 + v_\perp^2] = constant \; . \qquad \text{(A.32)}$$

If we did not make this approximation, but followed the true distribution function evolution, it would be possible to use Eq. (A.30.b) in concert with Eq. (A.30.a) to determine the frequency shift. However, given this approximation, Eq. (A.30.b) reduces to Eq. (A.30.a), and this determination is not possible in this way.

In the non-self-consistent simulations of Chapter 5, f_r will not contribute to the total damping, as stated earlier, and it is appropriate to use Eq. (A.30). However, in the self-consistent simulations, f_r does contribute, and should be accounted for. In particular, the

151

particles which we are simulating make some contribution to $f_{n\ell}$, f_i, and f_r, where $f_{n\ell}$ and f_i are the portions of $f_{n\ell}$ due to non-linear effects and Landau damping. In the self-consistent simulations, we assume that the entire contribution to $f_{n\ell}$ and f_i come from the particles we are simulating, so that the particles in other regions contribute only to f_r. If we split f_r into two pieces, f_1 being the contribution to f_r of the particles we are simulating, and f_2 being the contribution to f_r of the particles we are not, then it is only f_2 that we wish to subtract from the right-hand side of Eq. (A.30), not the entire f_r.

To determine what Eq. (A.30) becomes in this case, we return to Eq. (A.15) and re-write it in the form

$$i \underset{\sim}{k} \cdot [\underset{\sim}{D}_{kr} - \underset{\sim}{D}_{ki}] = 4\pi (\rho_{\underset{\sim}{k}} - \rho_{\underset{\sim}{k}2}) , \qquad (A.33)$$

where

$$-i \underset{\sim}{k} \cdot \underset{\sim}{D}_{ki} = 4\pi \rho_{\underset{\sim}{k}i} . \qquad (A.34)$$

Dividing $\underset{\sim}{\chi}_r$ into two pieces,

$$\underset{\sim}{\chi}_r (\underset{\sim}{k}, \omega) = \underset{\sim}{\chi}_1 (\underset{\sim}{k}, \omega) + \underset{\sim}{\chi}_2 (\underset{\sim}{k}, \omega) , \qquad (A.35)$$

where $\underset{\sim}{\chi}_1$ is the contribution to $\underset{\sim}{\chi}_r$ of the particles in the simulation, and $\underset{\sim}{\chi}_2$ is the contribution of particles not in the simulation, we find

$$i \underset{\sim}{k} \cdot \left(\underset{\sim}{D}_{\underset{\sim}{k}r} - \underset{\sim}{D}_{\underset{\sim}{k}i} \right)$$

$$= i \underset{\sim}{k} \cdot \int d\omega' \left[\underset{\approx}{\varepsilon}_r(\underset{\sim}{k}, \omega') - \underset{\approx}{\chi}_i(\underset{\sim}{k}, \omega') \right]$$

$$\exp\left[-i(\omega' - \omega_0)t\right] \cdot \underset{\sim}{E}_{\underset{\sim}{k}}(\omega')$$

$$= i \underset{\sim}{k} \cdot \int d\omega' \left[\left(\frac{\partial \underset{\approx}{\varepsilon}_r}{\partial \omega} - \frac{\partial \underset{\approx}{\chi}_i}{\partial \omega} \right)(\omega' - \omega_0) - \underset{\approx}{\chi}_i \right]$$

$$\exp\left[-i(\omega' - \omega_0)t\right] \cdot \underset{\sim}{E}_{\underset{\sim}{k}}(\omega')$$ (A.36)

$$= i \underset{\sim}{k} \cdot \left[\left(\frac{\partial \underset{\approx}{\varepsilon}_r}{\partial \omega} - \frac{\partial \underset{\approx}{\chi}_i}{\partial \omega} \right) \cdot i \frac{d}{dt} \underset{\sim}{E}_{\underset{\sim}{k}}(t) - \underset{\approx}{\chi}_i \cdot \underset{\sim}{E}_{\underset{\sim}{k}}(t) \right] \quad .$$

Noting that

$$\underset{\sim}{D}_r - \underset{\sim}{D}_i = \left(\underset{\sim}{D}_{\underset{\sim}{k}r} - \underset{\sim}{D}_i \right) \exp\left[i(\underset{\sim}{k} \cdot \underset{\sim}{x} - \omega_0 t) \right]$$

$$+ \left(\underset{\sim}{D}_{\underset{\sim}{k}r}^* - \underset{\sim}{D}_{\underset{\sim}{k}i}^* \right) \exp\left[-i(\underset{\sim}{k} \cdot \underset{\sim}{x} - \omega_0 t) \right] ,$$ (A.37)

and also that

$$\frac{\underset{\sim}{E}}{4\pi} \nabla \cdot \left(\underset{\sim}{D}_r - \underset{\sim}{D}_i \right) = 4\pi (\rho - \rho_i) \underset{\sim}{E} = \frac{d \underset{\sim}{P}}{dt} ,$$

$$-\frac{\underset{\sim}{E}}{4\pi} \cdot \frac{\partial \left(\underset{\sim}{D}_r - \underset{\sim}{D}_i \right)}{\partial t} = 4\pi \left(\underset{\sim}{j}_r - \underset{\sim}{j}_i \right) \cdot \underset{\sim}{E} = \frac{dU}{dt} ,$$ (A.38)

where P and U are the momentum and energy gained by the simulation par-
$\underset{\sim}{}$
ticles, we conclude, after averaging over y and z.

$$\frac{d \bar{P}_z}{dt} = -k_{\parallel} \left(\frac{\partial \varepsilon_r}{\partial \omega} - \frac{\partial \chi_i}{\partial \omega} \right) \frac{d E_0^2 / 16\pi}{dt} ,$$ (A.39.a)

$$\frac{d\bar{U}}{dt} = -\left(\frac{\partial \varepsilon_r}{\partial \omega} - \frac{\partial \chi_l}{\partial \omega}\right) \frac{d(\omega_0 + 2\delta\omega) E_0^2/16\pi}{dt}$$

$$+ \chi_l \frac{d E_0^2/16\pi}{dt} .$$

<div align="right">(A.39.b)</div>

In Chapter 5, numerical noise made it too difficult to use Eq. (A.39.b) to calculate the frequency shift.

To derive the energy and momentum equations in the boundary-value problem, we consider a wave of the form

$$\underset{\sim}{E} = \underset{\sim}{E}_0(z) \sin\left(k_{||} z + k_\perp y + \eta_z(z) - \omega t\right),$$

$$\eta_z(z) = \int_0^z \delta k_{||}(z') \, dz' .$$

<div align="right">(A.40)</div>

In the initial-value problem, particles can absorb momentum and energy from the wave because there are many Fourier modes spread over a frequency range which is the inverse of the time-scale on which the wave changes and $\varepsilon_r(\underset{\sim}{k},\omega)$ is not zero except at $\omega = \omega_0$. Similarly, in the boundary-value problem considered in Chapter 6, in which $k_\perp$ and ω are fixed, there will be many $k_{||}$'s in the system and the operator $(\partial \varepsilon_r/\partial \omega)(d/dt)$ is replaced by $-(\partial \varepsilon_r/\partial k_{||})(d/dz)$. One can derive this result in detail by going through exactly the same procedure we followed in the initial-value problem.

What we really calculate in the boundary-value problem is the momentum flux or energy flux deposited in a length dz. To establish this point, we begin with the general equation

$$\frac{d\,\underset{\sim}{P}}{d\,t} = \frac{\partial\,\underset{\sim}{P}}{\partial\,t} + \nabla \cdot \underset{\approx}{\pi} \; ,$$

(A.41)

where π is the momentum flux. Then, we average over t and y, as is
appropriate in the boundary-value problem, and note that, after aver-
aging, all quantities depend only on z, so that Eq. (A.23) becomes

$$\frac{d\,\overline{P_z}}{d\,t} = \frac{\partial}{\partial z} \, \overline{\underset{\approx}{\pi}}_z \; .$$

(A.42)

Similar conclusions hold for the particle flux and the energy flux.
Writing each one of these explicitly, we conclude

$$0 = \frac{d}{dz} \int \frac{dt}{T} \int \frac{dy}{\lambda_\perp} \int d^3v \; n_0 \, v_z \, (f - f_r)$$

$$\frac{\partial \varepsilon_r}{\partial k_\parallel} \, \frac{d\,(k_\parallel \; \delta k_\parallel) \, E_0^2 / 16\pi}{dz}$$

$$= \frac{d}{dz} \int \frac{dt}{T} \int \frac{dy}{\lambda_\perp} \int d^3v \; n_0 \, m \, v_z^2 \, (f - f_r) \, ,$$

(A.43)

$$\omega \frac{\partial \varepsilon_r}{\partial k_\parallel} \, \frac{d\,E_0^2 / 16\pi}{dz}$$

$$= \frac{d}{dz} \int \frac{dt}{T} \int \frac{dy}{\lambda_\perp} \int d^3v \; n_0 \, \frac{m v_z}{2} \, (v_z^2 + v_\perp^2) \, (f - f_r) \, ,$$

where $T = 2\pi/\omega$ is the wave's period of oscillation. In Chapter 6, the
field amplitude is held constant in evaluating the right-hand sides of
Eq. (A.25); so, the f_r terms contribute nothing and may be dropped. We

also neglect $\delta k_{||}$, so that Eq. (A.43) becomes

$$0 \quad = \frac{d}{dz} \int d^3v \ n_0 \ v_z \ f_0 (\underset{\sim}{v}, z) , \qquad \text{(A.44.a)}$$

$$k_{||} \frac{\partial \varepsilon_r}{\partial k_{||}} \frac{d \ E_0^2 / 16\pi}{dz} \quad = \frac{d}{dz} \int d^3v \ n_0 \ m \ v_z^2 \ f_0 (\underset{\sim}{v}, z) , \qquad \text{(A.44.b)}$$

where

$$f_0 = \int \frac{dt}{T} \int \frac{dy}{\lambda_\perp} f .$$

In the case of the parallel-propagating wave, all the particles which contribute significantly to the non-linear behavior have z-velocities of v_p, to lowest order in the electrostatic field, so that Eq. (A.44.b) may be rewritten

$$k_{||} \frac{\partial \varepsilon_r}{\partial k_{||}} \frac{d \ E_0^2 / 16\pi}{dz} \quad = v_p \frac{d}{dz} \int d^3v \ n_0 \ m \ v_z \ f_0 . \qquad \text{(A.45)}$$

Comparing Eqs. (A.21.a) and (A.27), we conclude

$$\frac{v_p}{v_g} \frac{\dfrac{d}{dz} \int d^3v \ n_0 \ m \ v_z \ f_0}{\dfrac{d}{dt} \int d^3v \ n_0 \ m \ v_z \ f_0} \quad = \quad \frac{\dfrac{d}{dz} \left(\dfrac{E_0^2}{16\pi} \right)}{\dfrac{d}{dt} \left(\dfrac{E_0^2}{16\pi} \right)} \quad , \qquad \text{(A.46)}$$

so that the total damping in the boundary-value problem is a factor of v_p/v_g greater than in the initial-value problem. Most of the resonances which contribute significantly to the total damping in an obliquely propagating wave are located close to $v_z = v_p$, implying that even in this case, the total spatial damping should be approximately a factor of v_p/v_g greater than the total temporal damping.